N73-16013
NASA CR-2127

NASA CONTRACTOR REPORT

NASA CR-2127

GODUNOV METHOD AND COMPUTER PROGRAM TO DETERMINE THE PRESSURE AND FLOW FIELD ASSOCIATED WITH A SONIC BOOM FOCUS

by Lee W. Parker and Robert G. Zalosh

Prepared by
MT. AUBURN RESEARCH ASSOCIATES, INC.
Newton, Mass. 02164
for Langley Research Center

NATIONAL AERONAUTICS AND SPACE ADMINISTRATION • WASHINGTON, D. C. • JANUARY 1973

1. Report No.	2. Government Accession No.	3. Recipient's Catalog No.
NASA CR-2127		

4. Title and Subtitle	5. Report Date
GODUNOV METHOD AND COMPUTER PROGRAM TO DETERMINE THE PRESSURE AND FLOW FIELD ASSOCIATED WITH A SONIC BOOM FOCUS	January 1973
	6. Performing Organization Code
7. Author(s)	8. Performing Organization Report No.
Lee W. Parker and Robert G. Zalosh	
	10. Work Unit No.
9. Performing Organization Name and Address	
Mt. Auburn Research Associates, Inc. 385 Elliot Street Newton, MA 02164	11. Contract or Grant No. NAS1-10276
	13. Type of Report and Period Covered
12. Sponsoring Agency Name and Address	Contractor Report
National Aeronautics and Space Administration Washington, D.C. 20546	14. Sponsoring Agency Code

15. Supplementary Notes

16. Abstract

A computer method has been developed to calculate the flow field associated with sonic boom focusing. Solutions are obtained for focusing caused by localized cold spots in the atmosphere, as well as for N-waves with concave fronts. Results include focus factors and the length scales of the focal region. Both strong and weak shock waves are studied.

17. Key Words (Suggested by Author(s))	18. Distribution Statement
Sonic Boom Focus Shock Wave Propagation Numerical Methods Nonlinear Waves	Unclassified - Unlimited

19. Security Classif. (of this report)	20. Security Classif. (of this page)	21. No. of Pages	22. Price*
Unclassified	Unclassified	109	$3.00

*For sale by the National Technical Information Service, Springfield, Virginia 22151

TABLE OF CONTENTS

LIST OF ILLUSTRATIONS

TABLES

GODUNOV METHOD AND COMPUTER PROGRAM TO DETERMINE THE PRESSURE AND FLOW FIELD ASSOCIATED WITH A SONIC BOOM FOCUS

By Lee W. Parker and Robert G. Zalosh

Mt. Auburn Research Associates, Inc.
Newton, Massachusetts

SUMMARY

A numerical method has been developed to calculate the flow field associated with sonic boom focusing. The computer code used in the calculations is capable of following weak N-waves (relative overpressures of the order of 10^{-3} before focusing) for large distances as they approach the focus, in addition to providing the flow field at the focus itself.

Results are presented for two types of problems. In one type of problem, the refraction and subsequent focusing of the N-wave is caused by a localized cold-spot in the atmosphere. In the second type of problem, the N-wave is assumed to be initially refracted (for example, by atmospheric inhomogeneities or aircraft maneuvers) into a prescribed concave shape.

Several sample problems in each category were run. Resulting overpressures at the foci range from 4.4 to 20 times the nominal overpressure. The typical length scale of the high-pressure focal region is of the order of one wavelength. These results are for hypothetical situations, not necessarily typical of supersonic aircraft booms. However, the computer code is now available for use with data taken from specific maneuvers and/or atmospheric disturbances.

An interesting result of this investigation is the resolution of the controversy concerning wave folding at a focus. The theory of geometric acoustics predicts that a concave shock front

will fold over upon itself as it propagates through a focus (ref. 2). As opposed to this, Whitham (ref. 9) has claimed that a concave shock will straighten out without folding over. It appears from the calculations reported here that both phenomena occur, but under different conditions. A weak shock wave with a relative overpressure much less than unity folds over, whereas a strong shock with a relative overpressure of the order of unity (or higher) tends to straighten out.

1. INTRODUCTION

The overpressures in a sonic boom N-wave can be intensified through the focusing phenomenon associated with concave shock fronts. Such concave shock fronts may be produced by atmospheric inhomogeneities and by aircraft maneuvers. This report is addressed to the computation of the flow fields that occur during focusing. Of particular interest is the calculation of the pressure at the focus as well as the extent of the high-pressure region surrounding the focus.

The far-field disturbance from a supersonic aircraft is in the form of an N-wave with two shocks, "fore" and "aft," separated by a linear rarefaction wave. Since the overpressures in a sonic boom N-wave are typically of the order of 10^{-3} times atmospheric pressure (i.e. extremely weak) before focusing, the theory of geometric acoustics is often employed to describe the approach to the focus. However, as explained later, geometric acoustics must be abandoned at the focus itself. On the other hand, standard numerical finite-difference techniques cannot be used to follow weak shocks for large distances because their artificial viscosity tends to smear out the shocks. The shock-following method developed during this study combines the advantages of both geometric acoustics and hydrodynamics. It preserves the weak shocks of the N-waves throughout the entire flow field, and accurately computes the pressure in the focus.

Throughout this report, both line foci and point foci will be discussed. Axisymmetric (r,z) geometry leads to a point focus, whereas two-dimensional (x,y) geometry leads to a line focus. For simplicity, the discussion to follow treats single shocks. It is understood that similar reasoning may be applied to both shocks of the N-wave.

The first mechanism for generating concave shock fronts that will be discussed here is the refraction of a shock wave through

a localized cold region in the atmosphere. Consider the situation illustrated in Figure 1-1, where the bow shock from a supersonic aircraft passes through a spherical atmospheric "cold spot" (leading to a point focus as described below). If the sound speed variation with altitude is neglected, the shock wave propagates at a uniform speed before it penetrates the cold spot. Since sound speed in the cold spot is lower than the ambient sound speed, the portion of the shock passing through the cold spot is slowed relative to the rest of the shock. The resulting concave shock front focuses in such a manner that a shock cusp is produced at the focus. Thus, the action of the cold spot in producing a focus is similar to that of an optical lens. As Figure 1-1 indicates, beyond the focus, the depth of the cusped region decays asymptotically with time.

The theory ordinarily used to predict sonic boom propagation (ref. 1) is based upon a modified form of geometric acoustics. According to geometric acoustics, the wave front propagates along rays which are everywhere perpendicular to the wave front. A geometric acoustics description of the propagation of a concave shock is illustrated in Figure 1-2, where the rays are drawn, and Figure 1-3, where successive shock fronts are drawn. The caustic sheets shown in Figures 1-2 and 1-3 are defined as imaginary surfaces along which adjacent rays cross. The two caustic sheets shown in Figure 1-3 correspond to a two-dimensional (x,y) geometry in which the focus is a line focus. In axisymmetric (r,z) geometry, the caustic sheets would become a single surface of revolution, and the focus would become a point focus.

One of the premises of geometric acoustics is that the local amplitude of the wave front is inversely proportional to the square root of the area of the ray tube formed by adjacent rays. Consequently, geometric acoustics predicts infinite overpressures at a caustic, where the ray tube areas vanish. Of course, non-linear diffraction effects, which are not accounted for in geometric acoustics,

limit the overpressure amplification to some finite value. This value may be computed by the method of the present report.

Although geometric acoustics fails to predict shock overpressures in the immediate vicinity of a caustic sheet, there is no reason to discount the qualitative geometric acoustics description in Figure 1-3.

Pierce (ref. 2) refers to the cusped intersection of the two caustic sheets in Figure 1-3 as an "arête."* Beyond the arête, which is also called the "focus" or "caustic cusp" in this report, the shock folds over upon itself. The fold-over is confined to the region bounded by the two caustic sheets. The above description is confined to weak shocks. As will be shown in Chapter 5, the fold-over occurs for weak shocks, but not for strong shocks which tend rather to straighten out smoothly. This verifies a hypothesis of Pierce (ref. 16).

Apparently, there have not been any direct measurements of sonic boom focusing caused by local atmospheric inhomogeneities, such as a cold spot as illustrated in Figure 1-1, or wind shear fluctuations as illustrated in Figure 1-4. On the other hand, there have been some measurements of focusing generated by maneuvering aircraft in supersonic flight. Schematic drawings of shock focusing resulting from turning and diving maneuvers are shown in Figures 1-5 and 1-6, respectively. Both Figures 1-5 and 1-6 have been redrawn from reference 3. Wanner (ref. 4) reports measured focus factors (defined as the overpressure at the focus divided by the nominal overpressure) up to about 5 for level turns. Maglieri (ref. 5) reports measured focus factors up to about 4 for the same type of maneuver. For the case of turn-entry, in which an arête similar to the one in Figure 1-3 is formed, Wanner reports measured focus factors of about 9.

---

* Computations of arête locations are included in the Boeing geometric acoustics program (ref. 15).

Most of the pressure-intensification data that is available refers to the so-called "sonic cut-off" phenomenon. The cut-off phenomenon occurs when an aircraft is flying faster than ambient sound speed but slower than sound speed at the ground. At the altitude at which the speed of sound is equal to the speed of the aircraft, the down-going wave front is reflected into an up-going wave front. The locus of points at which reflection occurs represents a caustic sheet. Figure 1-7 illustrates the situation for an accelerating aircraft, in which the altitude of the point of reflection moves down toward the ground with time.

It should be emphasized that the sonic cut-off intensification phenomenon, which produces overpressure intensification factors of the order of 2 (see Maglieri et al., ref. 6), is to be distinguished from proper focusing. In proper focusing, which is the phenomenon of interest here, much higher intensification factors are expected.

Confusing terminology exists in the literature. The cusp of an N-wave shock at a single caustic surface has been called a "focus" and the associated overpressure a "superboom." When the shock cusp occurs where two caustic sheets meet (at the "arête"), the shock cusp has been called a "super-focus" and the associated overpressure a "super-superboom," respectively. The distinction between the single caustic surface and the cusped caustic surface has been discussed by A. Pierce (ref. 2).

Except for Pierce's scaling law analysis (ref. 2), all the previous theoretical investigations of sonic boom intensification have been confined to phenomena associated with smooth single caustics, i.e., superbooms. The analyses of Hayes (ref. 7) and Seebass et al. (ref. 8) fall into this category. In contrast, the present report is concerned with proper focusing of a shock at a cusped double caustic, i.e., super-superbooms.

The primary approach adopted in this report is different from those of the past. Rather than attempt a correction to geometric-acoustic theory, or make restrictive assumptions about the nature of

the flow field, the full inviscid conservation equations are retained. A numerical solution is obtained through the use of a moving mesh that propagates with the N-wave (see Chapter 3). By confining the mesh to the spatial region of interest, the computer problems which would be encountered in following an N-wave for large distances with a code using a finite stationary grid are avoided.

A secondary approach based on Whitham's approximate model (ref. 9) of shock wave propagation is also presented. The Whitham-type model deals with a single shock wave, whereas the more rigorous model described in Chapter 3 treats the focusing of the entire N-wave.

The contents of the remainder of the report are summarized as follows:

Chapter 3

The shock following code called GODUNOV is described. GODUNOV computes the flow field within the N-wave as it propagates through the focus. The technique employed to solve the conservation equations is discussed, as well as the results of some test problems.

Chapter 4

The single-shock model code called WHITHAM is described. The model is based on a ray-tube-shock-segment formulation in which an empirical formula is used to relate ray-tube areas and shock-segment Mach numbers. WHITHAM is used as an independent auxiliary calculation that can follow the behavior of single curved shocks in much less computer time than would be required with GODUNOV.

Chapters 5 and 6

Solutions have been obtained for focusing problems involving two types of assumptions, namely,

(a) initially plane N-wave fronts, refracted into concave shapes by passing through cold spots

(b) initial concave-front configurations with prescribed geometric parameters such as curvature and rate-of-change of curvature.

In both cases, the solutions are carried through the focus. Case (a)

represents the full problem starting from the physically expected initial condition. However, Case (b) is useful for the following reasons. First, a significant amount of computer time is saved by avoiding the early part of the calculation, namely, that dealing with the propagation through the cold spot. Second, having geometric configurations based on analytic formulas (such as Gaussian and polynomial functions) allows one to study scaling laws involving, for example, the curvature and the derivatives of the curvature. Third, generally prescribed configurations are applicable, not only to cold-spot refraction, but to the refraction produced by any of several possible physical mechanisms. Hence, it is understood that, for the problems involving assumption (b), atmospheric disturbances or aircraft maneuvers can produce the refracted fronts. The flow variables as functions of two-dimensional space and time are obtained. Tests are made with changes in numerical parameters such as numbers of grid points in order to obtain numerically-convergent solutions. Focus factors are given for various values of the physical parameters. Also investigated is the question: Under what conditions will a concave shock fold over?

Chapter 7

Some conclusions that follow from our results are summarized. These include the confirmation of the geometric-acoustics wave-folding phenomenon for weak shocks, ($\Delta p/p \ll 1$) as well as the absence of wave-folding predicted by Whitham for strong shocks ($\Delta p/p \sim 1$). Focus factors of 19 and 13 have been obtained for polynomial and Gaussian front N-waves, respectively. In both cases, high overpressures are confined to spatial regions with scale lengths of the order of the wavelength. These results demonstrate the capability of solving the focusing problem with the numerical hydrodynamics formulation described in the report. Computations with initial conditions representative of proposed supersonic transport operations can now be carried out.

2. SYMBOLS

a = $\Delta r_i / \Delta r_{i-1}$ in GODUNOV

A = area of cell boundary in GODUNOV, area of shock segment in WHITHAM

A_{cross} = cross sectional area of cell in r,z plane

B = normal component of cell boundary velocity

c = sound speed

e = internal energy per unit mass

E = total energy per unit mass $E = e + \frac{1}{2}(u^2 + v^2)$

i = index for horizontal rows in GODUNOV mesh; index for shock segments and nodes in WHITHAM

j = index for columns parallel to shocks in GODUNOV

K = constant in area versus Mach number relation used in WHITHAM

ℓ_i = length of shock segment i (GODUNOV and WHITHAM)

m = mass flux across a wave appearing in Riemann problems

M = Mach number

p = pressure

q_i = shock velocity of segment i (GODUNOV and WHITHAM)

r = radial coordinate

$\dot{r}_i$ = vertical component of shock node velocity in WHITHAM

Δr_i = separation of horizontal grid lines in GODUNOV

t = time

u = velocity component in z (or x) direction

$\bar{u}_i$ = shock node velocity in WHITHAM

$\hat{u}_{i,j}$ = node velocity in GODUNOV (see Figure 3-2)

U = normal component of velocity flowing into a cell in GODUNOV

v = velocity component in r (or y) direction

V = cell volume in GODUNOV

V_w = wave propagation speed

x = coordinate parallel to direction of propagation

y = coordinate normal to propagation direction

z = axial coordinate

$\dot{z}_i$ = axial component of shock node velocity in WHITHAM

γ = ratio of specific heats

δ = symbol appearing in conservation equations. $\delta = 0$ for x,y geometry, $\delta = 1$ for r,z geometry

θ_i = angle of inclination of segment i to vertical

ρ = density

Subscripts

N, S, E, W = north, south, east, west cell boundary

old = value at beginning of time step

new = value at end of time step

1, 2, 3, 4 = regions 1, 2, 3, 4 in Figure 3-3

spot = cold spot

cs = contact surface (see Figure 3-3)

n = normal to cell boundary

3. THE GODUNOV CODE

A computer code, called GODUNOV, has been developed to solve the full set of two-dimensional time dependent conservation equations for the case of a focusing N-wave. The numerical method that is employed in GODUNOV is a modification of a technique originally devised by Godunov, et al. (ref. 10) to study the shock layer adjacent to a blunt body in supersonic flight. Since Godunov's original presentation, the Godunov technique has been applied successfully to a variety of blunt body problems, e.g. references 11 and 12. To the authors' knowledge, this is the first time the technique has been extended to a propagation problem.

One great advantage of the Godunov scheme is that it preserves the discontinuity across shock waves of arbitrary strength. In this respect, it is superior to the standard finite difference codes, such as SHELL, which use artificial viscosity to spread a shock over several mesh points and tend to obliterate weak shocks. It should be pointed out that GODUNOV also treats any internal discontinuity which may arise within the N-wave, through its intrinsic artificial viscosity.

3.1 Mesh Motion and Geometry

The mesh geometry employed in GODUNOV is illustrated in Figure 3-1. The leading and trailing shocks in the N-wave are shown as solid lines. The grid points lie on horizontal lines with fixed spacing in the vertical direction.

Since the high pressure region that results from focusing does not extend far from the axis of symmetry, it is desirable to place most of the grid points near the axis of symmetry. This can be achieved by placing the horizontal grid lines close together near the axis of symmetry and further apart at large radial distances. The separation between horizontal grid lines in GODUNOV follows the geometric progression

$$\frac{\Delta r_i}{\Delta r_{i-1}} = a$$

where a is a constant. We have found that the optimum value of a is 1.05 for these problems.

In order to follow the N-wave as it propagates, the grid points are allowed to move horizontally but not vertically. The N grid points within the N-wave (N = 5 in Figure 3-1) move in such a fashion that they are always equally spaced between the leading and trailing shocks. There are M grid points behind the N-wave (M = 2 in Figure 3-1), and they move so as to be equally spaced between the fixed left boundary of the grid and the trailing shock of the N-wave. The grid points behind the N-wave provide an indication of the net disturbance imparted to the atmosphere after the passage of the N-wave.

The procedure for moving the grid points is the following. First the propagation velocity of each segment of the leading and trailing shock is computed by solving a one-dimensional Riemann problem as described in Section 3.3 (below). Then the projection of each shock segment's normal velocity along the x axis is calculated. The propagation velocity of a node on the leading or trailing shock is determined by using an inverse length weighting of the projected velocity of the two adjacent shock segments. Using the notation indicated in Figure 3-2, the formula for the shock node velocity is

$$\hat{u}_{i,\mathrm{JFORE}} = \frac{1}{(\ell_i + \ell_{i+1})} \left[\frac{q_i \, \ell_{i+1}}{\sin \theta_i} + \frac{q_{i+1} \, \ell_i}{\sin \theta_{i+1}} \right] \qquad (1)$$

A node falling on the contour labeled j between the leading and trailing shocks, indicated by the dashed curve in Figure 3-2, is given a velocity

$$\hat{u}_{i,j} = \hat{u}_{i,JAFT} + (\hat{u}_{i,JFORE} - \hat{u}_{i,JAFT}) \frac{(j - JAFT)}{(JFORE - JAFT)} \qquad (2)$$

where JFORE and JAFT are the j-indices of the leading and trailing shocks, respectively.

An attractive feature of this floating mesh scheme is that it confines the grid points to the continually changing region of interest. Thus, for a given number of grid points, it allows for a higher resolution of the flow field than codes with fixed Eulerian or Lagrangian meshes.

3.2 Conservation Equations

The conservation equations which describe the two-dimensional unsteady flow of an inviscid fluid are given below.

Mass

$$\frac{\partial \rho}{\partial t} + \frac{\partial}{\partial x}(\rho u) + \frac{\partial}{\partial y}(\rho v) = - \delta \frac{\rho v}{y} \qquad (3)$$

x-Momentum

$$\frac{\partial}{\partial t}(\rho u) + \frac{\partial}{\partial x}(p + \rho u^2) + \frac{\partial}{\partial y}(\rho uv) = - \delta \frac{\rho uv}{y} \qquad (4)$$

y-Momentum

$$\frac{\partial}{\partial t}(\rho v) + \frac{\partial}{\partial x}(\rho uv) + \frac{\partial}{\partial y}(p + \rho v^2) = - \delta \frac{\rho v^2}{y} \qquad (5)$$

Energy

$$\frac{\partial}{\partial t}\left[\rho e + \frac{\rho}{2}(u^2 + v^2)\right] + \frac{\partial}{\partial x} u \left[p + \rho e + \frac{\rho}{2}(u^2 + v^2)\right]$$

$$+ \frac{\partial}{\partial y} v \left[p + \rho e + \frac{\rho}{2}(u^2 + v^2)\right] = - \delta \frac{v}{y}\left[p + \rho e + \frac{\rho}{2}(u^2 + v^2)\right] \qquad (6)$$

In the above equations $\delta = 0$ for x, y geometry and $\delta = 1$ for r,z geometry. These equations together with the equation of state represent a set of five nonlinear equations for the five unknowns p, ρ, e, u, and v. A perfect gas law equation of state has been incorporated into GODUNOV, i.e.

$$p = (\gamma - 1)\,\rho e \tag{7}$$

In applying the conservation equations to the moving mesh in GODUNOV, Eqs. (2) - (6) are integrated over a cell volume (V = cell volume). After applying Green's theorem, the result is

Mass

$$\frac{\Delta\,(\rho V)}{\Delta t} = \sum_{NSWE} \left[\rho A\,(U - B)\right] \tag{8}$$

x - Momentum

$$\frac{\Delta\,(\rho u V)}{\Delta t} = (pA \sin\theta)_W - (pA \sin\theta)_E + \sum_{NSEW} \left[\rho u A\,(U - B)\right] \tag{9}$$

y - Momentum

$$\frac{\Delta\,(\rho v V)}{\Delta t} = (pA \cos\theta)_E - (pA \cos\theta)_W$$

$$- (pA)_N + (pA)_S + \sum_{NSEW} \left[\rho v A\,(U - B)\right] + \delta 2\pi A_{cross} \tag{10}$$

Energy

$$\frac{\Delta (\rho EV)}{\Delta t} = \sum_{NSEW} \left[\rho AE\ (U - B) + pUA\right] \tag{11}$$

The subscripts in Eqs. (8) - (11) refer to the north, south, east, and west boundaries of the cell in question (see Figure 3-1). The areas of the cell boundaries are denoted by A, whereas A_{cross} denotes the cross sectional area of the cell in the r,z plane. U represents the normal component of inward-flowing velocity and B the normal component of the cell boundary velocity. The angle θ is measured from the positive x axis to the east or west cell boundary as illustrated in Figure 3-1.

During the course of a time step, the cell volume changes as a result of the mesh motion. The new cell volume at the end of a time step, V_{new}, must first be calculated before Eqs. (8) - (11) can be utilized. The resulting equations used to update the flow variable are

$$(\rho V)_{new} = (\rho V)_{old} + \Delta t \sum_{NSEW} \left[\rho A\ (U - B)\right] \tag{12}$$

$$(u\rho V)_{new} = (\rho uV)_{old} + \Delta t \left\{(pA \sin \theta)_W - (pA \sin \theta)_E + \sum_{NSEW} \left[\rho uA\ (U - B)\right]\right\} \tag{13}$$

$$(v\rho V)_{new} = (\rho vV)_{old} + \Delta t \left\{ (pA \cos\theta)_E - (pA \cos\theta)_W - (PA)_N + (PA)_S + \sum_{NSEW} \left[\rho vA\,(U - B) \right] + \delta 2\pi p A_{cross} \right\} \quad (14)$$

$$(E\rho V)_{new} = (\rho EV)_{old} + \Delta t \left\{ \sum_{NSEW} \left[\rho AE(U - B) + \rho UA \right] \right\} \quad (15)$$

Equations (12) - (15) are used to solve for ρ_{new}, u_{new}, v_{new}, and E_{new}, respectively.

3.3 Riemann Problems

Before the right-hand sides of Eqs. (12) - (15) can be evaluated, the values of the flow variables at the cell boundaries must be determined. This is accomplished in GODUNOV by solving a Riemann problem across the appropriate cell boundary.

The Riemann problem describes how an initial discontinuity between two uniform regions evolves with time. In this case, the two uniform regions are two adjacent cells separated by a cell boundary. There are four Riemann problems associated with each cell. Two of them involve moving boundaries (east and west), and two stationary boundaries (north and south).

Consider two adjacent cells in the same horizontal row as illustrated at the top of Figure 3-3. The boundary between the cells has a normal velocity, B, which is calculated by averaging the normal components of the node velocities at both ends of the boundary, i.e.

$$B = \frac{\sin\theta}{2} (\hat{u}_{i-1,j} + \hat{u}_{i,j}) \quad (16)$$

Once the fluid velocities in the two adjacent cells are resolved into components normal and parallel to the cell boundary, the solution of the one-dimensional Riemann problem proceeds as indicated in the x-t diagram in Figure 3-3.

In general, a compression or rarefaction wave, wave 1, will propagate into region (1), and another compression or rarefaction wave emanating from the interface, wave 4, will propagate into region (4). Between wave 1 and wave 4, a contact surface exists. To the extent that the width of the rarefaction waves can be neglected (acoustic limit), the three discontinuities divide the x-t plane into 4 uniform regions, labeled (1) - (4) in Figure 3-3.

At the fore and aft (or leading and trailing) shocks, wave 4 is a shock wave which coincides with the cell boundary in the x-t plane. At an interior east or west cell boundary, the boundary position has a velocity dx/dt = B as computed above, whereas a north or south boundary is fixed and its position coincides with the t axis in the x-t plane. In each case, the flow properties at the cell boundary are set equal to the flow properties of the region in which it lies.

If wave 4 is a shock wave, the Rankine-Hugoniot relations dictate that the mass flux across wave 4 is

$$m_4 = \sqrt{\frac{\rho_4}{2}\left[(\gamma + 1)\, p_3 + (\gamma - 1)\, p_4\right]} \qquad (17)$$

and, from momentum conservation,

$$p_4 - p_3 + m_4\,(u_{n4} - u_{n1}) = 0 \qquad (18)$$

where u_n is the fluid velocity relative to the wave. In the case that wave 1 is a rarefaction wave, the one-dimensional unsteady isentropic relations provide that

$$u_{n1} + \frac{2\sqrt{\gamma p_1/\rho_1}}{\gamma - 1} = u_{n2} + \frac{2\sqrt{\gamma p_2/\rho_2}}{\gamma - 1} \tag{19}$$

Since the pressure and normal component of fluid velocity are preserved across a contact surface, $p_2 = p_3 = p_{cs}$ and $u_{n2} = u_{n3} = U_{cs}$. Equations (18) and (19) may now be solved for p_{cs} and U_{cs} to give

$$p_{cs} = \frac{m_1 p_4 + m_4 p_1 + m_1 m_4 (u_{n1} - u_{n4})}{m_1 + m_4} \tag{20}$$

and

$$U_{cs} = \frac{p_1 - p_4 + m_4 u_{n4} + m_1 u_{n1}}{m_1 + m_4} \tag{21}$$

where

$$m_1 = \frac{(\gamma - 1)}{2\gamma}\sqrt{\gamma p_1 \rho_1}\left[\frac{1 - p_{cs}/p_1}{1 - (p_{cs}/p_1)^{(\gamma-1)/2\gamma}}\right] \tag{22}$$

An iterative solution for m_4 using Eqs. (17), (20), and (22) is obtained at each fore and aft shock segment. The shock velocity is then computed as

$$q_n = u_{n4} + \frac{m_4}{\rho_4} \tag{23}$$

This procedure is simplified at interior cell boundaries by using the weak wave relations across waves 1 and 4. In the acoustic limit,

$$m_1 = \sqrt{\gamma p_1 \rho_1} \quad \text{and} \quad m_4 = \sqrt{\gamma p_4 \rho_4} \tag{24}$$

and no iterative solution is required for p_{cs} and U_{cs}.

To determine the properties of an interior cell boundary, the boundary velocity, B, is compared to the wave speeds, where

$$\left.\begin{aligned} V_{w1} &= u_{n1} - \sqrt{\gamma p_1/\rho_1} + \frac{(\gamma+1)}{4}(U_{cs} - u_{n1}) \\ V_{w4} &= u_{n4} + \sqrt{\gamma p_4/\rho_4} + \frac{(\gamma+1)}{4}(U_{cs} - u_{n4}) \end{aligned}\right\} \tag{25}$$

For example, if $V_{w1} < B < U_{cs}$, then the cell boundary lies in region (2) in the x-t plane. and the flow variables at the boundary are:

$$\left.\begin{aligned} p &= p_{cs} \\ U &= U_{cs} \\ \rho &= \rho_2 = \rho_1 (p_{cs}/p_1)^{1/\gamma} \end{aligned}\right\} \tag{26}$$

If the cell boundary falls in region (3), the first two relations in (26) would remain the same while

$$\rho = \rho_3 = \rho_4 \, (p_{cs}/p_4)^{1/\gamma} \tag{27}$$

3.4 Time Step Computation

The time step used in updating the flow variables is computed on the basis of a Courant type stability criterion. This criterion limits the time step to less than the time required for an acoustic signal to travel across any cell, in either the x or y directions.

An acoustic signal travels northward across a cell at speed c + v, and southward at a speed c - v. Hence the vertical direction time step is

$$\Delta t_y = \frac{\Delta r}{\max\,(c + v,\ c - v)} \tag{28}$$

In calculating the horizontal direction time step, the motion of the cell boundary must be included. An acoustic signal propagates eastward at a speed c + u, and westward across a cell at speed c - u. A signal emanating from the west cell boundary will have to travel a distance $\Delta z_{min} + B_E \Delta t$, where Δz_{min} is the shortest horizontal leg of the trapezoidal cell, before it encounters the east boundary. Similarly, a signal leaving the east boundary will travel a distance $\Delta z_{min} - B_w \Delta t$ across the cell. Therefore, the horizontal time step is

$$\Delta t_x = \frac{\Delta z_{min}}{\max\ (c + u - B_E,\ c - u + B_W)} \tag{29}$$

In order to avoid difficulties that could arise when the cell boundaries and/or the fluid are moving much faster than sound speed, GODUNOV uses a modified horizontal time step of

$$\Delta t_x = \frac{\Delta z_{min}}{\max\ (c + |u| + |B_E|,\ c + |u| + |B_W|)} \tag{30}$$

Following Godunov, et al. (ref. 10), the overall time step for a cell is

$$\Delta t = \frac{\Delta t_x\ \Delta t_y}{\Delta t_x + \Delta t_y} \tag{31}$$

and the time step used during a cycle is the minimum value of Δt computed for every cell in the grid.

3.5 Boundary Conditions

Zero gradient boundary conditions are imposed at the top and left boundaries of the grid. This is implemented in GODUNOV by setting the flow variables at the west boundary of a cell in the first (far west) column of the grid equal to the corresponding values at the center of the cell. Similarly, the north boundary of a cell in the top (far north) row of the grid is assumed to possess the same properties as the center of the cell.

The right boundary of the grid coincides with the leading shock of the N-wave. The appropriate Riemann problem is solved (as described in the previous section) for each shock segment in order to compute the jump conditions across the shock. The flow field

ahead of the shock is assumed to be undisturbed except for the presence of the cold spot.

A symmetry condition exists at the bottom boundary of the grid. In the early stages of development, the symmetry was accounted for by placing the center of the first row of cells on the x axis, and constraining the east and west cell boundaries on the first row to be vertical. This configuration is illustrated at the top of Figure 3-4. The vertical component of velocity in the first row of cells must be zero in this arrangement.

Several runs with this symmetry configuration produced at late times an abrupt change in the slope of the shock between the first and second shock segments. In other words, both shocks in the N-wave tended to be inclined upon passing through the focus, and the constraint of a vertical segment on the axis was artificial. Downstream of the focus the discontinuity in slope seemed to propagate upward along the shocks, and it appeared as if the shocks "broke up." This situation is illustrated in Figure 3-5, and is a numerical artifact.

To alleviate this "break-up" the symmetry condition was re-posed in terms of an imaginary row of cells across the axis of symmetry. As the bottom of Figure 3-4 indicates, the imaginary row of cells was taken to be the mirror image of the first row. Now the first shock segment can be inclined and a vertical component of velocity is allowed in the first row of cells. Subsequent runs with this configuration produced smooth shock profiles.

3.6 Test Runs

A series of test runs was conducted with GODUNOV before it was used for the two-dimensional N-wave focusing problem.

The first test case concerned the one-dimensional propagation of an N-wave into a uniform atmosphere, without refraction.

The initial relative overpressure of the N-wave was $\Delta p_o/p_o = 0.1$, and the initial wavelength was 50 meters. Ten axial grid points were placed within the N-wave and two behind it. Figure 3-6 is a plot of the pressure distribution both initially and after it has propagated for 0.1807 secs (50 time steps or cycles).

The half wavelength, ℓ, of the N-wave should increase with time according to the formula (ref. 13)

$$\frac{\ell}{\ell_o} = \sqrt{1 + \frac{(\gamma + 1)}{2} \frac{\Delta v_o t}{\ell_o}} \tag{32}$$

where ℓ_o and Δv_o are the initial half wavelength and velocity amplitude, respectively. For the parameters of the N-wave in Figure 3-6, (Δv_o = 24.34 meters/sec), Eq. (32) predicts a value of $\ell/\ell_o = 1.100$ after 0.1807 secs. The value computed in GODUNOV was $\ell/\ell_o = 1.090$, which is within 1 percent of the theoretical value, indicating excellent agreement.

The same problem was run on the SHELL code, which is one of the standard hydrodynamic codes with a stationary mesh. The pressure profiles obtained with SHELL are illustrated in Figure 3-7. The artificial viscosity in SHELL has spread the shock waves to such an extent that they are barely recognizable as discontinuities with well-defined amplitudes. It is apparent that SHELL is not capable of following shock waves with relative overpressures much less than 0.1, which is the range in which we are interested.

The other test problem run on both SHELL and GODUNOV was a numerical simulation of a "cylindrical shock tube" problem. In this problem, the ordinary planar diaphragm separating the high and low pressure gases is replaced by an imaginary cylindrical diaphragm.

At time t = 0, the pressure ratio across the diaphragm is 4.45, the diaphragm is instantaneously removed, and the initial discontinuity resolves itself into a shock wave and a rarefaction wave propagating in opposite directions. The resulting flow is in the radial direction only.

The results of computations with SHELL and GODUNOV are illustrated in Figure 3-8. The initial pressure across the diaphragm (4.45) was chosen so as to produce a shock wave with a relative overpressure of 1 in the axial flow case. There is no equivalent analytical solution to the radial flow problem, but both SHELL and GODUNOV indicate that the shock wave is slightly weaker than it would be for axial flow. The excellent agreement between SHELL and GODUNOV confirms that GODUNOV is computing the radial flow correctly. This confirmation together with the axial flow test case results verifies that GODUNOV is a valid two-space-dimensional fluid dynamic code. The fact that the shock discontinuity is smeared slightly more by GODUNOV than by SHELL (in Figure 3-8) shows that the intrinsic artificial viscosity is slightly greater in GODUNOV than in SHELL.

4. THE WHITHAM CODE

An auxiliary computer code, entitled WHITHAM, has been created as a supplement to GODUNOV. WHITHAM follows the propagation of a single shock according to the approach described by Whitham in reference 9. In our case, the shock represents the leading shock of the N-wave, and the validity of the WHITHAM code is contingent upon a lack of interaction between the shock and the flow behind it.

Whitham's original premise was that a curved shock may be envisioned as a chain of planar elements, each of which propagates down a tube of varying cross section. The propagation velocity is determined by an empirical area versus Mach number relation. Thus, as the shock begins to focus, the segments near the focus are "compressed" and their propagation velocity increases. In this respect, WHITHAM is a higher order formulation than the ordinary geometric acoustic ray tube concept where every point on the wave front propagates at the local sound speed.

4.1 Numerical Description

A sketch of the shock front in WHITHAM is illustrated in Figure 4-1. Each line segment, which represents in the figure the cross-section of a planar element, has a velocity, q_i, normal to itself, where q_i is equal to the segment Mach number, M_i, multiplied by the ambient sound speed. The differential relationship between Mach number (M) and "segment area" (A) is the one proposed by Whitham (ref. 9), i.e.

$$\frac{dA}{A} = \frac{-2MdM}{(M^2 - 1)\,K(M)} \tag{33}$$

where K(M) is a slowly varying function of Mach number, given in

reference 9. Since K(M) only ranges from 0.5 for weak shocks to 0.394 for strong shocks, Whitham (ref. 9) suggests that its variation may be neglected in integrating Eq. (33). The resulting simple relationship

$$A^K (M^2 - 1) = \text{const} \tag{34}$$

is the one employed in WHITHAM. The area A_i associated with each shock segment is (a) the area of revolution of the segment about the axis of symmetry for r,z geometry, or (b) the area of a strip, per unit length in the z-direction, in x,y geometry.

The sequence of events occurring during one cycle, or time step, in WHITHAM is the following.

1. The lengths and areas of the shock segments are computed from the r,z (or x,y) coordinates of the shock nodes.
2. Mach numbers for every shock segment are computed from Eq. (34) (K is read in as input data; we have used K = .5 for most runs), yielding segment velocities, q_i.
3. The time step, Δt, is computed by taking the smallest value of ℓ_i/q_i. This criterion prevents the segments from moving a distance larger than their own length in one time step.
4. Using the shock segment velocities and geometry, compute the r and z (or x and y) components of the shock node velocities. The method used is described in detail in the next section.
5. Move each shock node a distance $\dot{r}_i \Delta t$ in the radial direction and $\dot{z}_i \Delta t$ in the axial direction.

4.2 Shock Node Velocities

Two different methods have been used to compute the shock node velocities, $\dot{r}_i$ and $\dot{z}_i$, from the segment velocities and geometry.

In the first method, the node velocity components are

computed as an inverse length weighting of the adjacent segment velocities. The equations are

$$\dot{r}_i = -\frac{\left[\frac{(z_i - z_{i-1})\, q_i \ell_{i+1}}{\ell_i} + \frac{(z_{i+1} - z_i)\, q_{i+1} \ell_i}{\ell_{i+1}}\right]}{(\ell_i + \ell_{i+1})} \tag{35}$$

$$\dot{z}_i = \frac{\left[\frac{(r_i - r_{i-1})\, q_i \ell_{i+1}}{\ell_i} + \frac{(r_{i+1} - r_i)\, q_{i+1} \ell_i}{\ell_{i+1}}\right]}{(\ell_i + \ell_{i+1})} \tag{36}$$

In the second method, the two adjacent shock segments are displaced a distance $q_i \Delta t$ normal to themselves and the new node position is computed as the geometric intersection of the two segments. The equations are

$$\dot{r}_i = \left[\frac{q_{i+1} \ell_i\, (r_{i-1} - r_i) + q_i \ell_i\, (r_{i+1} - r_i)}{(z_{i-1} - z_i)(r_{i+1} - r_i) - (z_{i+1} - z_i)(r_{i-1} - r_i)}\right] \tag{37}$$

$$\dot{z}_i = \left[\frac{q_i \ell_i\, (z_{i+1} - z_i) - q_{i+1} \ell_{i+1}\, (z_i - z_{i-1})}{(r_{i+1} - r_i)(z_{i-1} - z_i) - (r_{i-1} - r_i)(z_{i+1} - z_i)}\right] \tag{38}$$

Equations (37) and (38) are singular when the two segments are parallel. Therefore, Eqs. (35) and (36) are used only when the cosine of the angle between the segments differs from 1 by more than 10^{-3}.

5. RESULTS FOR INITIALLY-CONCAVE N-WAVES

5.1 Polynomial Front

Two different initially-refracted configurations are investigated, using GODUNOV. The first configuration to be discussed is called the "polynomial front" N-wave. Both the fore and aft shocks of the polynomial-front N-wave at $t = 0$ are represented by the formula

$$z - z_o = 100\left[\left(\frac{r}{100}\right)^2 - \frac{1}{2}\left(\frac{r}{100}\right)^4\right] \qquad 0 \leq r \leq 100 \qquad (39)$$

where z and r are in meters, and z_o locates the fore shock and the aft shock.

Consider the 4 pairs of approximately equally-spaced curves shown in Figure 5-1. For each pair, the curve on the right represents the fore shock profile at a given time, while the curve on the left represents the aft shock profile at the same time. The first pair of curves (labeled t = 0) corresponds to a polynomial-front N-wave with an initial wavelength of 10 meters and a radius of curvature at the axis of 50 meters. The initial relative overpressure is chosen to be $(\Delta p/p)_o = 10^{-3}$, where Δp is the pressure jump across the fore shock and p_o is the ambient pressure.

The shock profiles at the four indicated times in Figure 5-1 illustrate how the N-wave changes shape as it propagates to the right into a uniform atmosphere. Note that the point of inflection on either front migrates toward the axis as the N-wave approaches the focus, defined here to be the position of maximum pressure, which is located at z = 79 meters (corresponding to t = .172 sec, not shown in Figure 5-1). According to geometric acoustics, the focus is located at the center of curvature of the fore shock, at z = 70 meters in this case. We will designate the geometric-acoustic focal point as

the "nominal focus," to distinguish it from the "actual focus" deduced from the calculation. At the actual focus, the shock develops a cusp at the axis of symmetry. The profile at the focus resembles the geometric-acoustic wave-folding picture in Figure 1-3.

The incipient break-up of the last shock profiles at the axis in Figure 5-1 is a numerical artifact involving use of a vertical shock segment at the axis. A suitable modification which avoids this break-up has been discussed in Section 3.5.

The polynomial front N-wave shown in Figure 5-1 and defined above was run several times with different grid sizes. Although the shock profiles exhibit the general shapes shown in Figure 5-1 for all of the grids, the focus factors, $\Delta p_{max}/\Delta p_o$, depend on the number of grid points used. Table 5-1 displays the focus factors corresponding to each of the grids. The authors believe that the grid consisting of 100 equally spaced radial points and 20 axial points yields a reasonably accurate value for the focus factor, namely 18.7, in the sense that increasing further the number of grid points will not change this value significantly.

Moreover, the use of inclined cell segments on the axis is believed to yield more accurate results (see Section 3.5). Throughout the rest of this chapter, the results refer to inclined cell segments. Focus factors obtained with inclined cell segments are approximately 10 percent higher than those obtained with vertical cell segments. Thus, a better estimate of the focus factor for the polynomial front is about 20. It is interesting to note that the focus factor is 11.5 at the position of the "nominal" focus (geometric acoustics).

Figure 5-2 illustrates the pressure profiles (as computed with the 100 x 20 grid) along the axis at three different times. The last curve in Figure 5-2 corresponds to the pressure signature at the focus. The formation of spikes near the fore and aft shocks of

the N-wave is evident. Detailed structure behind the aft shock is not shown because the zoning was coarse behind the N-wave.

The pressure profiles at three different radial positions are illustrated in Figure 5-3. The lowest curve in Figure 5-3, which is the profile on the axis, is the same as the last curve in Figure 5-2, drawn to a different scale. The rapid drop of pressure with distance from the axis is apparent in Figure 5-3.

Figure 5-4 is a plot of the relative overpressure behind the fore shock of the N-wave versus axial position of the shock. The solid curve represents the results of the 100 x 20 grid GODUNOV calculation, while the dashed curve represents the equivalent (100-point) WHITHAM calculation. The maximum relative overpressure computed with WHITHAM (.0285) is 52% higher than the maximum relative overpressure computed with GODUNOV (.0187).

This is apparently due to the fact that there is no rarefaction wave in WHITHAM to relieve the pressure buildup. The calculations in WHITHAM are terminated when the shock segments overlap, or cross each other. (This occurs somewhat earlier than the GODUNOV focus.) It can be seen from Figure 5-4 that, along the axis, relative overpressures greater than .002 (twice nominal) occur in a spatial interval 40 meters long; and relative overpressures greater than .01 (about half the maximum) occur in a spatial interval 10 meters long. In the radial direction, the corresponding interval lengths are 20 and 10 meters, respectively.

In order to assess the relative intensities of point foci and line foci for the same initial conditions, the problem defined above was recomputed with WHITHAM in a two-dimensional x,y geometry (line focus). A maximum relative overpressure of .0117 was computed, as compared to the value of .0285 for the point focus.

The effect of varying the initial strength of the polynomial shock front was also investigated with WHITHAM. Calculations with initial relative overpressures, $\Delta p_o/p_o$, of 0.01 and 0.10, in r,z geometry, resulted in maximum relative overpressures of 0.154 and 0.63, respectively. These results indicate that the intensification due to focusing of stronger shocks is not as severe as for weaker shocks. Furthermore, the geometric-acoustics wave-folding description of focusing is not valid for shocks with relative overpressures of the order of 1 or higher. This is discussed below in connection with some GODUNOV calculations for "Gaussian front" N-waves.

5.2 Gaussian Front

We define a "Gaussian front" shock wave as one with a profile satisfying the equation

$$z = z_o + 10 - 10 \exp\left\{-20\left(\frac{r}{100}\right)^2\right\} \qquad (40)$$

where r and z are both in meters. The profile labeled "t = 0" in Figure 5-5 is an example of a Gaussian front. (Only the fore shock profiles are shown.) The other curves in Figure 5-5 represent the fore shock profile of the N-wave at later times. Initially, the N-wave has a nominal relative overpressure $\Delta p_o/p_o = 10^{-3}$ and a wavelength of 10 meters. The formation of a cusp at the axis as the focus is approached in Figure 5-5, and the gradual decay of the cusped portion of the shock beyond the focus, confirms the geometric-acoustics description of the primary shock shown in Figure 1-3.

The geometric-acoustics wave-folding picture in Figure 1-3 indicates that the primary shock should be reflected from the axis of symmetry. Further, the reflected shock ends at the caustic sheet, and

a third (logarithmic) discontinuity joins the "ends" of the reflected shock. The question arises whether this structure may be inferred from our calculations. The computed two-dimensional pressure distribution immediately behind the fore shock just after it has passed the focus has been plotted in Figure 5-6. A portion of the mesh used in the computation is shown in Figure 5-6, and the numbers within the cells represent the pressure at that location. If the presence of a reflected shock and a "logarithmic discontinuity" are to be inferred from the computations, there should be a jump in pressure as one scans from right to left along a horizontal row in the mesh. This type of pressure jump does not appear in Figure 5-6. It is perhaps not surprising that the GODUNOV calculations do not reveal the presence of secondary discontinuities, because the strong rarefaction behind the fore shock probably swamps such discontinuities. As opposed to this, the wave-folding picture shown is for a single shock without a strong rarefaction behind it.

A tabulation of focus factors calculated with different numbers of mesh points for the Gaussian-front N-wave discussed above is shown in Table 5-2. The relatively small change in focus factors between the last two grids in Table 5-2 indicates that approximate convergence has been obtained. The results discussed in this section refer to the 50 x 50 grid, which required 34 minutes of CDC 6600 computer time.

Pressure signatures along the axis of symmetry at three different times are plotted in Figure 5-7. Here again, the development of steep spikes adjacent to the fore and aft shocks of the N-wave is apparent. The pressure signature at the time corresponding to focusing in Figure 5-7 indicates a focus factor of 13.0 (relative overpressure = .013) for the Gaussian front N-wave.

Note that the location of the actual focus (z = 64 meters) is close to the center of curvature (the nominal focus) of the initial N-wave (z = 70 meters).

For the Gaussian-front N-wave, relative overpressures larger than .002 (twice nominal) occur in an axial interval 35 meters long, and relative overpressures greater than .0065 (about half the maximum) occur in an axial interval 20 meters long. In the radial direction, the corresponding interval lengths are 6 meters and 1.5 meters, respectively.

5.3 Strong Shocks

The same Gaussian front N-wave described above was rerun on GODUNOV with a much higher initial overpressure in order to investigate the focusing of relatively strong shocks. The shock profiles for an N-wave with $\Delta p_o/p_o = 0.90$ are shown in Figure 5-8. Notice the lack of a cusp in the shock profile at the focus in this case. In fact, the entire picture looks more like Whitham's picture of a concave shock "overshooting" than the geometric-acoustics wave-folding picture (compare figures 1 and 4 in ref. 9). The focus factor is 1.5.

GODUNOV has been used to investigate the propagation of other relatively strong concave and convex shocks. The convex shock that was studied is identical to one of the shocks that Collins and Chen (ref. 14) used in their study of shock wave diffraction.

As indicated in Figure 5-9, the initial shock profile is composed of three straight sections labeled A, B, C. Segments A and C have Mach numbers of 2.23 ($\Delta p_o/p_o = 4.63$), while the inclined segment, B, has a Mach number of 1.576 ($\Delta p_o/p_o = 1.73$). The decay of the convex portion of the shock at later times as illustrated in Figure 5-9 is in close agreement to Collins' and Chen's results.

A similar shock, with a concavity instead of a convexity, is shown in Figure 5-10. Although the shock does straighten out, the return to a planar configuration is not as smooth as it is for the convex shock. The spike in the last shock profile is a numerical artifact due to the symmetry constraint employed in that particular

run. (The modifications referred to in Section 3-5 of Chapter 3 would eliminate this artifact.)

Comparisons of Figure 5-8 and 5-10 with Figures 5-1 and 5-5 reveal that the focusing of concave shocks is much different for weak shocks than it is for strong shocks. Weak shocks with relative overpressures much smaller than unity focus according to the geometric-acoustic wave-folding mechanism, whereas strong shocks with relative overpressures of the order of unity or higher tend to straighten out as Whitham (ref. 9) predicted.

6. RESULTS FOR COLD-SPOT REFRACTION OF INITIALLY-PLANAR N-WAVES

In early runs, spherical cold-spots with uniform temperatures below ambient were investigated. The incident shocks were assumed to be initially planar, which is a good approximation if the radius of the cold-spot is much smaller than the radius of the Mach cone associated with the bow shock of a supersonic aircraft. The discontinuity in temperature at the cold-spot interface caused a reflected shock. The disturbance in the N-wave (as calculated by GODUNOV) that was caused by the reflected shock produced complicated solutions without providing further insight into the focusing mechanism. Consequently, in later runs a continuous transition in temperature was imposed at the cold-spot boundary, so that reflected shocks, if any, were weak and did not appear. The temperature variation within the cold-spot was taken to be

$$\frac{T}{T_o} = \left\{ 1 + \frac{\Delta\rho}{\rho_o} \exp\left[-3\left((z - z_{spot})^2 + r^2 \right) / r_{spot}^2 \right] - \frac{\Delta\rho}{\rho} \exp(-3) \right\}^{-1} \qquad (41)$$

where z_{spot} is the location of the center of the cold-spot, r_{spot} is the cold-spot radius, and $\Delta\rho/\rho_o$ is the relative density change between the center of the cold-spot and ambient conditions. The pressure in the cold-spot is taken to be the same as the ambient pressure.

The results of a run in which the temperature transition is continuous are shown in Figure 6-1. The solid curves represent the fore shock and the dashed curves the aft shock. This figure shows a numerical break-up occurring at late times, which is an artifact and was corrected in later runs (see Figure 6-2). The break-up occurs after the focus and has a negligible effect on the value of the focus factor. Therefore it may be ignored in the following remarks.

In the results illustrated in Figure 6-1, $\Delta\rho/\rho_0 = 1.0$, $z_{spot} = 120$ meters, and $r_{spot} = 50$ meters. The first pair of curves represent the impinging planar N-wave. The second pair of curves in Figure 6-1 illustrate the refraction that is caused by the cold-spot slowing down the inner portion of the N-wave. Note the resemblance between the cold-spot refracted shock fronts in Figure 6-1 and the Gaussian front of Figure 5-5. The initially-refracted concave shocks described in Chapter 5 started with uniform overpressures along the shock fronts. At the time the N-wave shown in Figure 6-1 emerges from the cold-spot, the overpressure variation along the fore shock is 55%, i.e., relatively small compared with 390% at the focus (see below).

The third pair of curves in Figure 6-1 have been drawn at a time when the fore shock has already propagated past the focus, which occurs at z = 231 meters. With a grid composed of 20 radial points and 7 axial points, a focus factor of 3.9 was computed for the problem shown in Figure 6-1. A finer mesh would result in a larger focus factor; if the results shown in Table 5-1 can be used as a guideline to extrapolate to a finer mesh, a focus factor of 11.3 can be estimated.

GODUNOV has also been employed to compute the two-dimensional (x,y geometry) cold-spot focusing that results from a situation equivalent to the one shown in Figure 6-1. In other words, the cold-spot is now cylindrical instead of spherical so that a line focus will result instead of a point focus. A focus factor of 1.5 was calculated using the same 20 x 7 mesh. Extrapolation to a finer mesh in this case would lead to a focus factor of 4.4.

Figure 6-2 shows the results of a computation with a mesh consisting of 50 radial points and 50 axial points. The cold-spot parameters are $\Delta\rho/\rho_0 = 1.0$, $z_{spot} = 250$ meters, and $r_{spot} = 150$ meters. Thus, the cold-spot in Figure 6-2 is larger than the one in Figure 6-1, although the central temperatures are the same. The three pairs of curves in Figure-6-2 represent the N-wave (a) impinging on the cold-

spot, (b) midway through the cold-spot, and (c) just after focusing (the focus is located at z = 430 meters). Note the absence of a break-up in the last pair of shocks in Figure 6-2. This is due to the improved symmetry condition employed in this calculation (see Section 3.5).

A plot of the relative overpressure behind the fore shock versus axial position of the fore shock is given in Figure 6-3. Significant increases in the overpressure are not observed until the fore shock is almost through the cold-spot. This is due to the small time lag between refraction and focusing. The focus factor in this calculation is 16.7, and the axial distance from the focus at which the overpressure is one-half the maximum value is about 30 meters (.6 wavelengths in this case).

All of the results quoted above are for cold-spots with center temperatures equal to one-half the ambient temperature. This is an example of an extreme temperature inhomogeneity that would not be encountered in the real atmosphere. Less extreme temperature inhomogeneities would produce lower focus factors. However, other inhomogeneities, such as wind shear fluctuations, may be more significant but were not considered in the calculations.

7. CONCLUSIONS

The results of this investigation demonstrate the capability of GODUNOV as a two-space-dimensional shock-following code for calculating sonic boom N-wave focusing.

The flow field at and near the focus has been computed by GODUNOV for two types of sample problems. The first type of problem involves the refraction and subsequent focusing of a planar N-wave by a cold-spot. Focus factors of 11.3 and 16.7 are obtained for the two spherical cold-spots (point foci) investigated. A cylindrical cold-spot (line focus) similar to the first spherical cold-spot yields a focus factor of 4.4.

The second type of focusing problem investigated in this study concerns the focusing of an N-wave with a concave front of prescribed shape. The curved front might be caused, for example, by atmospheric refraction or by aircraft maneuvers. Two different initial shock-front shapes are studied. In one case we obtain a focus factor of 13, and in the other case a factor of 20. In all cases, the focal region (as defined by the distance from the focus at which the N-wave overpressure falls to one-half the maximum overpressure) extends no more than 3 wavelengths from the focus. These results illustrate the dependence of the focus factor on the initial shape of the shock front.

The study has also provided valuable insight into the process of focusing. The wave-folding mechanism predicted by geometric acoustics (Figure 1-3) for a concave shock has been verified for weak shocks, although no evidence of secondary discontinuities, i.e. reflected shocks, has been observed. Wave-folding is the mechanism responsible for sonic boom focusing. On the other hand, strong concave shocks with relative overpressures, $\Delta p_o/p_o$, of the order of unity or higher tend to straighten out or overshoot rather than fold over. Thus, the hypothesis of Whitham (ref. 9) that a shock will straighten out without fold-over, and the fold-over hypothesis of geometric acoustics

(refs. 2, 16),are complementary to one another; both are valid but under different pressure conditions.

It may be noted that the GODUNOV code can be linked to a geometric-acoustics code (such as the codes described in references 1 and 15) in order to calculate sonic boom signatures from maneuvering aircraft. Predictions of the intensity and extent of "super-super-booms" (see Introduction) from prescribed aircraft maneuvers could provide the basis for defining acceptable flight operations for supersonic aircraft.

APPENDIX A

USER'S MANUAL FOR PROGRAM GODUNOV

GODUNOV is designed to compute the flow field that results from the focusing of an N-wave of arbitrary strength. The focusing is associated with a concavity in the wave front, which can be caused, for example, by a cold-spot in the path of the N-wave. One may also prescribe the initial concavity in the wave front. Thus, GODUNOV can be used to study focusing of (i) an initially straight-front N-wave upon passing through a cold-spot of prescribed size and intensity, or (ii) a curved-front N-wave of prescribed shape in a homogeneous atmosphere.

The input to GODUNOV determines the initial state of the fluid, the mesh spacing, and the frequency of printed output. A short output giving key data such as the shock positions and the positions and value of maximum pressure in the N-wave, is printed at every cycle. A long output describing the full two-dimensional state of the fluid is printed at the desired cycle frequency. In addition, tape dumps are made periodically to store information for a possible restart at a later date.

Input Data

The input data required to start a problem consists of a six-card package as described below. Any self consistent system of units can be employed. The cgs system is used for the problems described in this report, i.e. lengths are in cm, densities are in gm/cc, and pressures are in dynes/cm^2.

1st CARD

Columns 1 - 10	The problem number (CPROB) is required in a F10.3 format
Columns 11 - 20	The cycle (time step) number (CYCLE) is required in a F10.3 format. CYCLE = 0 to start a new problem. In restarting in order to continue a problem, CYCLE is the last cycle number of the previous run.
Columns 21 - 80	are left blank

The data in cards 2 - 6 are input in the Namelist format. The Namelist feature provides considerable flexibility by requiring only input that specifies the user's choice of options or is different from the preset data. However, it is only available on certain computers, e.g. CDC 6600. The procedure for inputting data via a Namelist format can be found in most FORTRAN IV manuals.

2nd CARD - $PRELIM

The following variables are contained in Namelist PRELIM:

IMAX	the number of grid points, or rows, in the r (radial or vertical) direction, indexed by i.
JFORE	the number of grid points, or columns, in the z (axial or horizontal) direction. JFORE is also the value of the j index corresponding to the fore shock.
JAFT	the number of grid points, or columns, in the z direction behind and including the aft shock. JAFT is also the value of the j index corresponding to the aft shock.
TMAX	time in seconds at which computations are to be terminated.
CYMAX	cycle number at which computations are to be terminated. (The program will stop computing whenever T > TMAX or CYCLE > CYMAX, whichever occurs first.)

CPRINT	cycle interval between long outputs
CDUMP	cycle interval between tape dumps
T	value of T (time) at start of run
GAMMA	ratio of specific heats

3rd CARD - $MESH1

Namelist MESH 1 contains the variables:

RMAX	value of r at outer boundary of grid
DZFORE	initial (uniform) spacing of grid contour lines within N-wave and parallel to shocks
DZAFT	initial spacing of grid contour lines behind N-wave, i.e. between the left boundary and the aft shock, and parallel to shocks
ZSPOT	value of z coordinate corresponding to center of cold-spot
DZSPOT	diameter of cross-section of cold-spot
A	ratio of spacing between successive radial grid lines
ZAXIS	array representing z coordinate of grid points on axis of symmetry (computed internally for standard problem corresponding to OPT = 0, 1, or 2 (see below))
OPT	integer indicating initial shock front shape

OPT = 0 planar front

OPT = 1 polynomial front

$$z = z_0 + RMAX\left[(r/RMAX)^2 - \frac{1}{2}(r/RMAX)^4\right]$$

OPT = 2 Gaussian front

$$z = z_0 + \frac{RMAX}{10}\left\{1 - \exp\left[-20\,(r/RMAX)^2\right]\right\}$$

where z_0 locates the fore and aft shocks and the contours in between

4th CARD - $MESH2

Namelist MESH2 contains the following variables:

R(i) vector consisting of the r-values of the fixed horizontal grid lines

Z(i,j) two-dimensional array consisting of the z-values of the mesh points. The first index (i) labels the horizontal line, and the second index (j) labels the node on the horizontal line between the shocks.

When one of the standard problems corresponding to OPT = 0, 1, 2 is to be run, MESH2 should be left blank, i.e.

$MESH2 $

5th CARD - $STATE1

STATE1 allows the initial fluid state to be described in compact form. The following variables are in STATE1.

PINIT(k) 6-component vector specifying fluid state ahead of N-wave (see 6th card)

PINIT(1) pressure

PINIT(2) density

(The other 4 components are not used. Energy and sound speed are computed in the program, assuming a static state.)

PSPOT(2) 1 + ratio of density at center of cold-spot to ambient density.

(The other 5 components are not used.)

The variation of density within the cold-spot obeys the equation

$$\rho = \rho_0 \left\{ 1 + \text{PSPOT}(2) \cdot \left[\exp - 3 \left| \left\{ (Z - \text{ZSPOT})^2 + R^2 \right\} / \text{RSPOT}^2 \right| \right] - \text{PSPOT}(2) \cdot \exp(-3) \right\}$$

where RSPOT is the radius of the cold spot, and ZSPOT is the axial position of the center of the cold spot.

S — the initial relative overpressure of the N wave, i.e. $S = \Delta p_o/p_o$ where Δp_o is the pressure jump across the fore shock, and p_o is the ambient pressure ahead of the N wave.

The program sets up a linear variation of all the state variables within the N-wave. The isentropic relations are used to relate the pressure to the other flow variables. The distribution of all the flow variables are approximately symmetric about ambient conditions (i.e., about the mid-point of the N-wave).

6th CARD - $STATE2

Namelist STATE2 allows the user to specify x,y or r,z geometry, as well as an arbitrary initial distribution of flow variables.

The following variables are in STATE2

IXY — IXY > 0 implies x,y geometry
IXY $\leq$ 0 implies r,z geometry

PINIT(k) — The ambient flow field ahead of the N-wave can be specified as a vector as follows:

PINIT(1) = ambient pressure

PINIT(2) = ambient density

PINIT(3) = z-component of ambient velocity

PINIT(4) = r-component of ambient velocity

PINIT(5) = ambient total energy per unit volume

PINIT(6) = ambient sound speed

P(i,j,k) three-dimensional array describing the initial flow field in the N-wave. The first index labels the horizontal row of the cell in the mesh, the second index (j) labels the cell on the horizontal line between the shocks, and the third index (k) labels the state variable as follows:

k = 1 - pressure
2 - density
3 - z-component of velocity
4 - r-component of velocity
5 - energy per unit volume
6 - sound speed

To run one of the standard problems, only IXY need be input in STATE2.

The input data package for restarting a problem consists of the two cards described below.

1st CARD

Columns 1 - 10	the problem number (CPROB) in a F10.3 format.
Columns 11 - 20	the cycle number at which the problem is to be restarted in a F10.3 format

2nd CARD

Columns 1 - 10	TMAX, the time at which calculations are to be terminated
Columns 11 - 20	CYMAX, cycle number at which calculations are to be terminated
Columns 21 - 30	CPRINT, cycle frequency for long outputs
Columns 31 - 40	CDUMP, cycle frequency for tape dumps

A subroutine-by-subroutine flow chart of GODUNOV is shown in Figure A-1. The purposes of the various subroutines are as follows.

INPUT reads all required input data regarding mesh geometry, initial values of the flow variables at all points in space, and physical parameters such as the ratio of specific heats.

NODES deals with changes of the mesh geometry as a function of time, and computes (at different points in the logical circuit):

(a) the lengths of shock segments (connecting adjacent shock nodes)
(b) the velocities of the shock segments normal to themselves, and the corresponding axial velocities of the shock nodes
(c) the velocities of the moving (non-shock) boundaries of the interior cells
(d) the new positions of all mesh nodes. (The various portions (a, b, c, or d) of NODES are called at different points in the flow sequence, as indicated in Figure A-1.)

SHOCK solves the Riemann problem according to the scheme suggested by Godunov et al. (ref. 10) at all shock segments (both fore and aft shocks), yielding the segment velocities normal to themselves, and the values of the flow-variables on both sides of each shock segment. These quantities are employed in evaluating the fluxes (of mass, momentum, and energy) on those special cell boundaries which coincide with shock segments (for cells adjacent to the shocks). SHIO ("shock-input-output") sets up the input to SHOCK, and processes its output for use by the main program.

RIEMANN solves the Riemann problem at all boundaries of each interior cell (not adjacent to shocks), taking into account the motion of the moving cell boundaries, yielding the values of the flow variables (continuous) on the cell boundaries. RIO ("Riemann-input-output") sets up the input to RIEMANN for each cell boundary, and processes its output. Accuracy can be maintained while employing a linearized version of the Riemann problem for the continuous portions of the flow, with a resulting economy in computation time.

FLUXES computes the fluxes of mass, momentum, and energy at the cell boundaries in preparation to updating the values of the flow variables at the cell centers. (FLUXES is called by NEWFLO.)

NEWFLO computes for a given cell:

(a) the cell boundary surface areas (of revolution in r,z geometry)

(b) the old cell volume (of revolution in r,z geometry) prior to updating the mesh node positions, and the new cell volume after updating the mesh node positions.

NEWFLO then updates the values of the flow variables at the cell center. This latter updating is done by means of the conservation of mass, momentum, and energy over the volume of the cell. First, the currents of mass, momentum, and energy at the cell boundary surfaces are obtained by multiplying the fluxes (obtained from FLUXES) by the cell boundary surface areas. Summing these currents and multiplying by the time increment gives the change in a quantity Q (not indicated in the figure), where Q represents the total mass, momentum, or energy contained in the cell. Q is approximated by multiplying the volume of the cell by the mass density, momentum density, or energy density within the cell (assumed constant across the cell). The new value of Q is proportional to the new cell volume. Hence, the new value of mass density, momentum density, or energy density within the cell is obtained by dividing the new value of Q by the new cell volume. The new values of the flow variables within the cell are subsequently readily calculated.

EOS ("equation of state") computes the pressure and sound speed when the mass density, energy density, and fluid velocity components are given. We are presently using an ideal gamma-law-gas equation.

DT determines the time interval to be used in updating the mesh and the flow variables. The time interval is chosen to satisfy the Courant stability criterion, which requires that the time interval be less than the time required for a sound signal (speed of

sound combined with fluid velocity) to travel across any cell, in either the radial or axial directions. The motion of the moving boundaries must also be taken into account here.

OUTPUT prints out appropriate information at desired intervals of time.

This completes the description of the subroutines used in GODUNOV.

A listing of GODUNOV follows.

```
RUN VERSION 2.3 --PSR LEVEL 298--

                PROGRAM GODUNOV(INPUT,OUTPUT,TAPE3,TAPE5=INPUT,TAPE6=OUTPUT,TAPE7)
000003          COMMON P(50,20,6), R(55), Z(55,20), ZSTART(50), ZEND(50), PINIT(6)
               1, PSPOT(6),ZOLD(50),PFORE(50,6),PAFT(50,6),FORSEG(50),FORVEL(50),
               2AFTSEG(50),AFTVEL(50), PN(20,6), PE(6), AN(20),UFORE(50),UAFT(50),
               3 VNE(20),IXY
               4,ZAXIS(20)
000003          COMMON RN, RS, ZNE, ZNW, ZSE, ZSW, ESEG, WSEG, GAMMA, T, TMAX, DT,
               1 CYMAX, CPRINT, DTMIN, IDT, JDT, PROB, CYCLE, CDUMP, LREAD, MWRITE
               2, LTAPE, DELR, ISPOT, VOLOLD, VOLNEW, AS, AW, AE, VNORME, VNORMW,
               3 UNORME, UNORMW, UTANGE, UTANGW, VFORE, VAFT, VNW, VSE,VSW, IMAX,
               4 JFORE, JAFT, I, J, PMAX,     HMACHF, HMACHA, IPMAX, JPMAX
000003          COMMON RSPOT, ZSPOT
000003          LREAD = 5
000004          MWRITE=6
000005          LTAPE=3
000006          REWIND LTAPE
000010          CALL SETPLTS
000011          CALL INPUT
000012          IF (CYCLE .GT. 0.) GO TO 5
          C                   START NEW CYCLE
000015    1     IF (CYCLE .GT. 0.) PMAX=0.
000020          PMIN = 1.E10
000022          DO 3 I=1,IMAX
000023          CALL NODES
000024          CALL SHIO
000025          CALL NODES2
000026          DO 2 J=1,JFORE
000030          CALL NODES3
000031          CALL RIO
000032          CALL DTCALC
000033          IF (CYCLE .EQ. 0.)  GO TO 2
000034          CALL NEWFLO
000035          CALL NODES4
000036          CALL NUFLOW
000037          CALL EOS(GAMMA,P(I,J,1),P(I,J,2),P(I,J,3),P(I,J,4),P(I,J,5),P(I,J,
               16))
000055          IF (P(I,J,1) .LT. PMAX)  GO TO 4
000063          PMAX = P(I,J,1)
000066          IPMAX = I
000066          JPMAX = J
000067        4 IF (P(I,J,1) .GT. PMIN)  GO TO 2
000076           PMIN = P(I,J,1)
000100          IPMIN = I
000101          JPMIN = J
000102        2 CONTINUE
000105        3 CONTINUE
000107          IF (PMIN .LE. 0.) CYMAX=CYCLE
000113          IF (CYCLE .EQ. 0.) DTMINO=0.
000115          IF (DTMIN .LT. DTMINO) DT=DTMIN**2/DTMINO
000121          IF (DTMIN .GE. DTMINO) DT=DTMIN
000124          DTMINO=DTMIN
000125    5     CALL OUTPUT
000126          IF (AMOD(CYCLE,CPRINT) .EQ. 0. .OR. T .GE. TMAX .OR. CYCLE  .GE.
               1 CYMAX)  CALL OUTLNG
```

```
000146          IF(T.GE.TMAX.OR.CYCLE.GE.CYMAX) GO TO 9
000160          T=T+DT
000162          CYCLE = CYCLE + 1.
000164          GO TO 1
000164        9 CALL ENDPLTS
000165          CALL EXIT
000166          END
```

```
RUN VERSION 2.3 --PSR LEVEL 298--

              SUBROUTINE INPUT
000002        COMMON P(50,20,6), R(55), Z(55,20), ZSTART(50), ZEND(50), PINIT(6)
             1, PSPOT(6),ZOLD(50),PFORE(50,6),PAFT(50,6),FORSEG(50),FORVEL(50),
             2AFTSEG(50),AFTVEL(50), PN(20,6), PE(6), AN(20),UFORE(50),UAFT(50),
             3 VNE(20),IXY
             4,ZAXIS(20)
000002        COMMON RN, RS, ZNE, ZNW, ZSE, ZSW, ESEG, WSEG, GAMMA, T, TMAX, DT,
             1 CYMAX, CPRINT, DTMIN, IDT, JDT, PROB, CYCLE, COUMP, LREAD, MWRITE
             2, LTAPE, DELR, ISPOT, VOLOLO, VOLNEW, AS, AW, AE, VNORME, VNORMW,
             3 UNORME, UNORMW, UTANGE, UTANGW, VFORE, VAFT, VNW, VSE,VSW, IMAX,
             4 JFORE, JAFT, I, J, PMAX,    HMACHE, HMACHA, IPMAX, JPMAX
000002        COMMON PSPOT, ZSPOT
000002        DIMENSION TITLE(8),XTITLE(8),YTITLE(8)
000002        DIMENSION ZCIRCL(55), RCIRCL(55)
000002        INTEGER OPT
000002        NAMELIST/PRELIM/ IMAX,JFORE,JAFT,GAMMA,T,TMAX,CYMAX,CPRINT,COUMP
000002        NAMELIST/MESH1/ RMAX,DZFORE,DZAFT,ZSPOT,DZSPOT,ISPOT,A,ZAXIS,OPT
000002        NAMELIST/MESH2/ R,Z,ZSTART,ZEND,ISPOT
000002        NAMELIST/STATE1/ PINIT, PSPOT, S
000002        NAMELIST/STATE2/ PINIT, PSPOT, P, PMAX,IXY
      C       READ IN PROBLEM AND CYCLE NUMBER
000002        READ (LREAD,100) CPROB, CCYCLE
      C                 IS IT A RESTART OR A NEW PROBLEM
000012        IF (CCYCLE .EQ. 0.) GO TO 2
      C         RESTART -READ INPUT FROM TAPE
000013      1 READ (LTAPE) PROB, CYCLE
000022        WRITE (MWRITE,104) CYCLE
000030  104   FORMAT (8H CYCLE =,F7.1)
000030        IF (EOF,LTAPE) 14,13
000033  13    IF (ABS(PROB-CPROB) .GT. .01)  GO TO 10
000041        READ (LTAPE) IMAX, JFORE, JAFT, GAMMA, T, TMAX, CYMAX, CPRINT,
             1 ISPOT, COUMP, PMAX, DT
000074        READ (LTAPE) (R(I),ZSTART(I),ZEND(I), I=1,IMAX)
000112        READ (LTAPE) ((Z(I,J),J=1,JFORE),I=1,IMAX)
000131        READ (LTAPE) (((P(I,J,K),K=1,6),J=1,JFORE),I=1,IMAX)
000155        READ(LTAPE) (PINIT(K), PSPOT(K),K=1,6)
000170        READ (LTAPE)
000173        IF (CYCLE .LT. CCYCLE) GO TO 1
000176     14 READ (LREAD,101) TMAX, CYMAX, CPRINT, COUMP
000212        GO TO 3
      C         NEW PROB -READ INPUT FROM CARDS
000213      2 PROB = CPROB
000215        CYCLE = 0.
000216        GAMMA = 1.4
000217        T = 0.
000220        READ (LREAD,PRELIM)
000222        READ (LREAD,MESH1)
      C       SET UP CLUSTERED GRID
000225        IF ((A-1.) .LT. .01) R(1)=RMAX/FLOAT(IMAX)
000233        IF ((A-1.) .LT. .01) GO TO 65
000237        R(1)=(A-1.)/((A**IMAX)-1.)*RMAX
000245  65    DO 66 I=2,IMAX
000247        R(I)=R(I-1) + A*(R(I-1)-R(I-2))
000254        IF (I.EQ.2) R(I)=R(1)*(1.+A)
```

```
000261       66 CONTINUE
000264          READ (LREAD,MESH2)
000266        4 DO 6 I=1,IMAX
000270          DO 5 J=1,JFORE
000271          IF (J .LE. JAFT) Z(I,J) = FLOAT(J)*DZAFT
000300          IF (J .GT. JAFT) Z(I,J) =FLOAT(JAFT)*DZAFT  +FLOAT(J-JAFT)*DZFORE
000312          IF (OPT.EQ.1) Z(I,J)=Z(I,J)+RMAX*((R(I)/RMAX)**2-(R(I)/RMAX)**4/2.
               1 )
000326          IF (OPT.EQ.2) Z(I,J)=Z(I,J)+0.1*RMAX*(1.-EXP(-20.*(R(I)/RMAX)**2))
000346          IF (I .EQ. 1) ZAXIS(J) = Z(I,J)
000354          IF (I .EQ. 1) ZOLD (J)=Z(I,J)
000361        5 CONTINUE
000364        6 CONTINUE
000366          RSPOT = DZSPOT/2.
000370          DO 17 J=1,JFORE
000370   17     ZOLD(J)=Z(1,J)
000401          PINIT(3) = 0.
000402          PINIT(4) = 0.
000403          PSPOT(3) = 0.
000404          PSPOT(4) = 0.
000405          READ (LREAD,STATE1)
000407          GM1 = GAMMA - 1.
000411          PINIT(5) = PINIT(1)/GM1
000413          PSPOT(5) = PSPOT(1)/GM1
000414          PINIT(6) = SQRT(GAMMA*PINIT(1)/PINIT(2))
000420          IF (PSPOT(2) .LE. 0.) GO TO 15
000421          PSPOT(6) = SQRT(GAMMA*PSPOT(1)/PSPOT(2))
000426   15      IF (S) 7,8,7
000427        7 DO 9 I=1,IMAX
000431          DO 9 J=1,JFORE
000432          IF (J .LE. JAFT ) GO TO 11
000434          X = (2.*Z(I,J)-(Z(I,JFORE)+Z(I,JAFT)))/(Z(I,JFORE)-Z(I,JAFT))
000452          P(I,J,1) = PINIT(1)*(1.+S*X)
000461          IF (P(I,J,1) .LE. PMAX) GO TO 16
000465          PMAX=P(I,J,1)
000470          IPMAX=I
000470          JPMAX=J
000471   16     CONTINUE
000471          P(I,J,2) = PINIT(2)*(1.+S*X/GAMMA)
000501          P(I,J,3) = PINIT(6)*S*X/GAMMA
000507          P(I,J,4) = 0.
000513          IF (I.EQ.1) GO TO 18
000514          ESEG=SQRT((R(I)-R(I-1))**2+(Z(I,J)-Z(I-1,J))**2)
000527          SINE=(R(I)-R(I-1))/ESEG
000532          COSINE=(Z(I,J)-Z(I-1,J))/ESEG
000536          GO TO 19
000536   18     ESEG = SQRT(R(1)**2 + (Z(1,J)-ZAXIS(J))**2)
000546          SINE = R(1)/ESEG
000547          COSINE = (Z(1,J)-ZAXIS(J))/ESEG
000554   19     P(I,J,3) = PINIT(6)*S*X/GAMMA*SINE
000564          P(I,J,4) =-PINIT(6)*S*X/GAMMA*COSINE
000574          P(I,J,5)=P(I,J,1)/GM1+P(I,J,2)*P(I,J,3)**2/2.
000606          P(I,J,6) = SQRT(GAMMA*P(I,J,1)/P(I,J,2))
000617          GO TO 9
000620       11 DO 12 K=1,6
```

```
RUN VERSION 2.3 --PSR LEVEL 298--                                INPUT

000622       12 P(I,J,K) = PINIT(K)
000634        9 CONTINUE
000641        8 READ (LREAD,STATE2)
000644          IF (P(1,1,2) .GT. 1.E-10) GO TO 3
        C                THE FOLLOWING DATA REFER TO THE COLLINS AND CHEN BUMP
000650          DO 99 I=1,IMAX
000651          IF (R(I).LT.1.5663) Z(I,JFORE)= 8.437
000657          IF (R(I) .GT. 1.5663 .AND. R(I).LT.3.127) Z(I,JFORE)=.85*R(I)+7.2
000675          IF (R(I).GT.3.127) Z(I,JFORE)=10.
000704          Z(I,JAFT)=Z(I,JFORE)-DZAFT
000713          DO 20 J=1,JFORE
000715          IF (J .GT. JAFT .AND. J .LT. JFORE) Z(I,J)=Z(I,JAFT)+DZFORE
               1 *FLOAT(J-JAFT)
000736          IF (R(I) .GT. 1.567 .AND. R(I) .LT. 3.127) GO TO 97
000747          P(I,J,1) = 1.126E04
000753          P(I,J,2) = .6681E-02
000757          P(I,J,3) =1667.
000762          P(I,J,4) = 0.
000765          GO TO 98
000765    97    CONTINUE
000765          P(I,J,1) = 5462.
000772          P(I,J,2) = .4448E-02
000775          P(I,J,4) =-622.
001000          P(I,J,3) = 622.
001004    98    P(I,J,5)=P(I,J,1)/GM1+P(I,J,2)*(P(I,J,3)**2+ P(I,J,4)**2)/2.
001022          P(I,J,6)=SQRT(GAMMA*P(I,J,1)/P(I,J,2))
001032    20    CONTINUE
001035    99    CONTINUE
        C                    WRITE OUT INITIAL STATE
001037        3 WRITE(MWRITE,102) PROB, CYCLE
001047          WRITE (MWRITE, PRELIM)
001052          WRITE (MWRITE,MESH1)
001055          WRITE (MWRITE,STATE1)
001060          WRITE (MWRITE, MESH2)
001063          READ(LREAD,106) TITLE
001071          READ(LREAD,106) XTITLE
001077          READ(LREAD,106)  YTITLE
001105      106 FORMAT(8A10)
001105          Z(IMAX+2,1)=0.0
001107          R(IMAX+2)=0.0
001110          Z(IMAX+3,1)=2.0*R(IMAX)
001112          R(IMAX+3)=0.0
001113          Z(IMAX+4,1)=0.0
001114          R(IMAX+4)=0.0
001115          Z(IMAX+5,1)=0.0
001116          R(IMAX+5)=R(IMAX)
001117          CALL XYPLOT(Z(IMAX+2,1),R(IMAX+2),4,1,0,0,0,10.0,6.0,XTITLE,5,
               1 YTITLE,4,TITLE,80)
001136          RETURN
        C                    WRONG PROBLEM
001137       10 WRITE(MWRITE,103) PROB,CPROB
001147      100 FORMAT(2F10.2)
001147      101 FORMAT (4F10.3)
001147      102 FORMAT(1H1,20X,15HPROGRAM GODUNOV//9X,12H PROBLEM NO.,F6.1,5X,
              1 9HCYCLE NO.,F8.1)
```

```
RUN VERSION 2.3 --PSR LEVEL 298--                                INPUT

001147      103 FORMAT (14H WRONG PROBLEM/16H CARD PROB NO. =,F8.3,17H TAPE PROB
               1NO. =,F8.3)
001147           END
```

```
RUN VERSION 2.3 --PSR LEVEL 298--

              SUBROUTINE NODES
000002        COMMON P(50,20,6), R(55), Z(55,20), ZSTART(50), ZEND(50), PINIT(6)
             1, PSPOT(6),ZOLD(50),PFORE(50,6),PAFT(50,6),FORSEG(50),FORVEL(50),
             2AFTSEG(50),AFTVEL(50), PN(20,6), PE(6), AN(20),UFORE(50),UAFT(50),
             3 VNE(20),IXY
             4,ZAXIS(20)
000002        COMMON RN, RS, ZNE, ZNW, ZSE, ZSW, ESEG, WSEG, GAMMA, T, TMAX, DT,
             1 CYMAX, CPRINT, DTMIN, IDT, JDT, PROB, CYCLE, CDUMP, LREAD, MWRITE
             2, LTAPE, DELR, ISPOT, VOLOLD, VOLNEW, AS, AW, AE, VNORME, VNORMW,
             3 UNORME, UNORMW, UTANGE, UTANGW, VFORE, VAFT, VNW, VSE,VSW, IMAX,
             4 JFORE, JAFT, I, J, PMAX,     HMACHF, HMACHA, IPMAX, JPMAX
000002        COMMON RSPOT, ZSPOT
000002        IF (I .GT. 1)  GO TO 2
000006        FORSEG(1) = SQRT(R(1)**2 + (Z(1,JFORE)-ZAXIS(JFORE))**2)
000016        AFTSEG(1) = SQRT(R(1)**2 + (Z(1,JAFT)-ZAXIS(JAFT))**2)
000026        FORSEG(2) = SQRT((R(2)-R(1))**2 + (Z(2,JFORE) - Z(1,JFORE))**2)
000040        AFTSEG(2) = SQRT((R(2)-R(1))**2 + (Z(2,JAFT) - Z(1,JAFT))**2)
000052        RETURN
000052    2   IF (I .EQ. IMAX) RETURN
000055        FORSEG(I+1)=SQRT((R(I+1)-R(I))**2 + (Z(I+1,JFORE)-Z(I,JFORE))**2)
000072        AFTSEG(I+1)=SQRT((R(I+1)-R(I))**2 + (Z(I+1,JAFT)-Z(I,JAFT))**2)
000106        RETURN
000107        ENTRY NODES2
000114        I1 = I+1
          C                   COMPUTE CELL  NODE VELOCITIES
000116      3 IF (I .EQ. IMAX) GO TO 4
000120        VNFORE=FORSEG(I)*FORSEG(I1)/(FORSEG(I)+FORSEG(I1))*(FORVEL(I)/(R(I
             1)-R(I-1)) +FORVEL(I1)/(R(I+1)-R(I)))
000135        VNAFT=AFTSEG(I)*AFTSEG(I1)/(AFTSEG(I)+AFTSEG(I1))*(AFTVEL(I)/(R(I)
             1-R(I-1)) +AFTVEL(I1)/(R(I+1)-R(I)))
000152        RETURN
000153      4 VNFORE = FORSEG(I)*FORVEL(I)/(R(IMAX)-R(IMAX-1))
000160        VNAFT  = AFTSEG(I)*AFTVEL(I)/(R(IMAX)-R(IMAX-1))
000164        RETURN
000165        ENTRY NODES3
000172        IF (J .EQ. 1) GO TO 6
000174        VNW = VNE(J-1)
000176        VSW=VSE
000177        VSE = VNE(J)
000200        GO TO  7
000201      6 VNW = 0.
000202        VSW = 0.
000203        IF (I .GT. 1) VSE=VNE(1)
000207      7 IF (J .LE. JAFT) VNE(J)=VNAFT*FLOAT(J)/FLOAT(JAFT)
000217        IF (J .GT. JAFT) VNE(J)=VNAFT + (VNFORE-VNAFT)*FLOAT(J-JAFT)/FLOAT
             1(JFORE-JAFT)
000233        IF ( I .EQ. 1 .AND. J .LE. JAFT) VSE=AFTVEL(1)*AFTSEG(1)/R(1)*
             1 FLOAT(J)/FLOAT(JAFT)
000250        IF ( I .EQ. 1 .AND. J .GT. JAFT)  VSE=AFTVEL(1)*AFTSEG(1)/R(1)
             1  + (FORVEL(1)*FORSEG(1) - AFTVEL(1)*AFTSEG( 1))/R(1) *FLOAT(J -
             2 JAFT)/FLOAT(JFORE-JAFT)
          C                   COMPUTE NORMAL VELOCITIES AT EAST AND WEST BOUNDARIES
000275        RN=R(I)
000277        ZNE=Z(I,J)
```

```
000303          ZSW=ZSE
000304          IF (I .GT. 1) ZSE = ZOLD(J)
000307          ZNW=ZOLD(J-1)
000311          IF (CYCLE .EQ. 0.)  ZSE=Z(I-1,J)
000316          IF (CYCLE .EQ. 0.) ZSW=Z(I-1,J-1)
000323          IF (CYCLE .EQ. 0.) ZNW=Z(I,J-1)
000330          IF (J .EQ. 1) ZNW=0.
000333          IF (J .EQ. 1) ZSW=0.
000335          IF (I .EQ. 1 .AND. J .GT. 1) ZSW=ZSE
000345          IF (I .EQ. 1) ZSE=ZAXIS(J)
000350          RS=R(I-1)
000352          IF (I .EQ. 1) RS=0.
000355        9 DELR = RN - RS
000357          ESEG =SQRT(DELR**2+(ZNE-ZSE)**2)
000365          WSEG = SQRT(DELR**2+(ZNW-ZSW)**2)
000373          VNORME = .5*DELR/ESEG*(VNE(J)+VSE)
000400          VNORMW = .5*DELR/WSEG*(VNW+VSW)
000404          RETURN
000405          ENTRY NODES4
          C                    COMPUTE NEW NODE POSITIONS, I.E. MOVE MESH
000412          ZOLD(J)= Z(I,J)
000416          Z(I,J) = Z(I,J) + DT*VNE(J)
000423          IF (I .GT. 1) RETURN
000426          ZAXIS(J) = ZAXIS(J) + DT*VSE
000432          RETURN
000433          END
```

```
RUN VERSION 2.3 --PSR LEVEL 298--

            SUBROUTINE SHOCK
      C                   SHOCK SOLVES THE FULL RIMANN PROBLEM AT THE FORE AND
      C                   AFT SHOCKS TO DETERMINE THE SHOCK VELOCITY AND FLUID
      C                   PROPERTIES BEHIND THE SHOCK
000002      COMMON/SHOCK/P1,RHO1,U1,V1,P4,RHO4,U4,V4,    G,VSHOCK,P3,RHO3,U3,M
000002      GAMMA=G
      C           IS THERE REALLY A SHOCK WAVE
000003      IF (ABS(1.-P1/P4) .LT. 1.E-10)  GO TO 4
      C                   START BY GUESSING PRESSURE ACROSS CONTACT SURFACE
000011      PCS =(P1+P4)/2.
      C                   COMPUTE FLUX DENSITY OF W4 (SHOCK WAVE)
000013      ITER =0
000014      GM1 = GAMMA-1.
000016      GP1 = GAMMA+1.
000020    1 EM4 =SQRT(RHO4/2.*(GP1*PCS+GM1*P4))
      C                   COMPUTE FLUX DENSITY OF W1 (RAREFACTION WAVE)
000027      EM1 = GM1/2./GAMMA*SQRT(GAMMA*P1*RHO1)*(1.-PCS/P1)/(1.-(PCS/P1)**
           1(GM1/2./GAMMA))
000054      IF (P1.LT.P4) EM4=SQRT(RHO1/2.*(GP1*PCS+GM1*P1))
000066      IF (P1.LT.P4) EM1=GM1/2./GAMMA*SQRT(GAMMA*P4*RHO4)*(1.-PCS/P4)/
           1 (1.-(PCS/P4)**(GM1/2./GAMMA))
      C                   CHECK GUESS FOR PCS
000114      PCSP =(EM1*P4+EM4*P1+EM1*EM4*(U1-U4))/(EM1+EM4)
000125      IF (ABS(1.-PCS/PCSP) .LE. 1.E-03) GO TO 2
000133      ITER = ITER + 1
000135      IF (ITER .GE. 50) GO TO 3
000137      PCS = (PCSP+PCS)/2.
      C                   HAVE NOT CONVERGED, GUESS AGAIN AND REPEAT CYCLE
000142      GO TO 1
      C                   CONVERGENCE, COMPUTE JUMP CONDITIONS AND SHOCK VELOCI
000142    2 P3 = PCSP
000143      RHO3 = RHO4* (GP1*P3+GM1*P4)/(GP1*P4+GM1*P3)
000153      U3 =(P1 -P4+EM4*U4+EM1*U1)/(EM1+EM4)
000163      VSHOCK = U4 + EM4/RHO4
000166      V3 = V4
000170      RETURN
000170    3 WRITE (M,100)        P1, P4, PCS, PCSP
000204  100 FORMAT (44H SHOCK HAS NOT CONVERGED AFTER 50 ITERATIONS/ 17H P1,P4
           1,PCS,PCSP =,4E15.4)
000204      CALL ENDPLTS
000205      CALL EXIT
000206  4   VSHOCK = U4+SQRT(G*P4/RHO4)
000214      RHO3=RHO4
000215      P3=P4
000217      U3=U4
000217      V3=V4
000221      RETURN
000222      END
```

```
RUN VERSION 2.3 --PSR LEVEL 298--


              SUBROUTINE OUTPUT
000002        COMMON P(50,20,6), R(55), Z(55,20), ZSTART(50), ZEND(50), PINIT(6)
             1, PSPOT(6),ZOLD(50),PFORE(50,6),PAFT(50,6),FORSEG(50),FORVEL(50),
             2AFTSEG(50),AFTVEL(50), PN(20,6), PE(6), AN(20),UFORE(50),UAFT(50),
             3 VNE(20),IXY
             4,ZAXIS(20)
000002        COMMON RN, RS, ZNE, ZNW, ZSE, ZSW, ESEG, WSEG, GAMMA, T, TMAX, DT,
             1 CYMAX, CPRINT, DTMIN, IDT, JDT, PROB, CYCLE, CDUMP, LREAD, MWRITE
             2, LTAPE, DELR, ISPOT, VOLOLD, VOLNEW, AS, AW, AE, VNORME, VNORMW,
             3 UNORME, UNORMW, UTANGE, UTANGW, VFORE, VAFT, VNW, VSE,VSW, IMAX,
             4 JFORE, JAFT, I, J, PMAX,    HMACHF, HMACHA, IPMAX, JPMAX
000002        COMMON RSPOT, ZSPOT
000002        DIMENSION ZPRIME(55,2),RPRIME(55)
000002        MIMAX=-IMAX-1
000004        CPLOT = 2.*CPRINT
000006        IF (AMOD(CYCLE,CPLOT)) 25,16,25
000011   16   ZPRIME(1,1) = ZAXIS(JFORE)
000013        ZPRIME(1,2) = ZAXIS(JAFT)
000015        RPRIME(1)=0.0
000016        DO 14 I=1,IMAX
000017        ZPRIME(I+1,1    )=Z(I,JFORE)
000023        ZPRIME(I+1,2    )=Z(I,JAFT)
000026        RPRIME(I+1)=R(I)
000030     14 CONTINUE
000032        CALL XYPLOT(ZPRIME(1,1    ),RPRIME(1),MIMAX,1,0,1)
000036        IF (JAFT.EQ.1) GO TO 33
000040        CALL XYPLOT(ZPRIME(1,2    ),RPRIME(1),MIMAX,1,0,3)
000044   33   CONTINUE
000044        IPLOT=IPLOT+1
000046        WRITE(MWRITE,115) CYCLE
000053     25 WRITE (MWRITE,100) PROB, CYCLE, T
000065        WRITE (MWRITE,101) DT,IDT,JDT
000077        WRITE (MWRITE,102) PMAX,IPMAX,JPMAX
000111        WRITE (MWRITE,103) ZAXIS(JFORE), ZAXIS(JAFT)
000121        IF (AMOD(CYCLE,CDUMP)) 1,3,1
000125      1 IF (T-TMAX) 2,3,3
000130      2 IF (CYCLE-CYMAX) 4,3,3
000133      3 WRITE (LTAPE) PROB, CYCLE
000142        WRITE (LTAPE) IMAX,JFORE, JAFT, GAMMA, T, TMAX, CYMAX, CPRINT,
             1 ISPOT, CDUMP, PMAX, DT
000175        WRITE (LTAPE) (R(I),ZSTART(I),ZEND(I), I=1,IMAX)
000213        WRITE (LTAPE) ((Z(I,J),J=1,JFORE),I=1,IMAX)
000232        WRITE (LTAPE) (((P(I,J,K), K=1,6),J=1,JFORE),I=1,IMAX)
000256        WRITE (LTAPE) (PINIT(K), PSPOT(K), K=1,6)
000271        WRITE (LTAPE) (ZOLD(J),J=1,JFORE)
000303        WRITE (MWRITE,111)  CYCLE
000311      4 RETURN
000312        ENTRY OUTLNG
000317        IF (IXY.LE.0) WRITE (MWRITE,104)
000325        IF (IXY.GT.0) WRITE (MWRITE,114)
000332        DO 11 I=1,IMAX
000334        DO 10 J=1,JFORE
000335        IF (J .EQ. 1)  WRITE (MWRITE,110)
000342        WRITE (MWRITE,105) I, J, R(I), Z(I,J), P(I,J,1), P(I,J,2), P(I,J,3
```

```
            1), P(I,J,4), P(I,J,5)
000401       10 CONTINUE
000404       11 CONTINUE
000406          WRITE (MWRITE,117)
000412          WRITE (MWRITE,116) (J,ZAXIS(J),J=1,JFORE)
000426          M=MWRITE
000430          WRITE (M,106)
000433          WRITE (M,107)
000437          DO 12 I=1,IMAX
000441       12 WRITE (M,109) I,FORVEL(I),HMACHF,(PFORE(I,K),K=1,5)
000465          WRITE (M,108)
000470          WRITE (M,107)
000474          DO 13 I=1,IMAX
000476       13 WRITE (M,109) I,AFTVEL(I),HMACHA,(PAFT(I,K),K=1,5)
000522      100 FORMAT(    10X, 8H PROBLEM,F7.2, 6H CYCLE,F8.1, 4H T =,E12.4)
000522      101 FORMAT (/5H DT =,E12.4,12H AT CELL I =,I3,4H J =,I3)
000522    102   FORMAT (/7H PMAX =,E12.5,12H AT CELL I =,I3,4H J =,I3)
000522      103 FORMAT (10X,21H FORE SHOCK IS AT Z =,E12.4,20H AFT SHOCK IS AT Z =
            1,E12.4)
000522      104 FORMAT(4X,1HI,4X,1HJ,9X,1HR,14X,1HZ,14X,1HP,12X,3HRHO,14X,1HU,14X,
            11HV,9X,6HENERGY)
000522      105 FORMAT (2I5,     7(3X,E12.4))
000522      106 FORMAT (1H1,20X,22H FORE SHOCK PROPERTIES)
000522      107 FORMAT (7X,1HI,8X,6HVSHOCK,7X,6HMSHOCK,12X,1HP,12X,3HRHO,14X,1HU,
            114X,1HV,10X,6HENERGY)
000522      108 FORMAT (20X,21H AFT SHOCK PROPERTIES)
000522      109 FORMAT (5X,I5,7(3X,E12.4))
000522    110   FORMAT (1X,/)
000522    111   FORMAT (//19H TAPE DUMP ON CYCLE,F7.1/)
000522    112    FORMAT (/7H PMIN =,E12.4,12H AT CELL I =,I3,4H J =,I3)
000522      114 FORMAT(4X,1HI,4X,1HJ,9X,1HY,14X,1HX,14X,1HP,12X,3HRHO,14X,1HU,14X,
            11HV,9X,6HENERGY)
000522     115  FORMAT(1H1,5X,37H FORE AND AFT SHOCKS PLOTTED AT CYCLE,F8.1)
000522    116   FORMAT (4(I5,1X,E12.4))
000522    117   FORMAT (12H ZAXIS ARRAY)
000522          RETURN
000522          END
```

```
RUN VERSION 2.3 --PSR LEVEL 298--

                SUBROUTINE EOS(G,P,RHO,ZDOT,RDOT,ENERGY,SOUND)
000012          P=(G-1.)*(ENERGY - RHO*(ZDOT**2 + RDOT**2)/2.)
000020          SOUND = SQRT(G*P/RHO)
000030          RETURN
000030          END
```

```
RUN VERSION 2.3 --PSR LEVEL 298--


                SUBROUTINE FLUXES
          C             COMPUTES MASS, RADIAL MOMENTUM, AXIAL MOMENTUM, AND ENERGY
          C             FLUXES ON THE NORTH, SOUTH, EAST, AND WEST BOUNDARIES
000002            COMMON P(50,20,6), R(55), Z(55,20), ZSTART(50), ZEND(50), PINIT(6)
                 1, PSPOT(6),ZOLD(50),PFORE(50,6),PAFT(50,6),FORSEG(50),FORVEL(50),
                 2AFTSEG(50),AFTVEL(50), PN(20,6), PE(6), AN(20),UFORE(50),UAFT(50),
                 3 VNE(20),IXY
                 4,ZAXIS(20)
000002            COMMON RN, RS, ZNE, ZNW, ZSE, ZSW, ESEG, WSEG, GAMMA, T, TMAX, DT,
                 1 CYMAX, CPRINT, DTMIN, IDT, JDT, PROB, CYCLE, CDUMP, LREAD, MWRITE
                 2, LTAPE, DELR, ISPOT, VOLOLD, VOLNEW, AS, AW, AE, VNORME, VNORMW,
                 3 UNORME, UNORMW, UTANGE, UTANGW, VFORE, VAFT, VNW, VSE,VSW, IMAX,
                 4 JFORE, JAFT, I, J, PMAX,    HMACHF, HMACHA, IPMAX, JPMAX
000002            COMMON RSPOT, ZSPOT
000002            COMMON/FLUX/ FLUXN(20,5), FLUXS(5), FLUXW(5),FLUXE(5)
          C                    SOUTH BOUNDARY
000002            IF (I .EQ. 1) GO TO 5
000004            DO 2 K=2,5
000006    2       FLUXS(K)=-FLUXN(J,K)
000015            GO TO 10
000015    5       DO 6 K=2,5
000017    6       FLUXS(K)=0.
          C                    NORTH BOUNDARY
000022    10      FLUXN(J,2)=-PN(J,2)*PN(J,4)
000025            FLUXN(J,3)=-PN(J,2)*PN(J,4)*PN(J,3)
000030            FLUXN(J,4)=-PN(J,2)*PN(J,4)**2 - PN(J,1)
000034            FLUXN(J,5)=-(PN(J,5)+PN(J,1))*PN(J,4)
          C                    WEST BOUNDARY
000037            IF (J .EQ. 1) GO TO 15
000041            DO 12 K=2,5
000042    12      FLUXW(K)=-FLUXE(K)
000045            GO TO 16
000046    15      FLUXW(2)=P(I,1,2)*P(I,1,3)
000051            FLUXW(3)=P(I,1,2)*P(I,1,3)**2 + P(I,1,1)
000054            FLUXW(4)=P(I,1,2)*P(I,1,4)*P(I,1,3)

000056            FLUXW(5)=(P(I,1,5) + P(I,1,1))*P(I,1,3)
000061    16      FLUXE(2) = -PE(2)*(UNORME-VNORME)
000064            FLUXE(3) = -PE(2)*PE(3)*(UNORME-VNORME) - PE(1)*DELR/ESEG
000072            FLUXE(4) = -PE(2)*PE(4)*(UNORME-VNORME) + PE(1)*(ZNE-ZSE)/ESEG
000103            FLUXE(5) = -PE(5)*(UNORME-VNORME) - PE(1)*UNORME
000107            RETURN
000110            END
```

```
RUN VERSION 2.3 --PSR LEVEL 298--


                SUBROUTINE DTCALC
          C                    COMPUTE TIME STEP FROM COURANT CONDITION
000002            COMMON P(50,20,6), R(55), Z(55,20), ZSTART(50), ZEND(50), PINIT(6)
                 1, PSPOT(6),ZOLD(50),PFORE(50,6),PAFT(50,6),FORSEG(50),FORVEL(50),
                 2AFTSEG(50),AFTVEL(50), PN(20,6), PE(6), AN(20),UFORE(50),UAFT(50),
                 3 VNE(20),IXY
                 4,ZAXIS(20)
000002            COMMON RN, RS, ZNE, ZNW, ZSE, ZSW, ESEG, WSEG, GAMMA, T, TMAX, DT,
                 1 CYMAX, CPRINT, DTMIN, IDT, JDT, PROB, CYCLE, CDUMP, LREAD, MWRITE
                 2, LTAPE, DELR, ISPOT, VOLOLD, VOLNEW, AS, AW, AE, VNORME, VNORMW,
                 3 UNORME, UNORMW, UTANGE, UTANGW, VFORE, VAFT, VNW, VSE,VSW, IMAX,
                 4 JFORE, JAFT, I, J, PMAX,     HMACHF, HMACHA, IPMAX, JPMAX
000002            COMMON RSPOT, ZSPOT
000002            NAMELIST/CDT/ DT1,I,J,DTR,DTZ
          C                    RADIAL VELOCITY TIME STEP
000002            DR=DELR
000004            RSIG =AMAX1((P(I,J,6)+P(I,J,4)),(P(I,J,6)-P(I,J,4)))
000017            DTR = DR/RSIG
          C                    AXIAL VELOCITY TIME STEP
000021            DZ = AMIN1(    (ZNE-ZNW),    (ZSE-ZSW))
000030            ZSIG = AMAX1((P(I,J,6)+ABS(UNORME)+ABS(VNORME)),(P(I,J,6)+ABS(
                 1 UNORMW)+ABS(VNORMW)))
000050            DTZ = DZ/ZSIG
          C                    TIME STEP FOR CELL I,J
000052            DT1 = DTR*DTZ/(DTR+DTZ)
000055            IF (DT1 .LE. 0.)  GO TO 6
000056            IF (I.EQ.1 .AND. J.EQ.1) DTMIN=DT1
000066            IF (DT1 .GT. DTMIN) GO TO 5
000072            DTMIN = DT1
000072            IDT=I
000074            JDT=J
000075    5       RETURN
000076    6       WRITE (MWRITE,CDT)
000101            CALL ENDPLTS
000102            CALL EXIT
000103            END
```

```
RUN VERSION 2.3 --PSR LEVEL 299--

              SUBROUTINE NEWFLO
        C             COMPUTES CELL SURFACE AREAS AND VOLUMES
        C             AND UPDATES FLOW VARIABLES WITH THE DEFFERENCE EQNS.
000002          COMMON P(50,20,6), R(55), Z(55,20), ZSTART(50), ZEND(50), PINIT(6)
               1, PSPOT(6),ZOLD(50),PFORE(50,6),PAFT(50,6),FORSEG(50),FORVEL(50),
               2AFTSEG(50),AFTVEL(50), PN(20,6), PE(6), AN(20),UFORE(50),UAFT(50),
               3 VNE(20),IXY
               4,ZAXIS(20)
000002          COMMON RN, RS, ZNE, ZNW, ZSE, ZSW, ESEG, WSEG, GAMMA, T, TMAX, DT,
               1 CYMAX, CPRINT, DTMIN, IDT, JDT, PROB, CYCLE, CDUMP, LREAD, MWRITE
               2, LTAPE, DELR, ISPOT, VOLOLD, VOLNEW, AS, AW, AE, VNORME, VNORMW,
               3 UNORME, UNORMW, UTANGE, UTANGW, VFORE, VAFT, VNW, VSE,VSW, IMAX,
               4 JFORE, JAFT, I, J, PMAX,    HMACHF, HMACHA, IPMAX, JPMAX
000002          COMMON RSPOT, ZSPOT
000002          COMMON/FLUX/ FLUXN(20,5), FLUXS(5), FLUXW(5),FLUXE(5)
000002          NAMELIST/FLUX/ I,J,RATE,OMASSO,VOLNEW,VOLOLD,FLUXN,FLUXS,FLUXW,
               1 FLUXE, PN,PE,UNORME,VNORME, ZNE,ZSE,ZNW,ZSW,APLANE,AN,AS,RN,RS
               2,AW,AE,DELR,ESEG
        C                     SURFACE AREAS
000002          PI = 3.14159
000004          IF (IXY.GT.0) GO TO 1
000006          IF (I .EQ. 1) AS=0.
000011          IF (I .GT. 1) AS=AN(J)
000015          AN(J)=PI*2.*RN*(ZNE-ZNW)
000022          IF (J .GT. 1)  AW = AE
000026          IF (J .EQ. 1)  AW = PI*(RN+RS)*DELR
000033          AE = PI*(RN+RS)*ESEG
000037          GO TO 2
000037        1 AS=AN(J)
000041          AN(J)=ZNE-ZNW
000044          IF (I.EQ.1) AS=AN(J)
000047          AW=AE
000051          IF (J.EQ.1) AW= DELR
000054          AE=ESEG
000055        2 APLANE= 0.5*DELR*(ZNE-ZNW+ZSE-ZSW)
        C                     OLD CELL VOLUME
000063          IF (IXY.LE.0) VOL=
               1    PI/3.*DELR*((2.*RS+RN)*(ZSE-ZSW)+ (2.*RN+RS)*(ZNE-ZNW))
000102          IF (IXY.GT.0) VOL=(RN-RS)*(ZNE-ZNW+ZSE-ZSW)/2.
000112          VOLOLD=VOL
000114          RETURN
000114          ENTRY NUFLOW
        C                     NEW CELL VOLUME
000121          ZNNE=Z(I,J)
000125          ZNSW=Z(I-1,J-1)
000130          ZNSE=Z(I-1,J)
000133          ZNNW=Z(I,J-1)
000136          IF (I .EQ. 1) ZNSW = ZAXIS(J-1)
000141          IF (I .EQ. 1) ZNSE = ZAXIS(J)
000144          IF (J .EQ. 1)  ZNNW=0.
000147          IF (J .EQ. 1) ZNSW=0.
000151          IF (IXY.LE.0) VOL=
               1    PI/3.*DELR*((2.*RS+RN)*(ZNSE-ZNSW)+(2.*RN+RS)*(ZNNE-ZNNW))
000171          IF (IXY.GT.0) VOL=(RN-RS)*(ZNNE-ZNNW+ZNSE-ZNSW)/2.
```

```
000201          VOLNEW = VOL
          C               SOLVE CONSERVATION EQNS FOR NEW FLUID PROPERTIES
000203          CALL FLUXES
000204          QMASSO = P(I,J,2)*VOLOLD
000211          DO 20 K=2,5
000212          RATE = AN(J)*FLUXN(J,K)+AS*FLUXS(K)+AE*FLUXE(K)+AW*FLUXW(K)
000225          IF (K .NE. 4) GO TO 10
000227          IF (IXY .GT. 0) GO TO 10
000231          RATE = RATE + 2.*PI*APLANE*P(I,J,1)
000240    10    IF (K.EQ.2 .OR. K.EQ.5) P(I,J,K)=(VOLOLD*P(I,J,K)+RATE*DT)/VOLNEW
000261          IF (K.EQ.3 .OR. K.EQ.4) P(I,J,K)=(QMASSO*P(I,J,K)+RATE*DT)/P(I,J,
                1 2)/VOLNEW
000306    20    CONTINUE
000310          IF (P(I,J,5) .LT. 0.) WRITE (6,FLUX)
000317          IF (I .EQ. 1 .AND. J .EQ. 7 .AND. CYCLE .LE. 2.) WRITE (6,FLUX)
000337          IF (I .EQ. 1 .AND. J .EQ. 1 .AND. CYCLE .LT. 2.) WRITE (6,FLUX)
000357          RETURN
000360          END
```

```
RUN VERSION 2.3 --PSR LEVEL 298--

                SUBROUTINE RIO
          C                  RIO EVALUATES THE FLOW VARIABLES ON THE EAST
          C                  AND NORTH CELL BOUNDARIES BY SOLVING A RIEMANN PROBLE
000002            COMMON P(50,20,6), F(55), Z(55,20), ZSTART(50), ZEND(50), PINIT(6)
                 1, PSPOT(6),ZOLD(50),FFORE(50,6),PAFT(50,6),FORSEG(50),FORVEL(50),
                 2AFTSEG(50),AFTVEL(50), PN(20,6), PE(6), AN(20),UFORE(50),UAFT(50),
                 3 VNE(20),IXY
                 4,ZAXIS(20)
000002            COMMON RN, RS, ZNE, ZNW, ZSE, ZSW, ESEG, WSEG, GAMMA, T, TMAX, DT,
                 1 CYMAX, CPRINT, DTMIN, IDT, JDT, PROB, CYCLE, CDUMP, LREAD, MWRITE
                 2, LTAPE, DELR, ISPOT, VOLOLD, VOLNEW, AS, AW, AE, VNORME, VNORMW,
                 3 UNORME, UNORMW, UTANGE, UTANGW, VFORE, VAFT, VNW, VSE,VSW, IMAX,
                 4 JFORE, JAFT, I, J, PMAX,    HMACHF, HMACHA, IPMAX, JPMAX
000002            COMMON RSPOT, ZSPOT
000002            COMMON/RIEMANN/P1,U1,RHO1,V1,C1,P4,U4,RHO4,V4,U,C4, G,PB,UB,RHOB,
                 1VB
000002            G=GAMMA
          C                     NORTH BOUNDARY
000004            GM1=GAMMA-1.
000006            IF (I .EQ. IMAX) GO TO 10
000010            P1 = P(I,J,1)
000013            U1 = P(I,J,4)
000016            RHO1=P(I,J,2)
000021            V1=P(I,J,3)
000024            C1 = P(I,J,6)
000027            U = 0.
000030            P4=P(I+1,J,1)
000033            U4=P(I+1,J,4)
000036            RHO4=P(I+1,J,2)
000041            V4=P(I+1,J,3)
000044            C4=P(I+1,J,6)
000047            CALL RIEMANN
000050            PN(J,1)=PB
000052            PN(J,2)=RHOB
000054            PN(J,3)=VB
000055            PN(J,4)=UB
000057            PN(J,5)=PB/GM1 + RHOB/2.*(UB**2+VB**2)
000066            GO TO 15
000067    10      DO 11 K=1,5
000071    11      PN(J,K) = P(IMAX,J,K)
          C                     EAST BOUNDARY
000105    15      IF (J .EQ. JAFT) GO TO 25
000107            IF (J .EQ. JFORE) GO TO 30
000111            SINE = DELR/ESEG
000113            COSINE = (ZNE-ZSE)/ESEG
000115            P1 = P(I,J,1)
000121            RHO1=P(I,J,2)
000124            P4=P(I,J+1,1)
000127            RHO4=P(I,J+1,2)
000132            U1 = P(I,J,3)*SINE - P(I,J,4)*COSINE
000141            U4 = P(I,J+1,3)*SINE - P(I,J+1,4)*COSINE
000147            V1 = P(I,J,3)*COSINE + P(I,J,4)*SINE
000155            V4 = P(I,J+1,3)*COSINE + P(I,J+1,4)*SINE
000162            C1 = P(I,J,6)
```

```
000165          C4 = P(I,J+1,6)
000166          U = VNORME
000170          CALL RIEMANN
000171          UNORMW = UNORME
000173          VNORMW = VNORME
000174          IF (J .EQ. 1) UNORMW = P(I,J,3)
000202          IF (J .EQ. 1) VNORMW = 0.
000204          UNORME = UB
000206          PE(1) = PB
000207          PE(2) = RHOB
000211          PE(3) = UB*SINE + VB*COSINE
000214          PE(4) = VB*SINE - UB*COSINE
000217          PE(5) = PB/GM1 + RHOB/2.*(UB**2 + VB**2)
000225          RETURN
000226    25    DO 26 K=1,5
000230    26    PE(K) = PAFT(I,K)
000240          UNORMW=UNORME
000241          VNORMW=VNORME
000243          UNORME = UAFT (I)
000244          RETURN
000245    30    DO 31 K=1,5
000247          PE(K) = PFORE(I,K)
000255    31    CONTINUE
000257          VNORMW=VNORME
000260          UNORMW=UNORME
000262          UNORME = UFORE(I)
000263    5     RETURN
000264          END
```

```
RUN VERSION 2.3 --PSR LEVEL 298--


              SUBROUTINE SHIO
000002        COMMON P(50,20,6), R(55), Z(55,20), ZSTART(50), ZEND(50), PINIT(6)
             1, PSPOT(6),ZOLD(50),PFORE(50,6),PAFT(50,6),FORSEG(50),FORVEL(50),
             2AFTSEG(50),AFTVEL(50), PN(20,6), PE(6), AN(20),UFORE(50),UAFT(50),
             3 VNE(20),IXY
             4,ZAXIS(20)
000002        COMMON RN, RS, ZNE, ZNW, ZSE, ZSW, ESEG, WSEG, GAMMA, T, TMAX, DT,
             1 CYMAX, CPRINT, DTMIN, IDT, JDT, PROB, CYCLE, CDUMP, LREAD, MWRITE
             2, LTAPE, DELR, ISPOT, VOLOLD, VOLNEW, AS, AW, AE, VNORME, VNORMW,
             3 UNORME, UNORMW, UTANGE, UTANGW, VFORE, VAFT, VNW, VSE,VSW, IMAX,
             4 JFORE, JAFT, I, J, PMAX,    HMACHF, HMACHA, IPMAX, JPMAX
000002        COMMON RSPOT, ZSPOT
000002        COMMON/SHOCK/P1,RHO1,U1,V1,P4,RHO4,U4,V4,    G,VSHOCK,P3,RHO3,U3,M
000002        IF (I .EQ. IMAX) RETURN
000005        G=GAMMA
000007        II=I+1
000011        IF (I .EQ. 1) II=1
      C                     SET UP AFT SHOCK INPUT FOR SHOCK
000013      1 P4 = P(II,JAFT+1,1)
000017        P1 = P(II,JAFT,1)
000022        RHO4 = P(II,JAFT+1,2)
000025        RHO1 = P(II,JAFT,2)
000030        DELR = R(II)-R(II-1)
000032        STHETA = DELR/AFTSEG(II)
000034        IF (II .EQ. 1) GO TO 2
000036        CTHETA = (Z(II,JAFT)- Z(II-1,JAFT))/AFTSEG(II)
000045        GO TO 3
000045      2 STHETA = R(1)/AFTSEG(1)
000047        CTHETA = (Z(1,JAFT)-ZAXIS(JAFT))/AFTSEG(1)
000054      3 U1 = P(II,JAFT,3)*STHETA- P(II,JAFT,4)*CTHETA
000064        U4 = P(II,JAFT+1,3)*STHETA- P(II,JAFT+1,4)*CTHETA
000072        UAFT(II)= U1
000074        C1 = P(II,JAFT,6)
000076        C4 = P(II,JAFT+1,6)
000100        V4 = P(II,JAFT+1, 3)*CTHETA + P(II,JAFT+1,4)*STHETA
000104        CALL SHOCK
000105        V3=V4
      C                     PROCESS AFTSHOCK OUTPUT FROM SHOCK
000107        IF (PROB .EQ.19.) VSHOCK=0.
000112        AFTVEL(II)=VSHOCK
000114        PAFT(II,1)=P3
000116        PAFT(II,2)=RHO3
000117        PAFT(II,3)=U3*STHETA + V3*CTHETA
000123        PAFT(II,4) =V3*STHETA-U3*CTHETA
000126        PAFT(II,5) = P3/(GAMMA-1.) + RHO3/2.*(U3**2+V3**2)
000137        HMACHA=(VSHOCK-U4)/C4
      C                      IF J=1, DO THE SECOND TUBE ALSO
000142        IF (II .GT. 1) GO TO 4
000146        II = 2
000146        GO TO 1
000147      4 IF (I .EQ. 1) II = 1
      C                     FORE SHOCK ANGLE
000152      7 CTHETF = (Z(II,JFORE)-Z(II-1,JFORE))/FORSEG(II)
000162        STHETF = DELR/FORSEG(II)
```

```
RUN VERSION 2.3 --PSR LEVEL 298--                                SHIO

000164          IF (II .EQ. 1) STHETF = R(1)/FORSEG(1)
000170          IF (II .EQ. 1) CTHETF = (Z(1,JFORE)-ZAXIS(JFORE))/FORSEG(1)
          C                     SET UP FORE SHOCK INPUT TO SHOCK
000176          P1 = P(II,JFORE,1)
000202          RHO1 = P(II,JFORE,2)
000205          U1 = P(II,JFORE,3)*STHETF - P(II,JFORE,4)*CTHETF
000214          UFORE(II)=U1
000216          V1 = P(II,JFORE,4)*STHETF + P(II,JFORE,3)*CTHETF
000223          C1 = P(II,JFORE,6)
          C                          ARE WE IN COLD SPOT   OR UNDISTURBED REGION
000226        5 P4=PINIT(1)
000230        6 U4 = 0.
000231          V4 = 0.
000232          IF (RSPOT.LT. 1.E-4) GO TO 8
000234          RHO4 = PINIT(2)*(1.+PSPOT(2)*EXP(-3.*((Z(I,JFORE)-ZSPOT)**2
                1 +R(I)       **2)/RSPOT**2) -PSPOT(2)*EXP(-3.))
000256        8 RADSQR = (Z(I,JFORE)-ZSPOT)**2 +R(I)**2
000264          IF (RADSQR .GT. RSPOT**2) RHO4=PINIT(2)
000271          C4=PINIT(6)*SQRT(PINIT(2)/RHO4)
000277          CALL SHOCK
          C                     PROCESS FORE SHOCK OUTPUT
000300          FORVEL(II)=VSHOCK
000302          PFORE(II,1) = P3
000304          PFORE(II,2) = RHO3
000305          PFORE(II,3) = U3*STHETF
000307          PFORE(II,4)=-U3*CTHETF
000311          PFORE(II,5)= P3/(GAMMA-1.) + RHO3/2.*U3**2
000317          HMACHF = VSHOCK/C4
000321          IF (II .GT. 1) RETURN
000324          II = 2
000325          GO TO 7
000326          END
```

```
RUN VERSION 2.3 --PSR LEVEL 298--

                SUBROUTINE RIEMANN
        C                    SOLVE WEAK WAVE RIEMANN PROBLEM
000002          COMMON/RIEMANN/P1,U1,RHO1,V1,C1,P4,U4,RHO4,V4,U,C4, G,PB,UB,RHOB,
               1VB
        C                 COMPUTE PRESSURE AND VELOCITY ACROSS CONTACT SURFACE
000002          GAMMA=G
000003          EM1 = SQRT(GAMMA*P1*RHO1)
000007          EM4 = SQRT(GAMMA*P4*RHO4)
000014          UCS =(P1 - P4 +EM1*U1+EM4*U4)/(EM1+EM4)
000025          PCS = (EM1*EM4*(U1-U4) + P4*EM1 + P1*EM4)/(EM1+EM4)
        C                 COMPUTE WAVE SPEEDS
000036          VW1 = U1 - C1 + (GAMMA+1.)/4.*(UCS-U1)
000046          VW2 = U4 + C4 + (GAMMA+1.)/4.*(UCS-U4)
000057          IF (VW1 .GE. U) GO TO 5
000062          IF (UCS .GE. U) GO TO 10
000064          IF (VW2 .GE. U) GO TO 15
000066          PB = P4
000067          UB = U4
000070          RHOB = RHO4
000072          VB = V4
000074          RETURN
000074    5     PB=P1
000075          UB=U1
000077          RHOB=RHO1
000100          VB=V1
000102          RETURN
000103    10    PB=PCS
000104          UB=UCS
000106          RHOB= RHO1*(PCS/P1)**(1./GAMMA)
000114          VB = V1
000116          RETURN
000117    15    PB=PCS
000120          UB=UCS
000122          RHOB = RHO4*(PCS/P4)**(1./GAMMA)
000130          VB=V4
000132          RETURN
000133          END
```

APPENDIX B

THE SHELL CODE

As part of the evolution of GODUNOV, comparisons were made with another two-dimensional time-dependent hydrodynamic code called SHELL. SHELL was created several years ago for nuclear detonation calculations. It was intended originally in the present investigation to use SHELL in the focal region of the calculation. However, it is inappropriate for sonic boom studies because it tends to smear out weak shocks with relative overpressures less than 0.07. Nevertheless, SHELL was useful in checking out GODUNOV in certain test calculations (see Chapter 3).

A flow chart for SHELL is shown in Figure A-2. The input for SHELL is generated by an auxiliary program called CLAM. In the course of one time step in SHELL, the fluid properties at the center of each cell in the grid are updated in two phases. In the first phase, the conservation equations are solved with the convective terms neglected. In the second phase, material is allowed to flow across cell boundaries and transport mass, momentum, and energy. A detailed discussion of the calculation procedure can be found in General Atomic report number GAMD-5580, "OIL, A Continuous Two-Dimensional Eulerian Hydrodynamic Code," 1965, by W. E. Johnson.

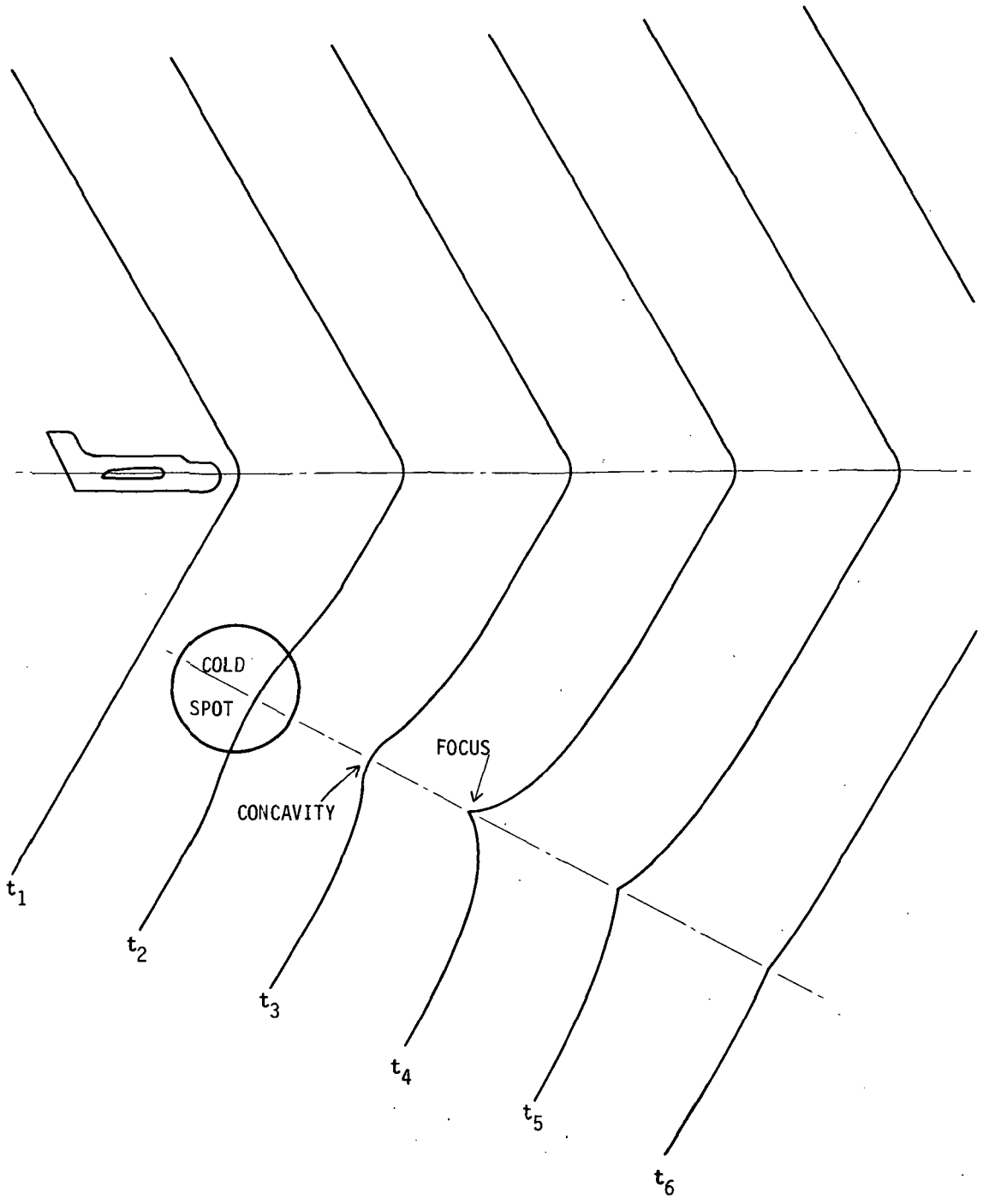

FIGURE 1-1. FOCUSING OF BOW SHOCK WAVE BY A COLD SPOT

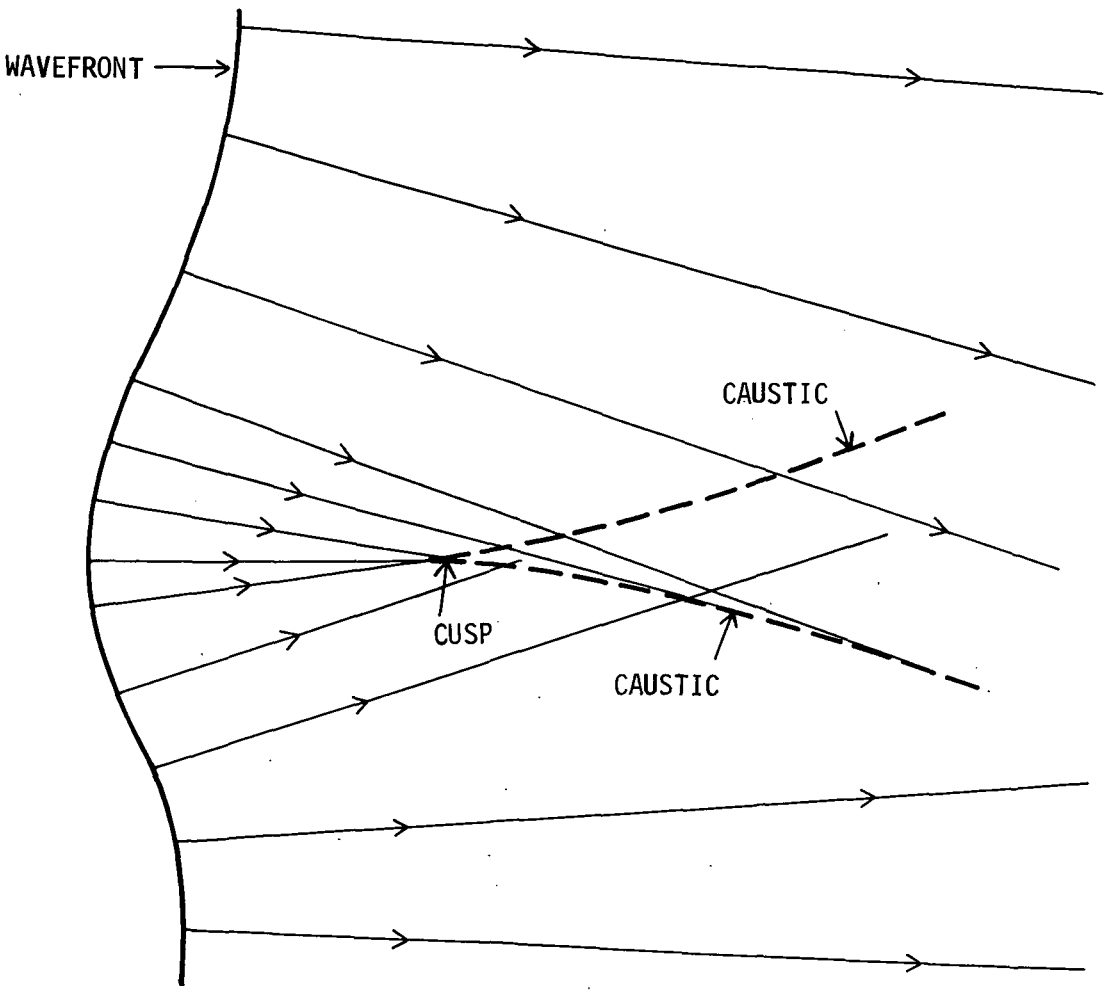

FIGURE 1-2. GEOMETRIC ACOUSTICS DESCRIPTION OF FOCUSING, SHOWING RAYS AND CAUSTIC CUSP

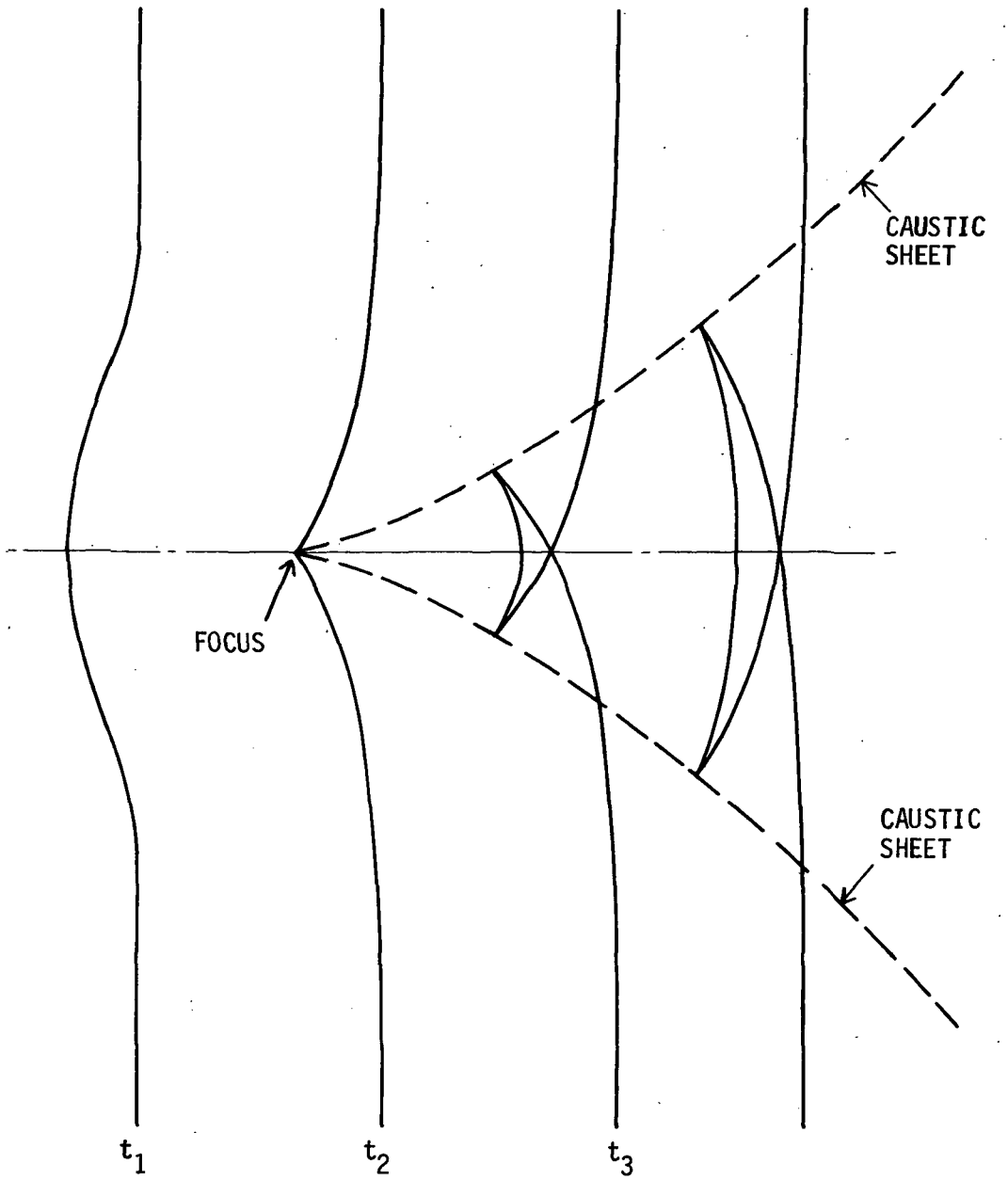

FIGURE 1-3. GEOMETRIC ACOUSTIC WAVE-FOLDING

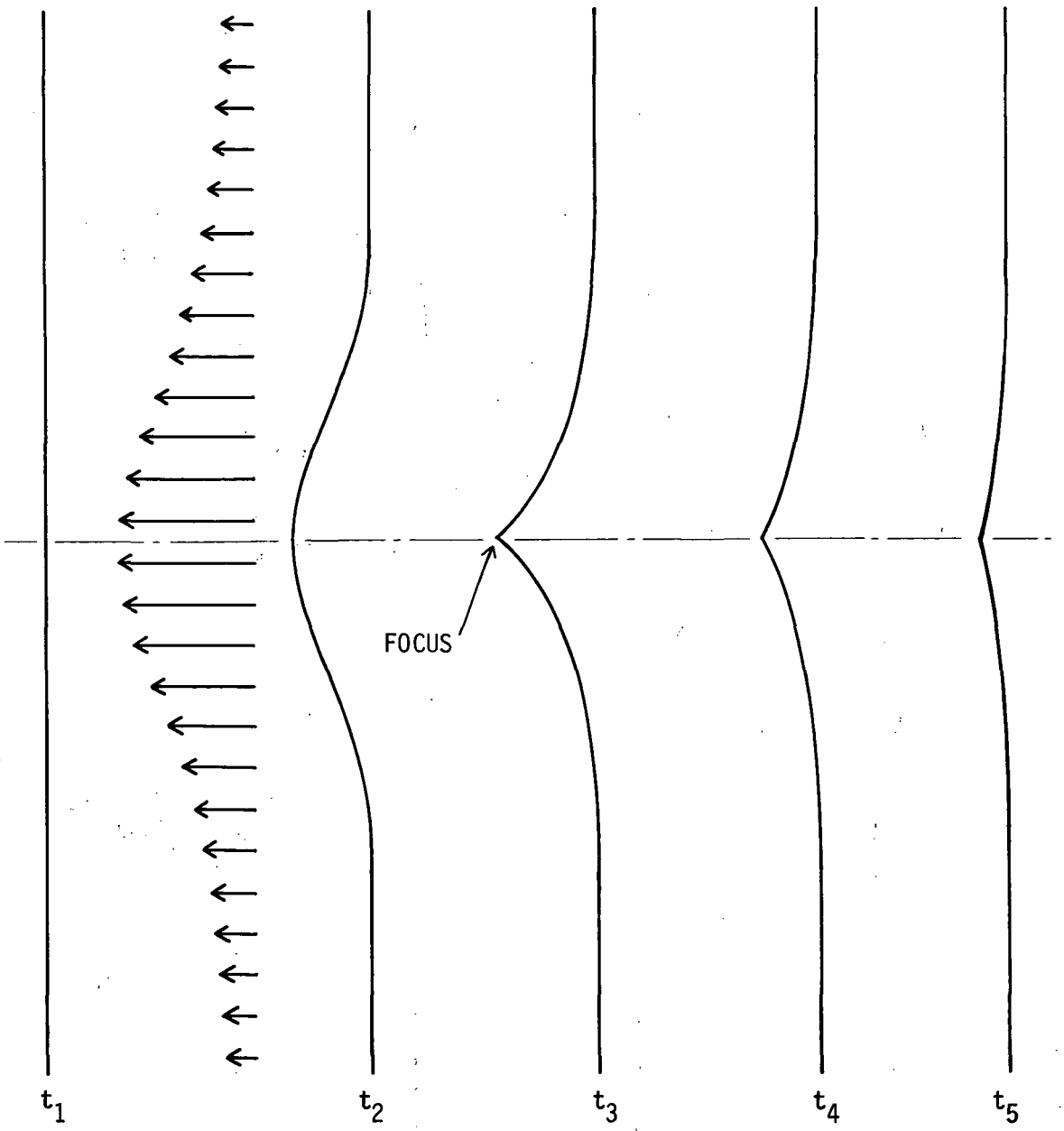

FIGURE 1-4. REFRACTION AND FOCUSING BY ATMOSPHERIC WIND SHEAR

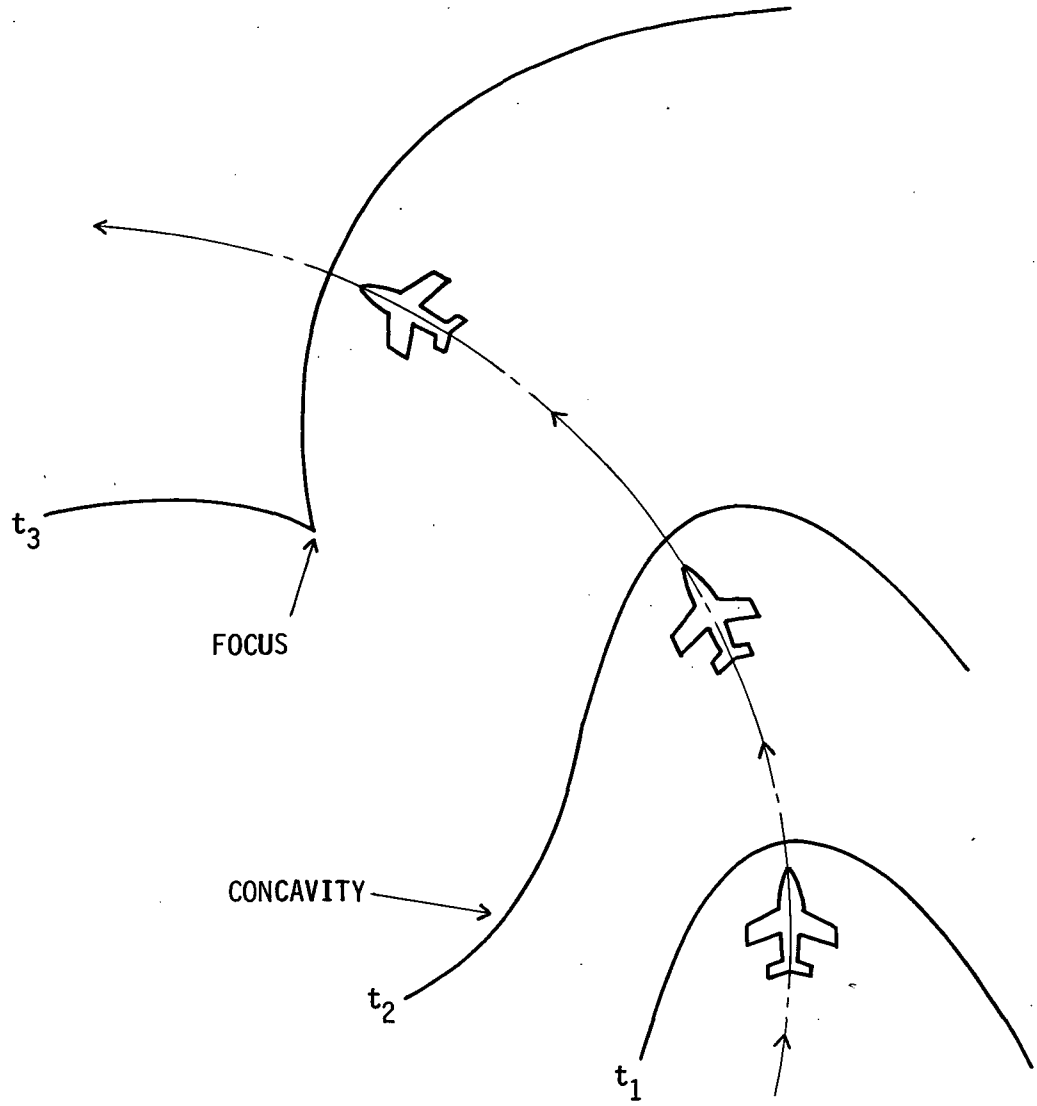

FIGURE 1-5. FOCUSING OF A SHOCK WAVE FROM A TURNING AIRCRAFT

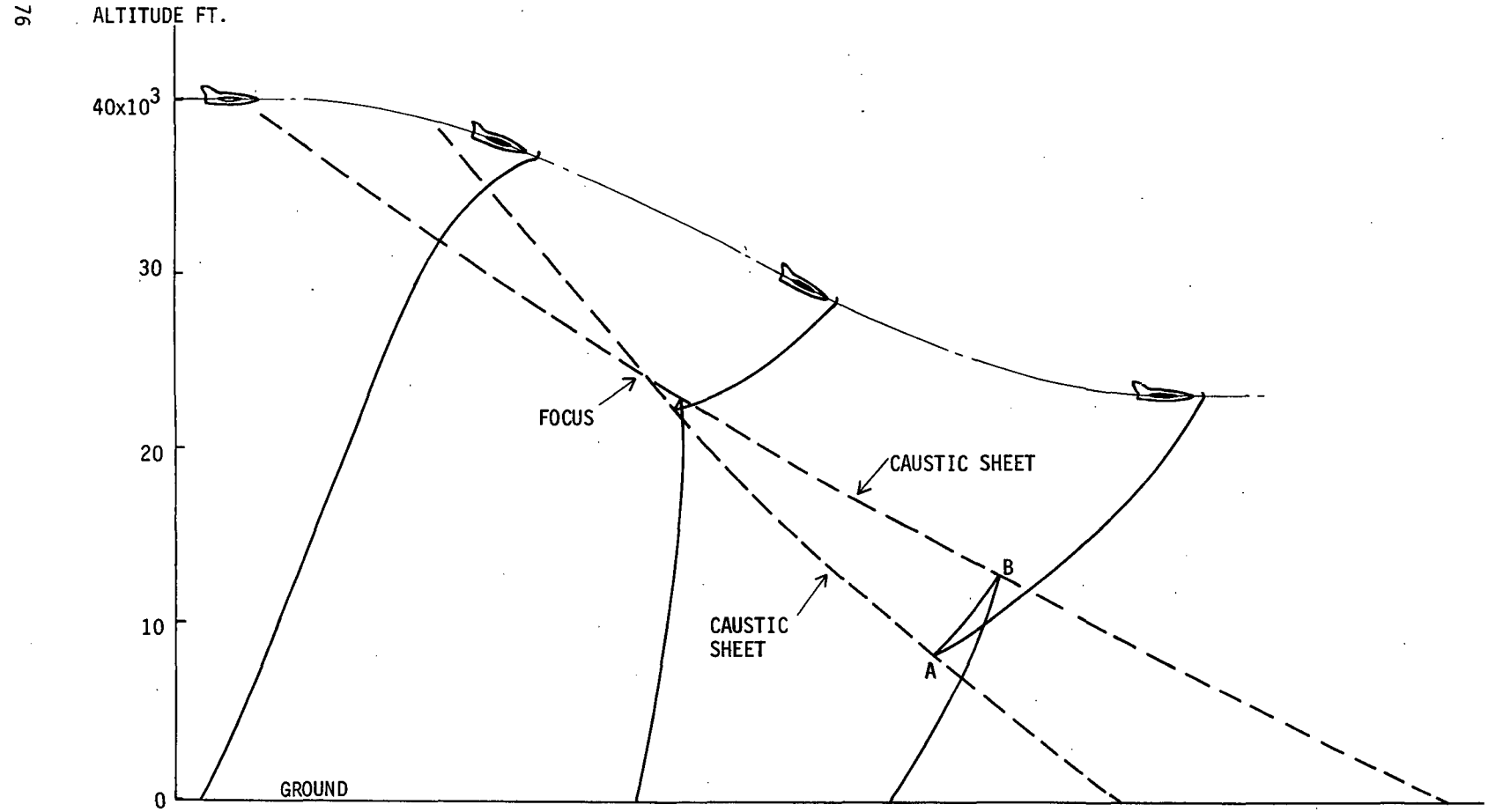

FIGURE 1-6. FOCUSING OF A SHOCK WAVE FROM A DIVE MANEUVER

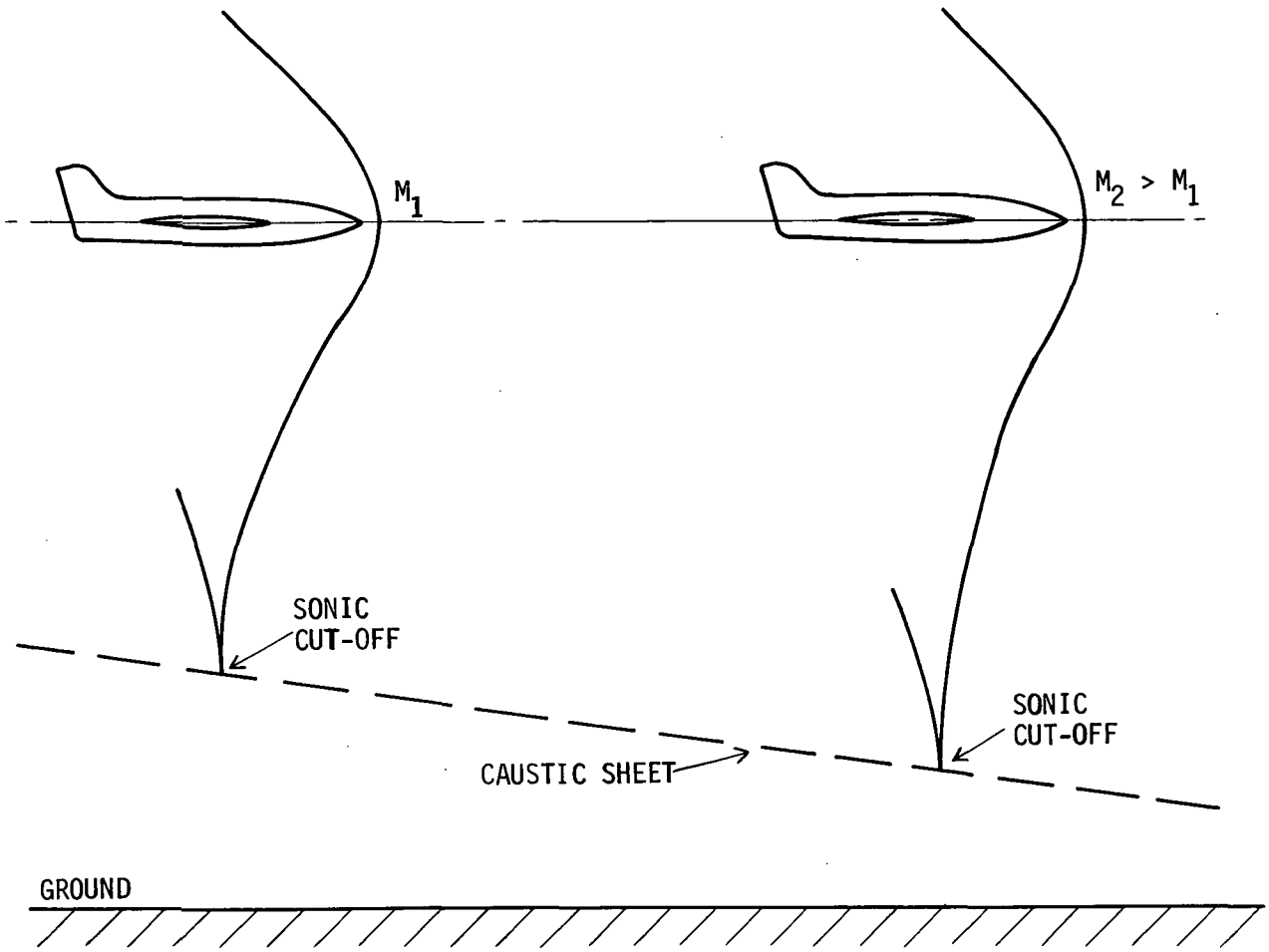

FIGURE 1-7. SONIC CUT-OFF FOR AN ACCELERATING AIRCRAFT

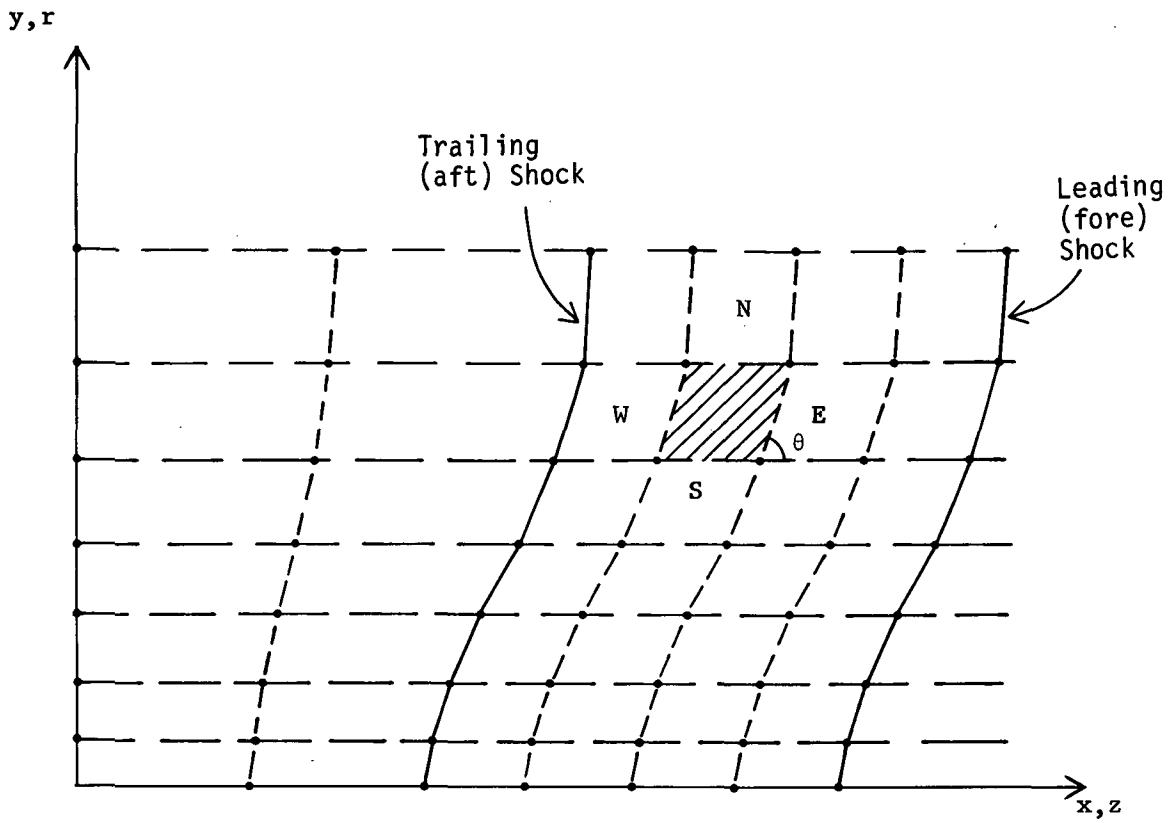

FIGURE 3-1. GODUNOV MESH

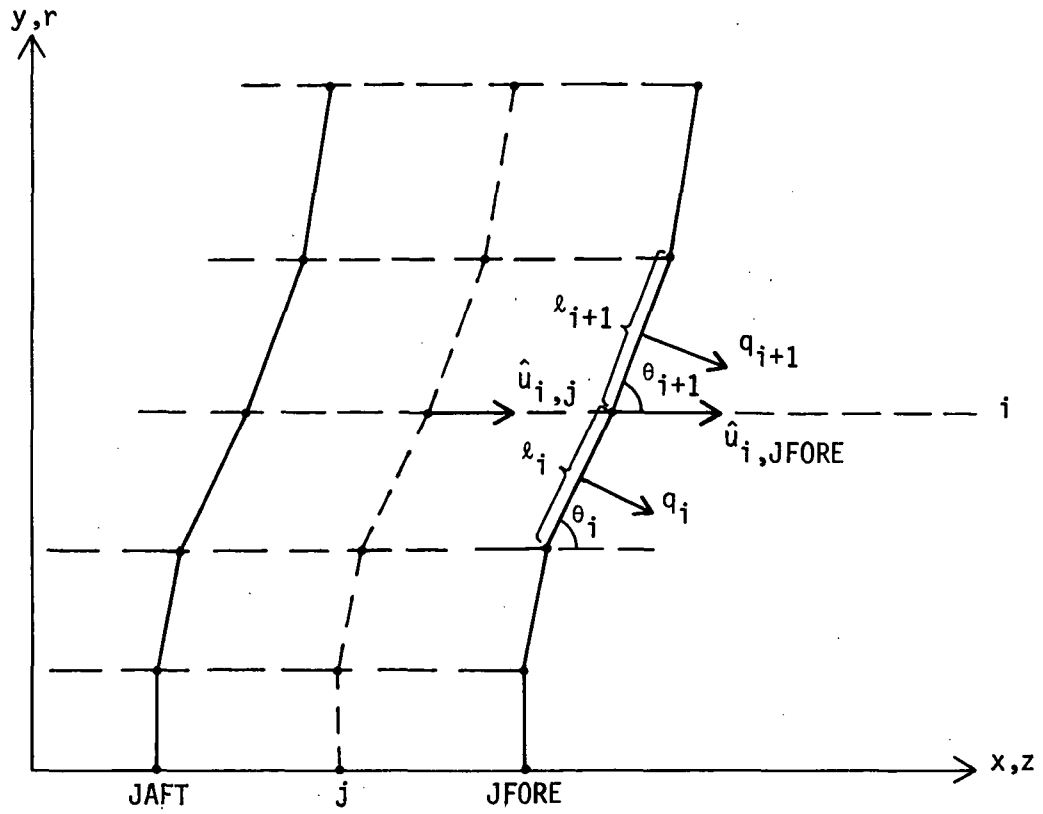

FIGURE 3-2. NODE VELOCITIES IN GODUNOV

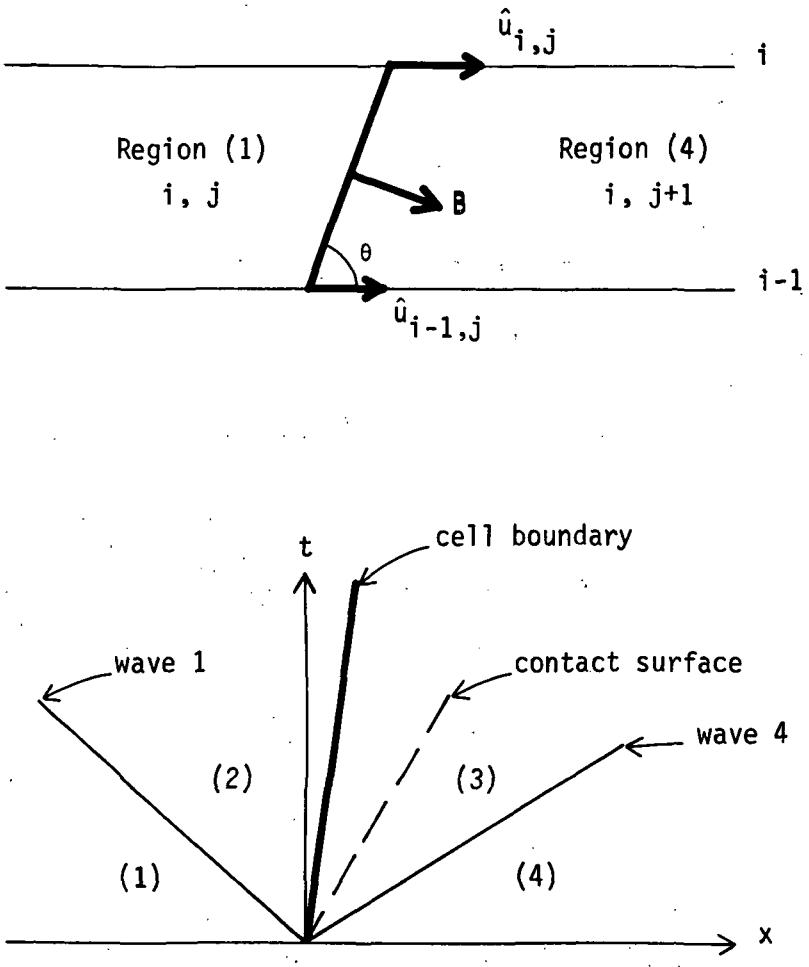

FIGURE 3-3. RIEMANN PROBLEM AT A CELL BOUNDARY

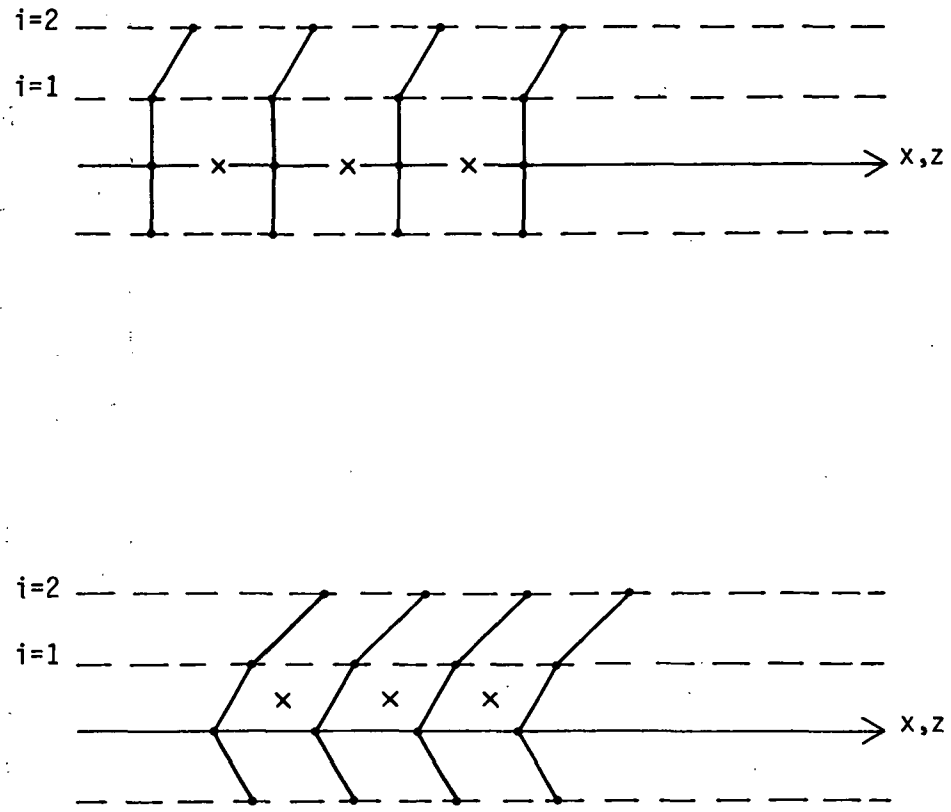

FIGURE 3-4. AXIAL SYMMETRY CONDITIONS IN GODUNOV

TOP: VERTICAL CELL-BOUNDARIES AT AXIS
BOTTOM: INCLINED CELL-BOUNDARIES AT AXIS
(*x DENOTES CENTER OF CELL*)

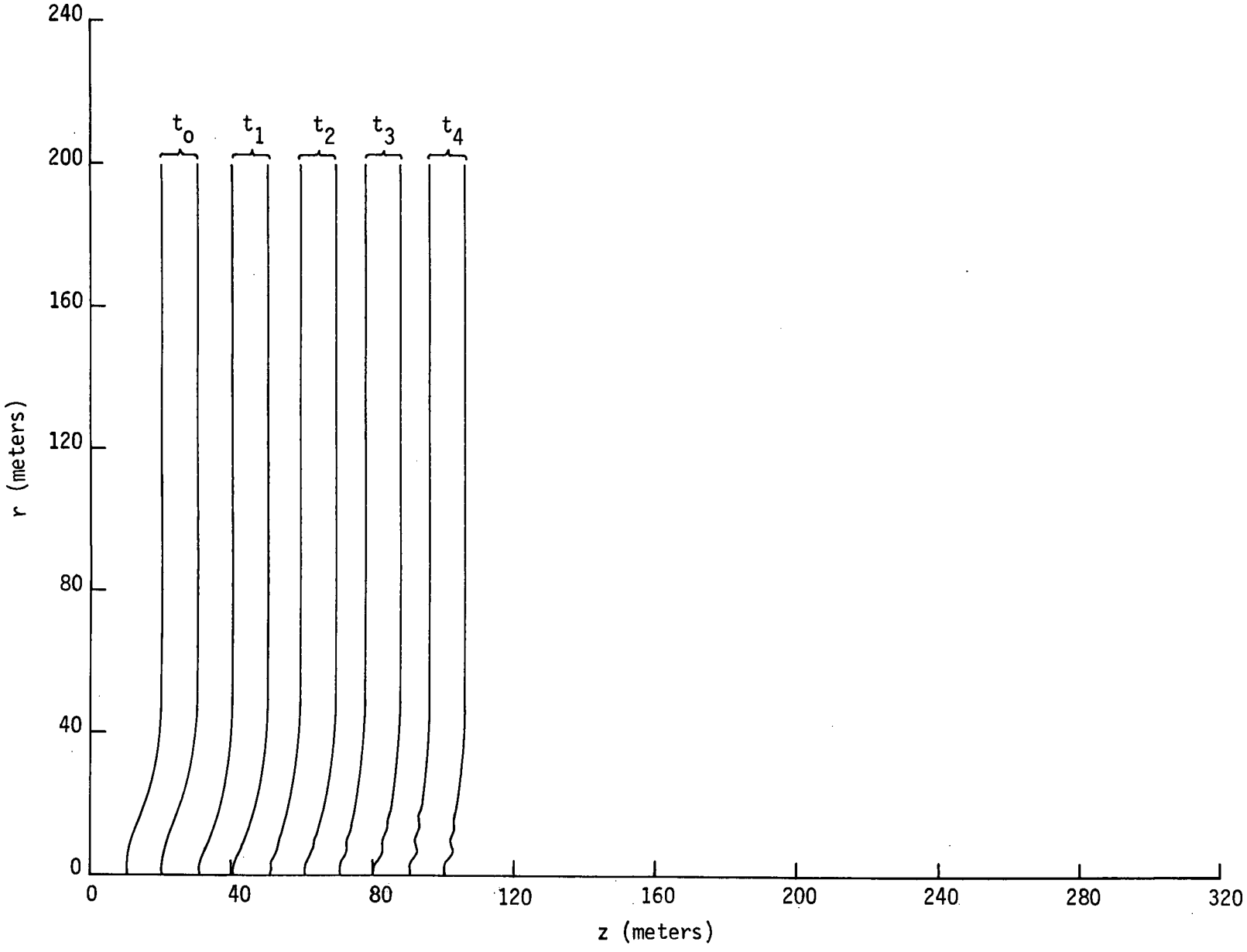

FIGURE 3-5. FORE AND AFT SHOCK PROFILES OF AN N-WAVE PROPAGATING TO THE RIGHT (VERTICAL CELL-BOUNDARY SYMMETRY CONDITION) AT FIVE DIFFERENT TIMES

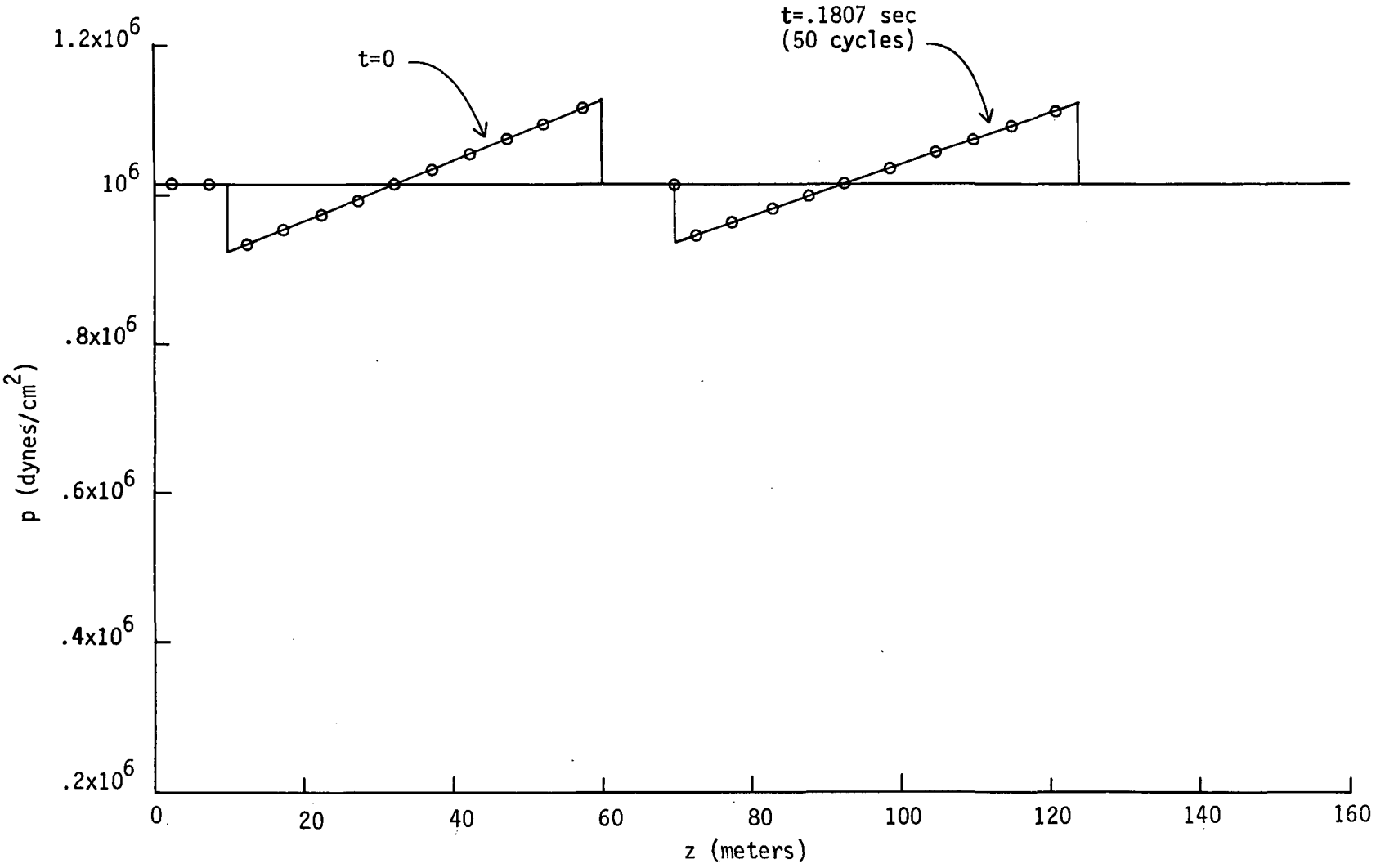

FIGURE 3-6. PRESSURE PROFILES IN AN N-WAVE ($\Delta p_o/p_o$ = 0.1) (GODUNOV CALCULATION)

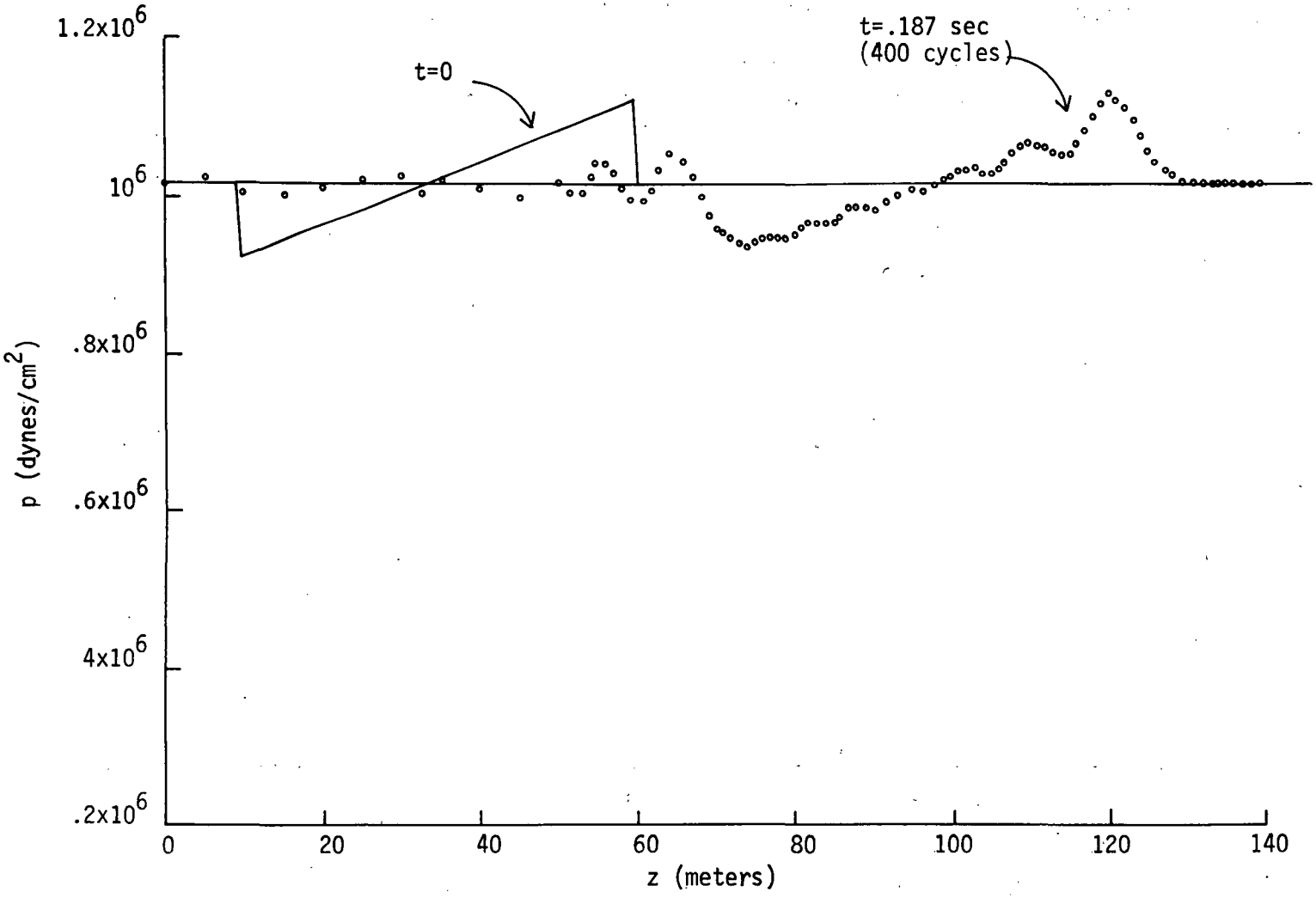

FIGURE 3-7. PRESSURE PROFILES IN AN N-WAVE ($\Delta p_o/p_o$ = 0.1) (SHELL CALCULATION)

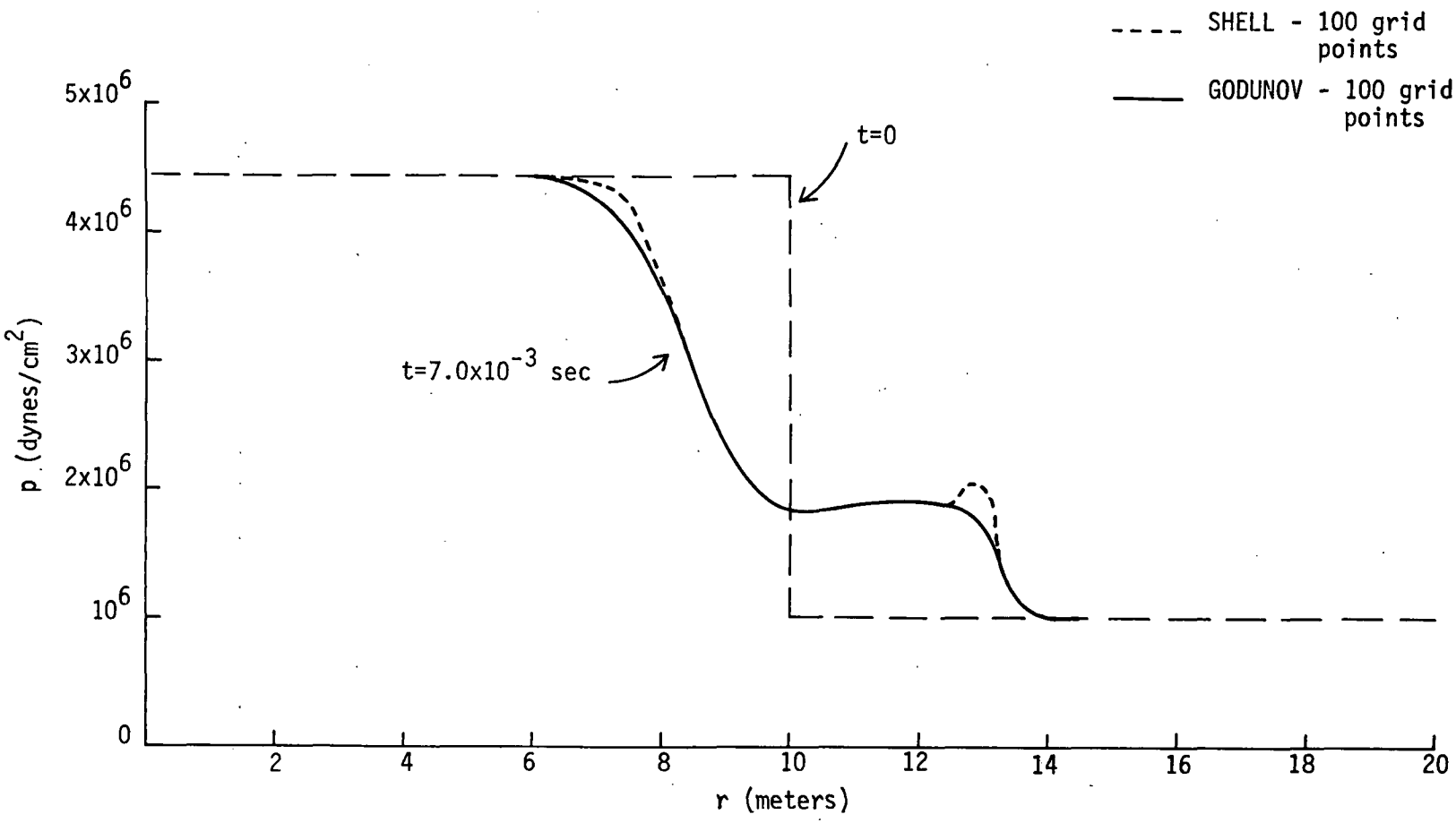

FIGURE 3-8. PRESSURE PROFILES IN A RADIAL FLOW PROBLEM ("CYLINDRICAL SHOCK TUBE", PRESSURE RATIO = 4.45) COMPARISON OF GODUNOV AND SHELL CALCULATIONS

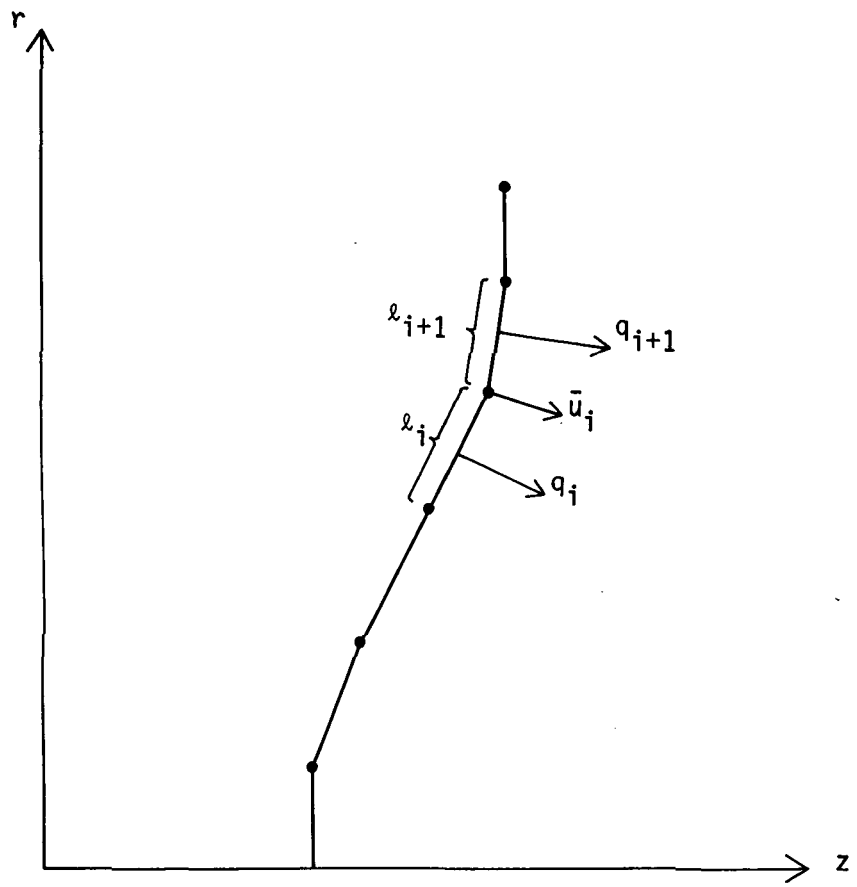

FIGURE 4-1. SHOCK SEGMENTS AND NODES IN WHITHAM

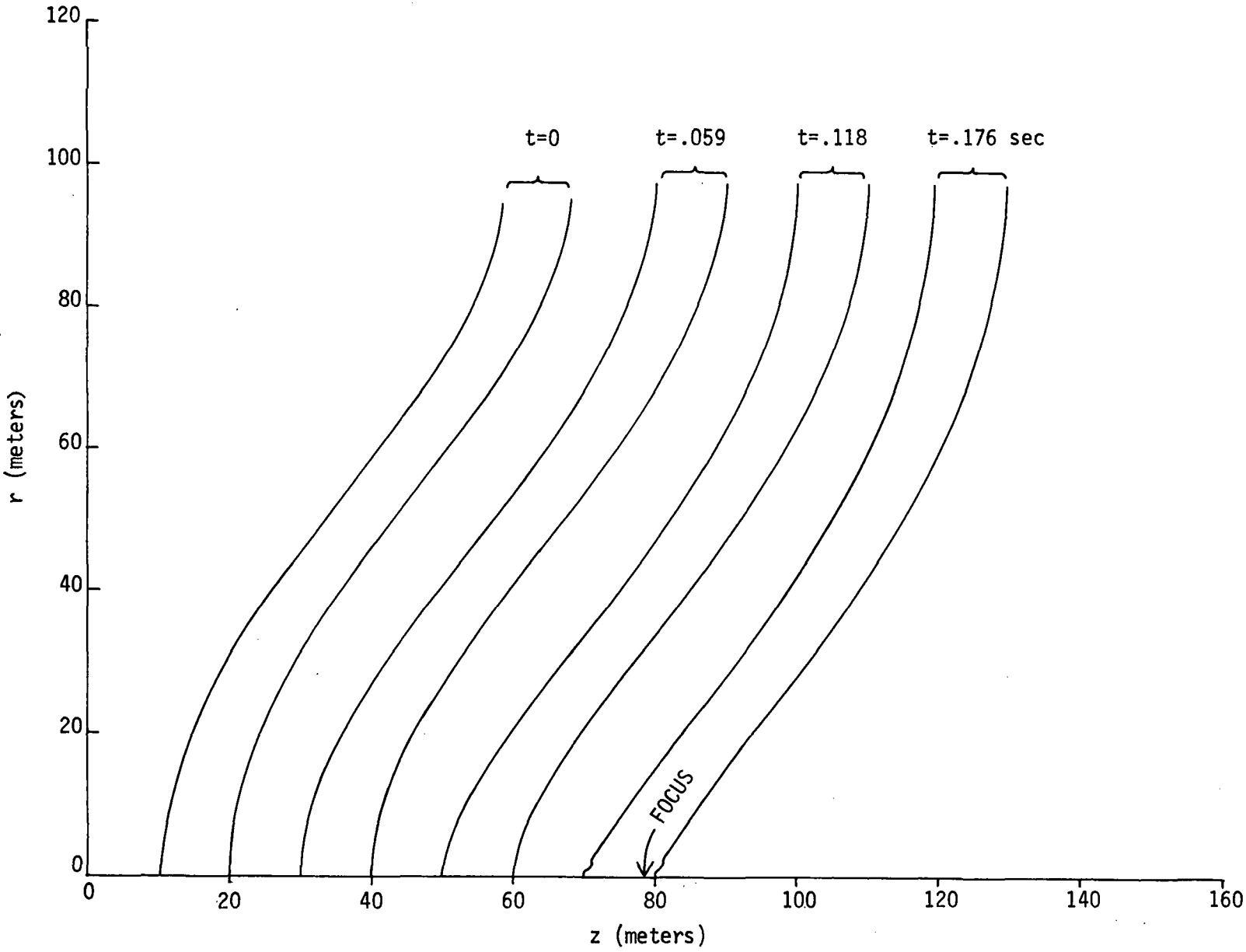

FIGURE 5-1. SHOCK PROFILES OF A POLYNOMIAL-FRONT N-WAVE ($\Delta p_o/p_o = 10^{-3}$) (ACTUAL FOCUS IS AT z=79 METERS)

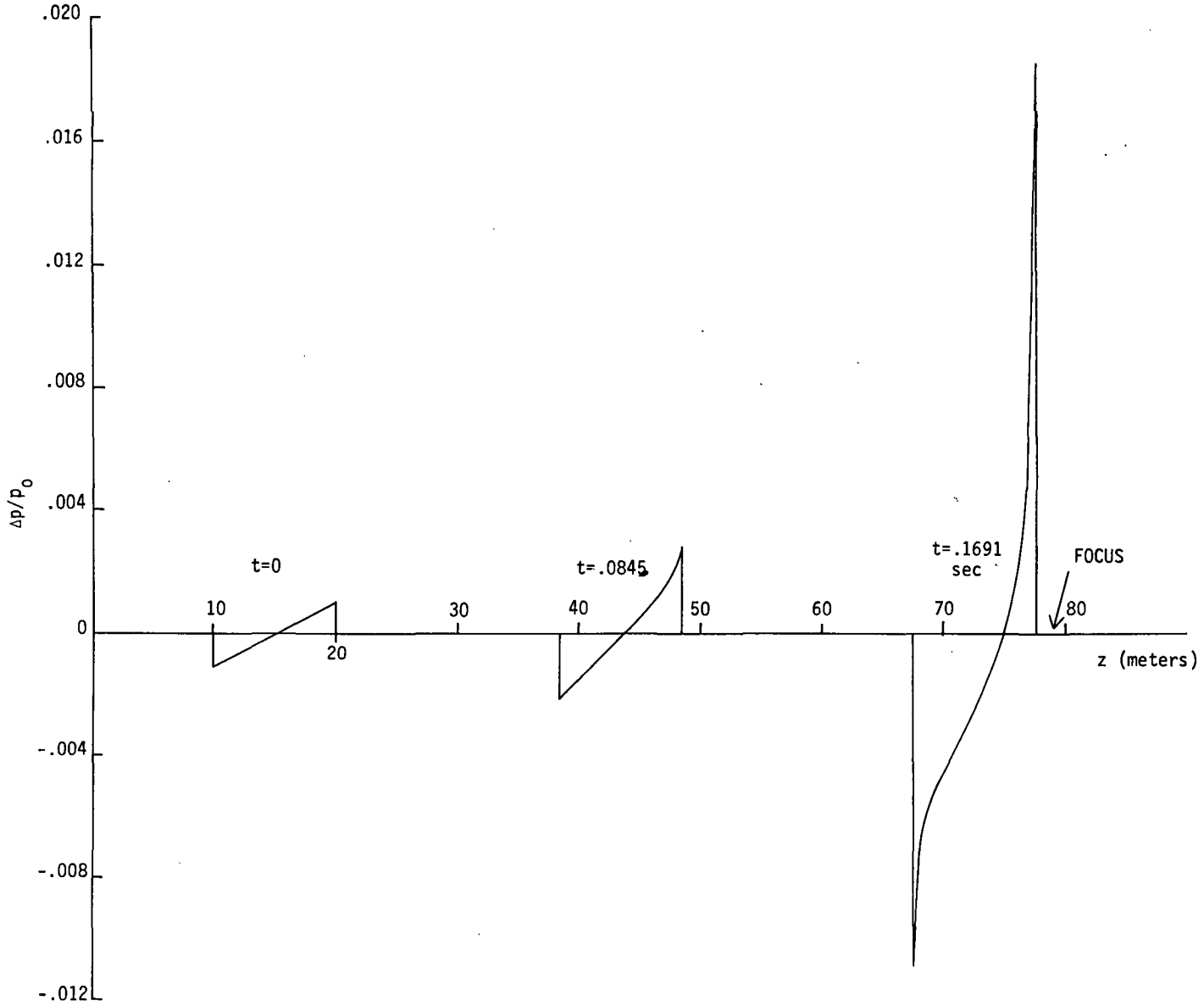

FIGURE 5-2. PRESSURE PROFILES AT THE AXIS AT THREE DIFFERENT TIMES FOR A POLYNOMIAL-FRONT N-WAVE ($\Delta p_o/p_o = 10^{-3}$, $\Delta p_{max}/\Delta p_o = 18.7$)

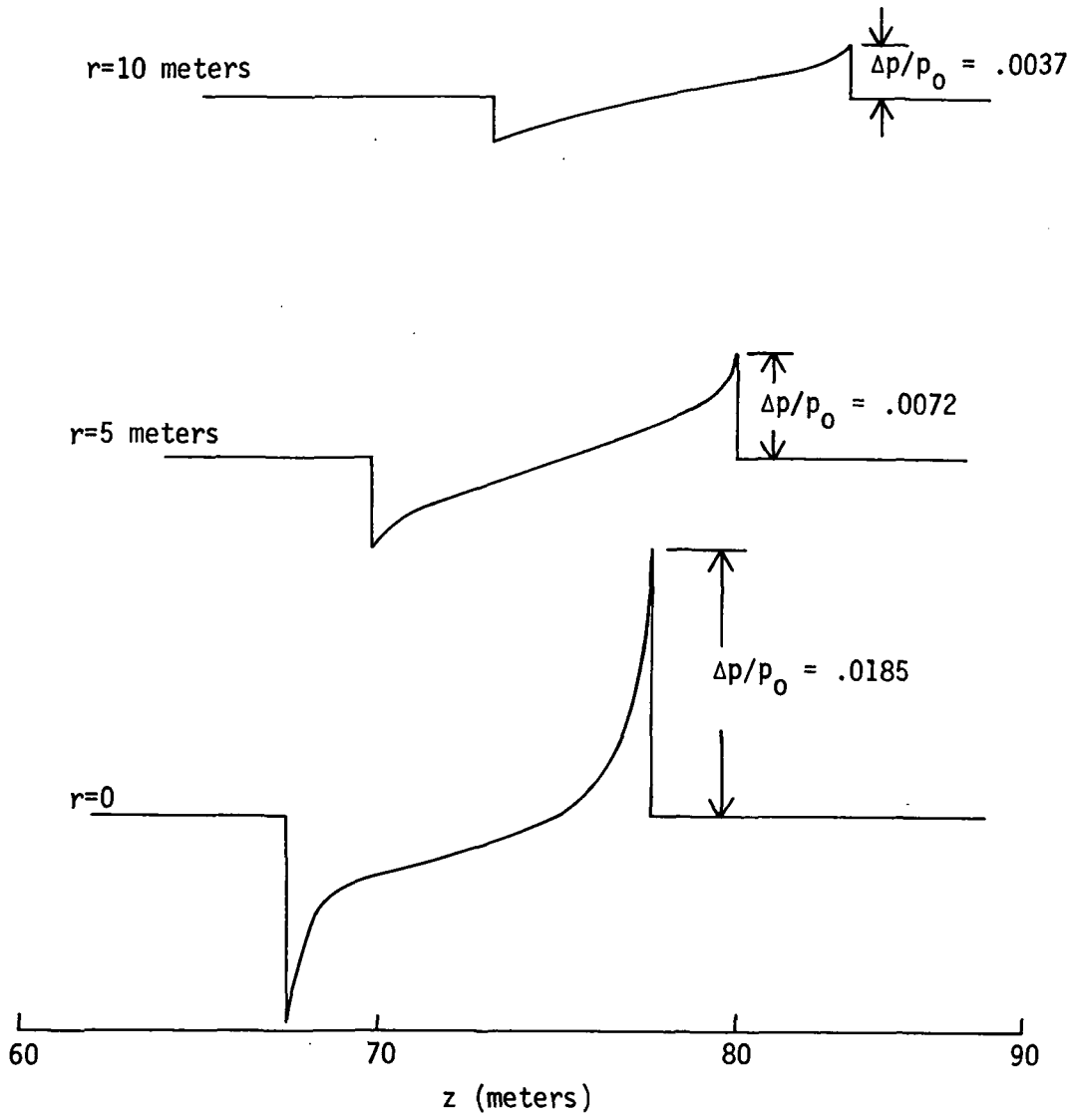

FIGURE 5-3. PRESSURE PROFILES AT THREE DIFFERENT RADIAL POSITIONS JUST PRIOR TO FOCUSING FOR A POLYNOMIAL-FRONT N-WAVE ($\Delta p_o/p_o = 10^{-3}$)

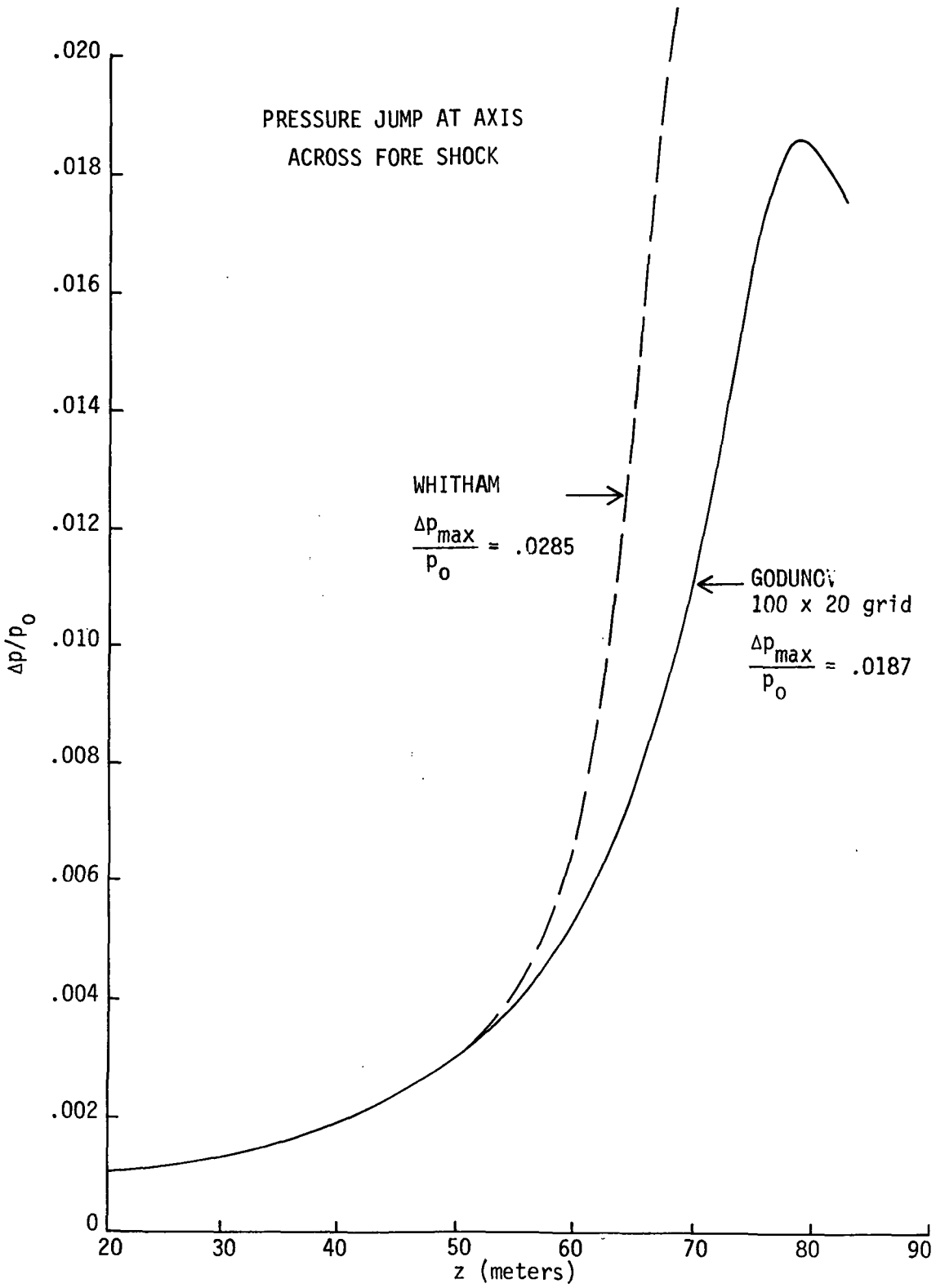

FIGURE 5-4. RELATIVE OVERPRESSURE VERSUS AXIAL POSITION OF FORE SHOCK FOR A POLYNOMIAL-FRONT N-WAVE ($\Delta p_o/p_o = 10^{-3}$)

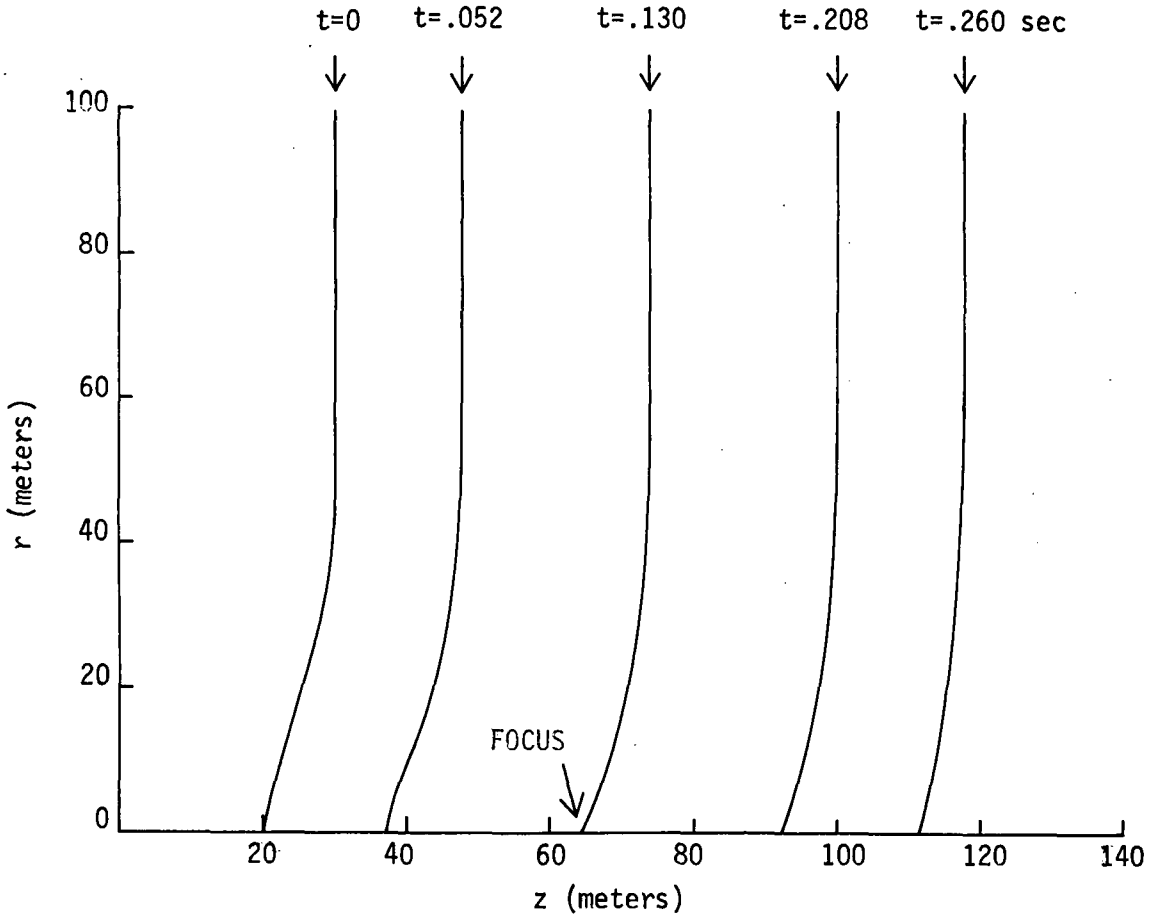

FIGURE 5-5. FORE SHOCK PROFILES OF A GAUSSIAN-FRONT N-WAVE ($\Delta p_o/p_o = 10^{-3}$)
(ACTUAL FOCUS OCCURS AT t = .130 SEC AT z = 64 METERS)

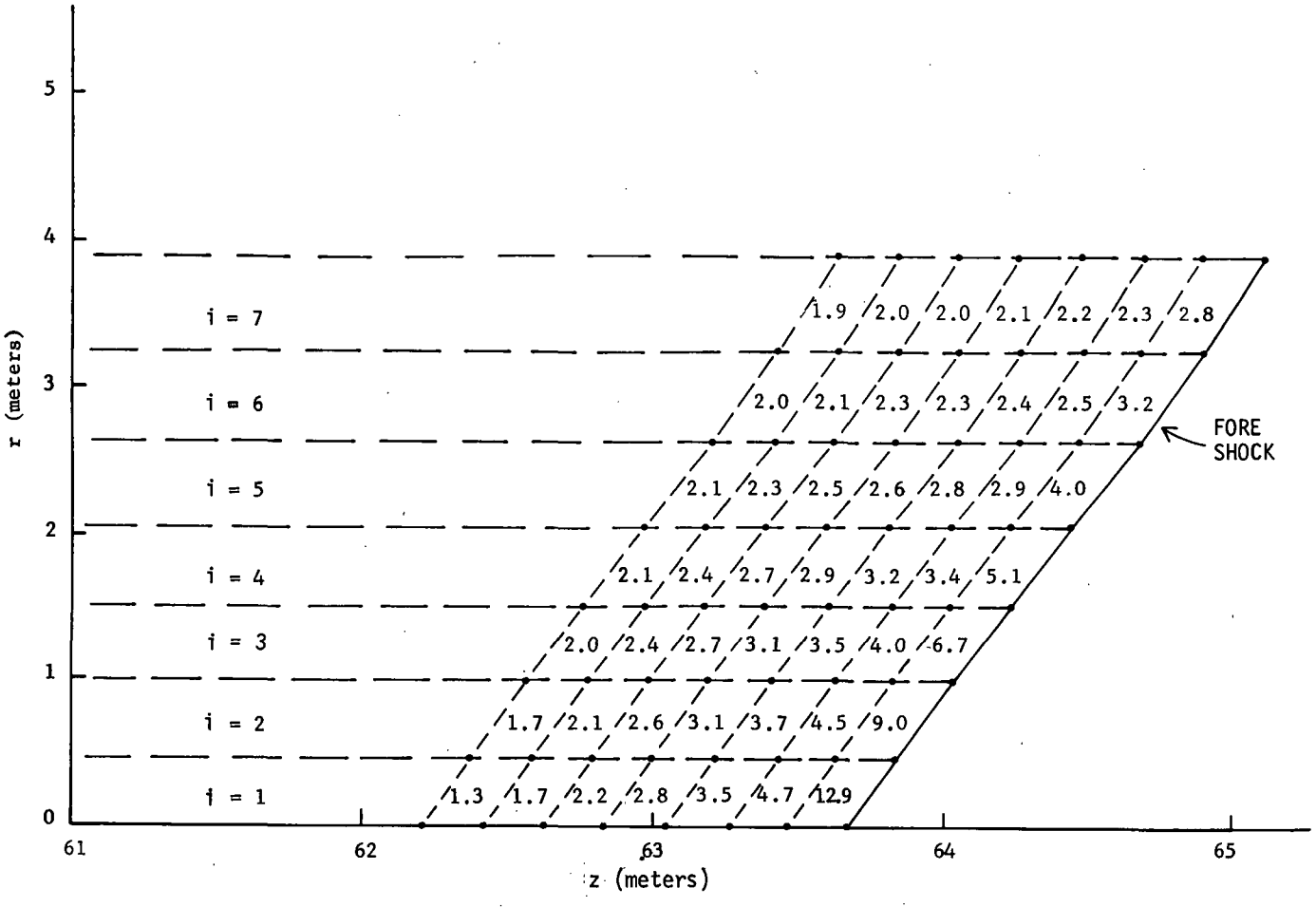

FIGURE 5-6. DISTRIBUTION OF RELATIVE OVERPRESSURE IN GAUSSIAN-FRONT N-WAVE IMMEDIATELY AFTER FOCUSING ($\Delta p_o/p_o = 10^{-3}$; figures in cells denote $\Delta p/\Delta p_o$)

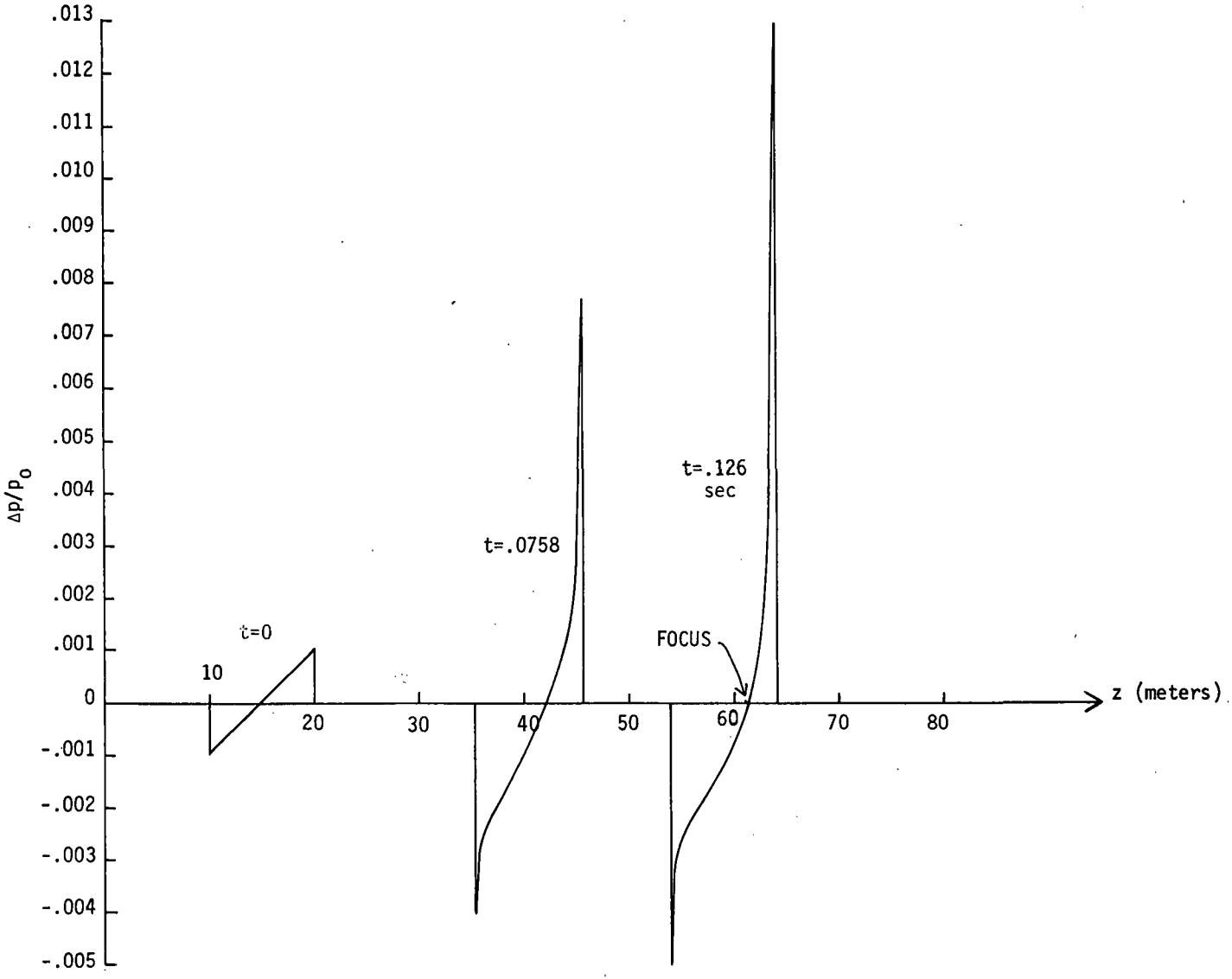

FIGURE 5-7. PRESSURE PROFILES AT AXIS AT THREE DIFFERENT TIMES FOR A GAUSSIAN-FRONT N-WAVE. ($\Delta p_o/p_o = 10^{-3}$, $\Delta p_{max}/\Delta p_o = 13.0$)

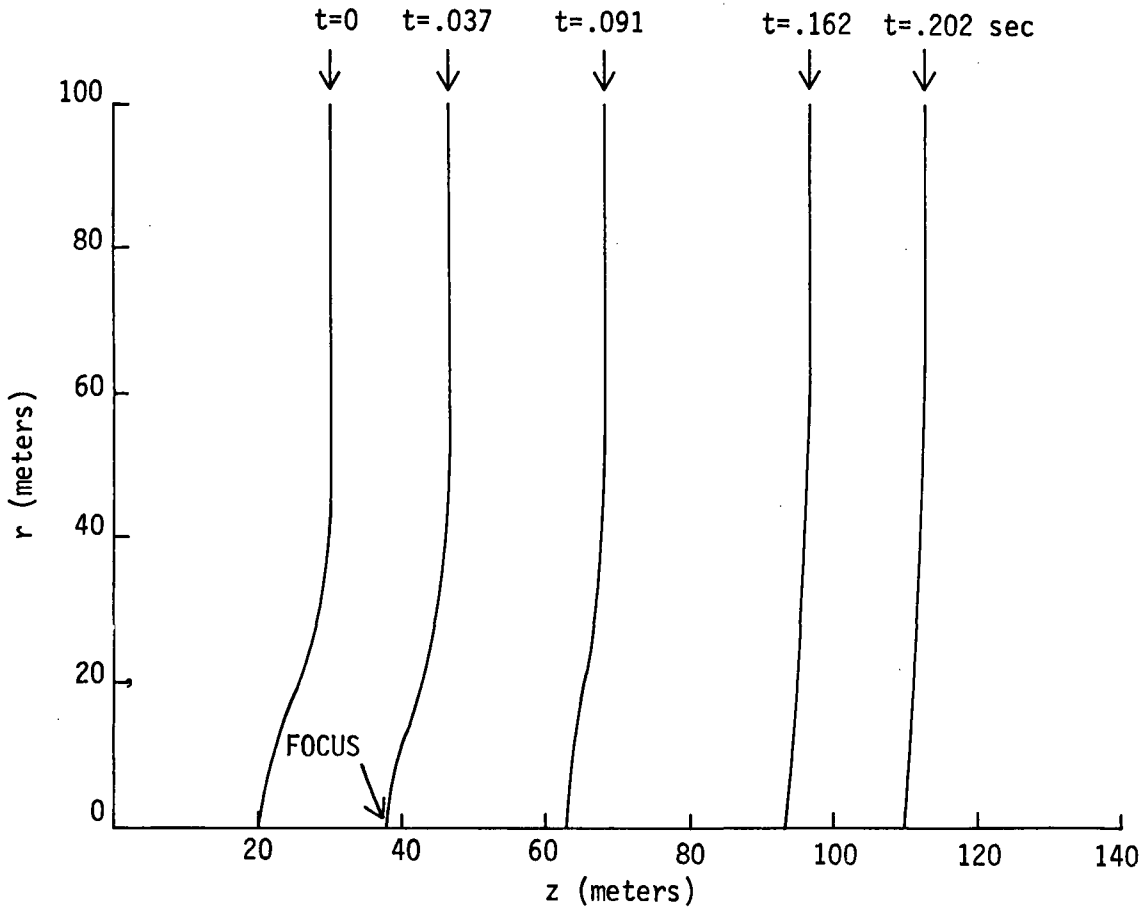

FIGURE 5-8. FORE SHOCK PROFILES OF A RELATIVELY STRONG GAUSSIAN-FRONT N-WAVE ($\Delta p_o/p_o$ = 0.90; FOCUS OCCURS AT t = .037 SEC AT z = 38 METERS)

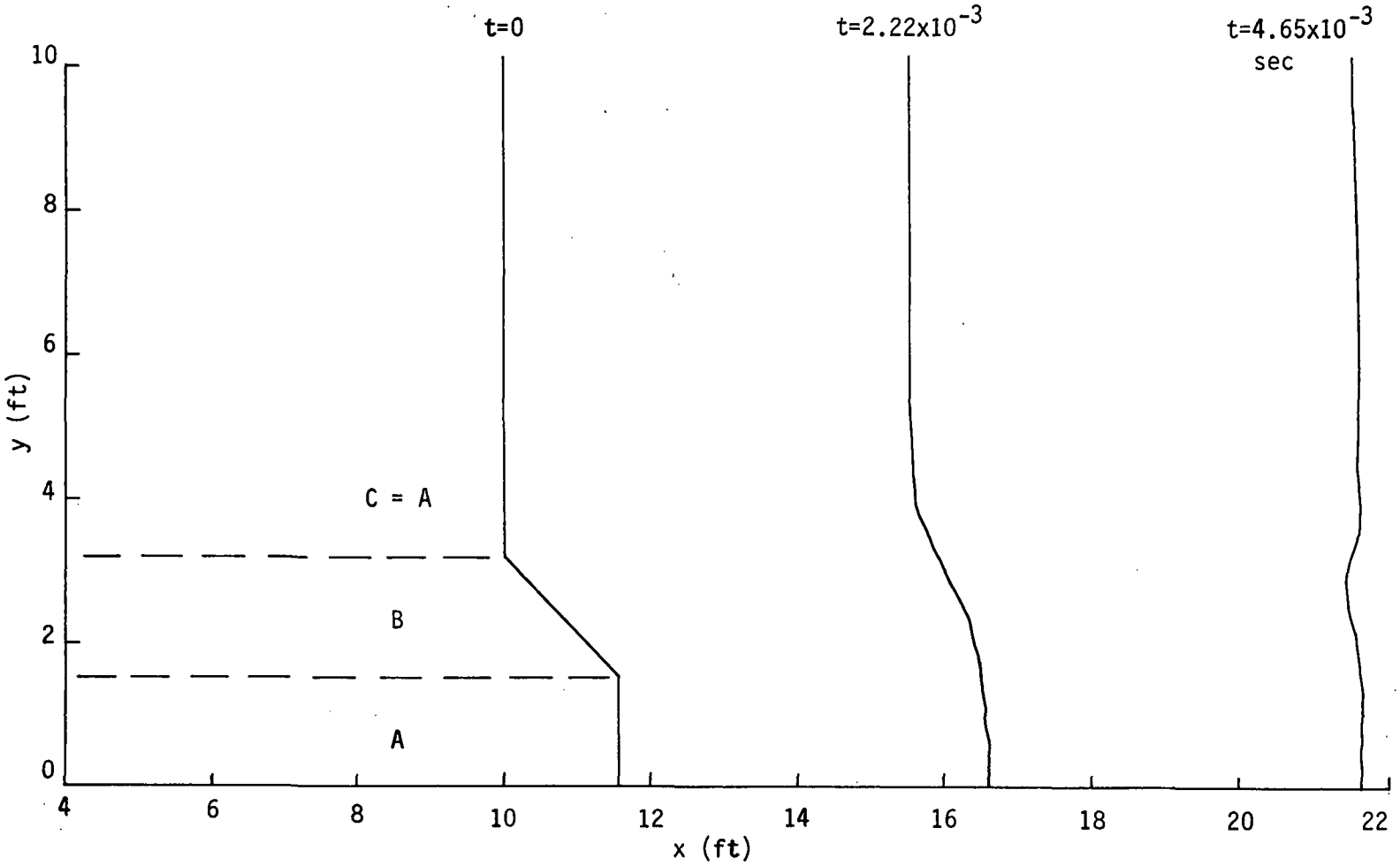

FIGURE 5-9. SINGLE RELATIVELY STRONG CONVEX SHOCK (GODUNOV CALCULATION)

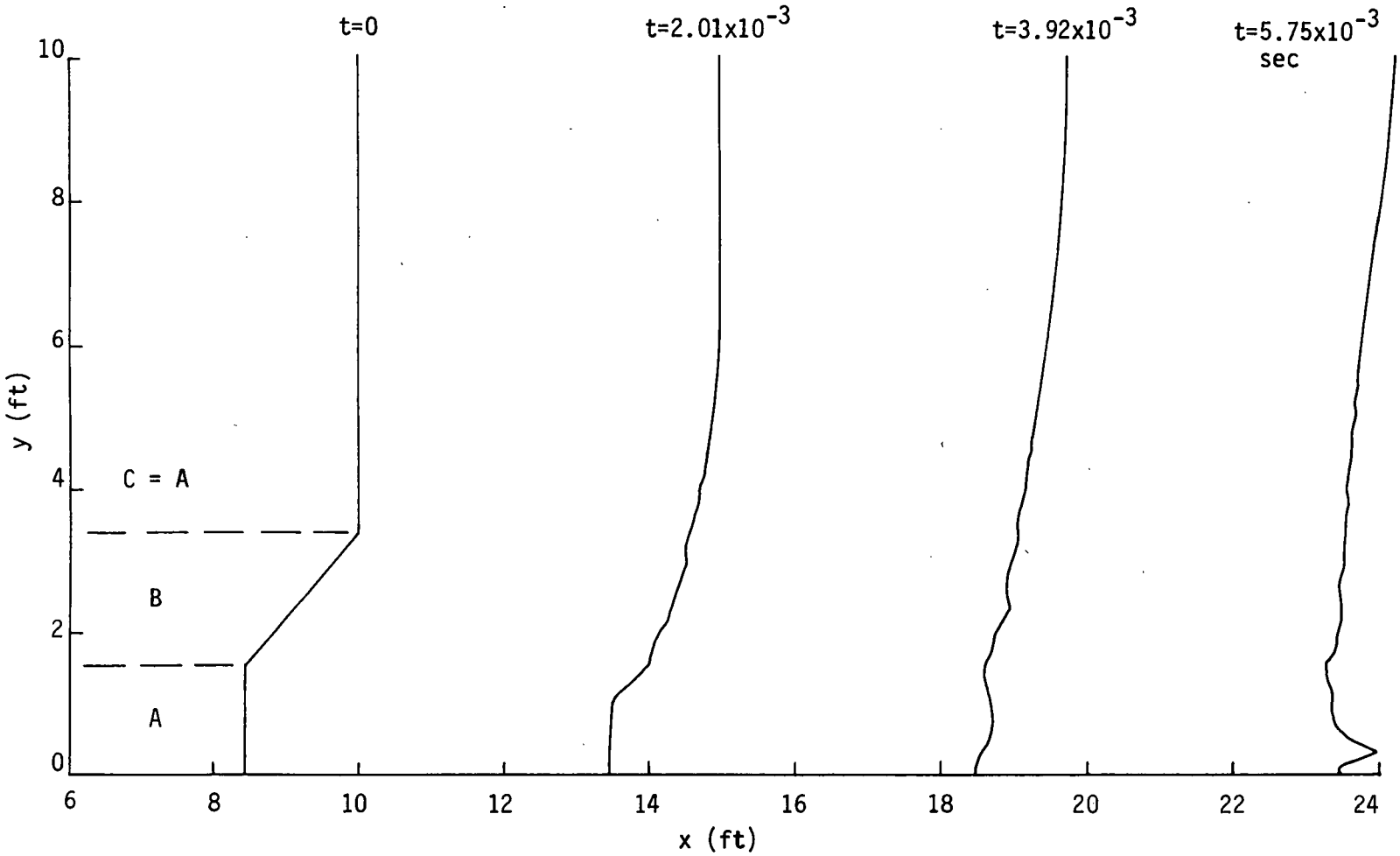

FIGURE 5-10. SINGLE RELATIVELY STRONG CONCAVE SHOCK (GODUNOV CALCULATION)

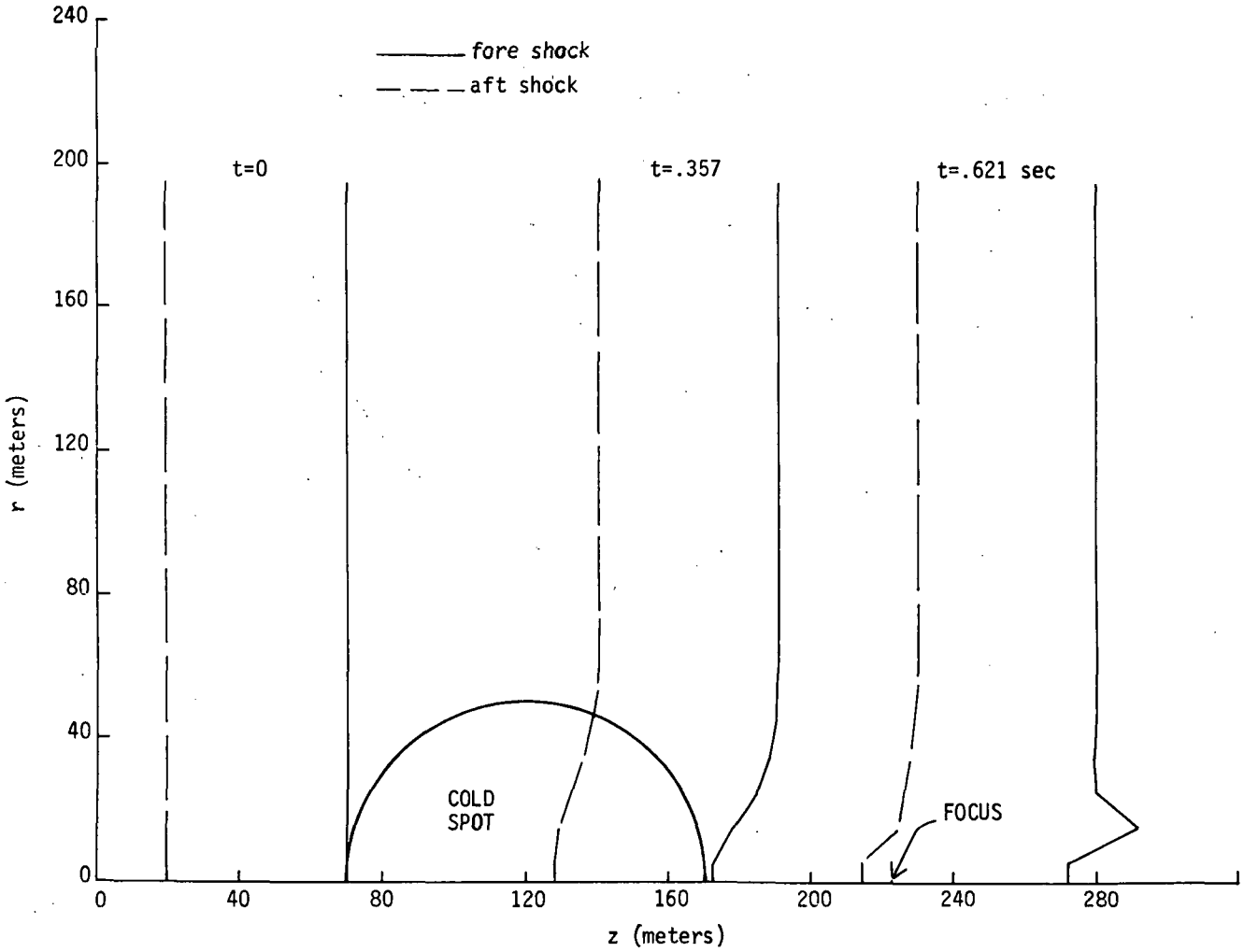

FIGURE 6-1. FORE AND AFT SHOCK PROFILES OF AN N-WAVE REFRACTED BY A COLD-SPOT AND SUBSEQUENTLY FOCUSED (r_{spot} = 50 METERS, TEMPERATURE RATIO = 0.5)

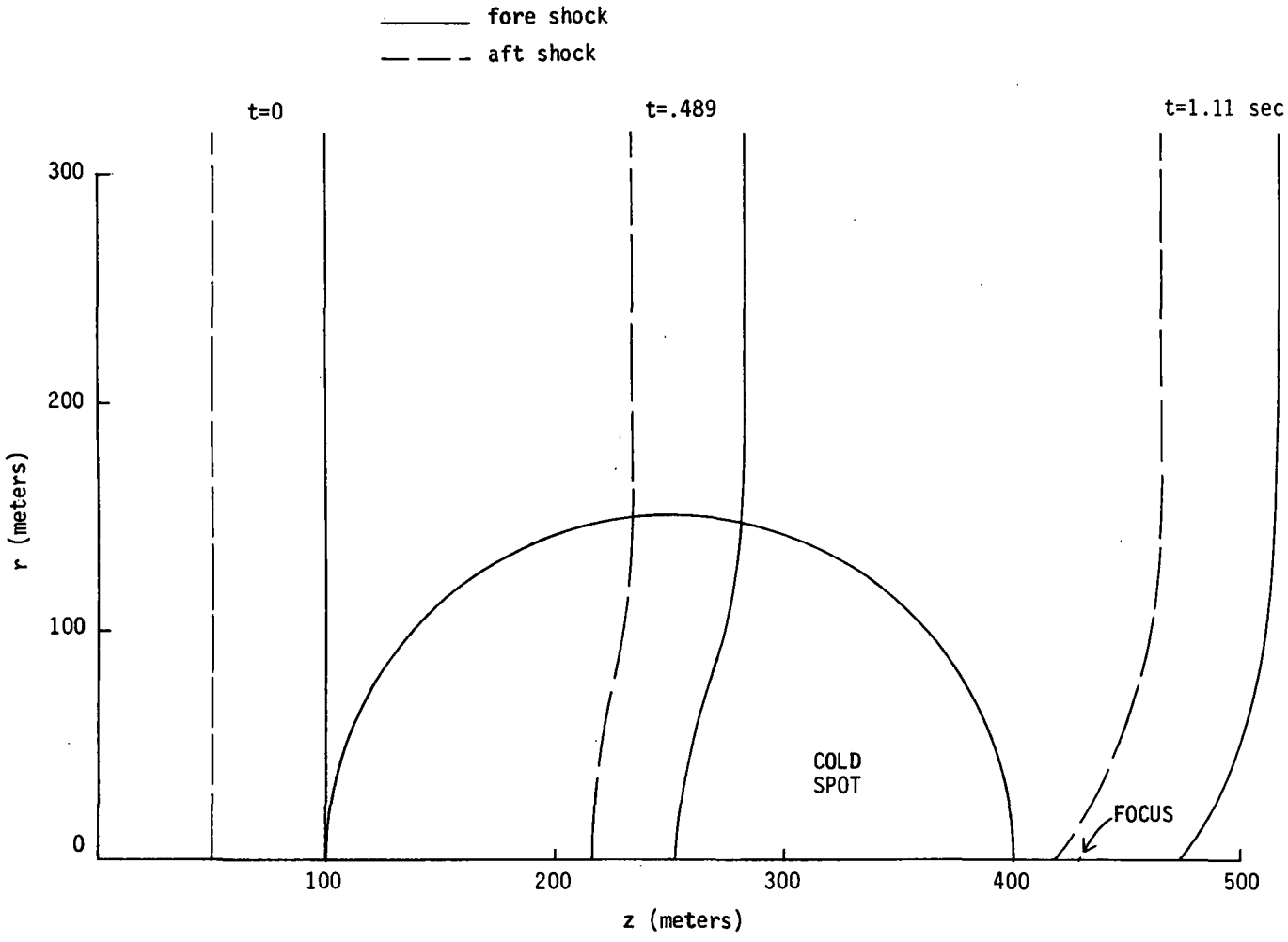

FIGURE 6-2. FORE AND AFT SHOCK PROFILES OF AN N-WAVE REFRACTED BY A COLD-SPOT AND SUBSEQUENTLY FOCUSED (r_{spot} = 150 METERS, TEMPERATURE RATIO = 0.5)

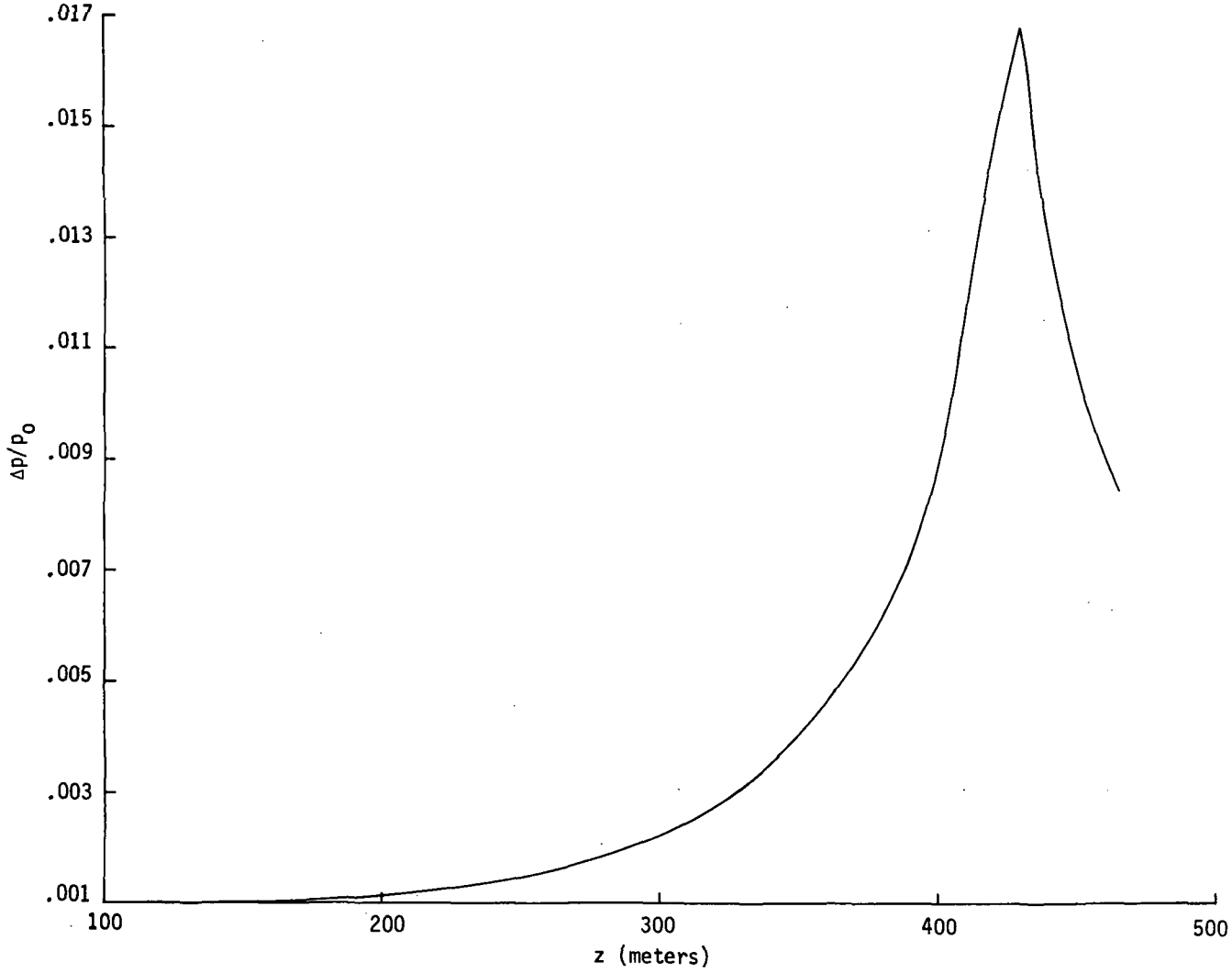

FIGURE 6-3. RELATIVE OVERPRESSURE VERSUS AXIAL POSITION OF FORE SHOCK FOR N-WAVE REFRACTED BY A COLD-SPOT. ($\Delta p_{max}/p_o$ = .0167)

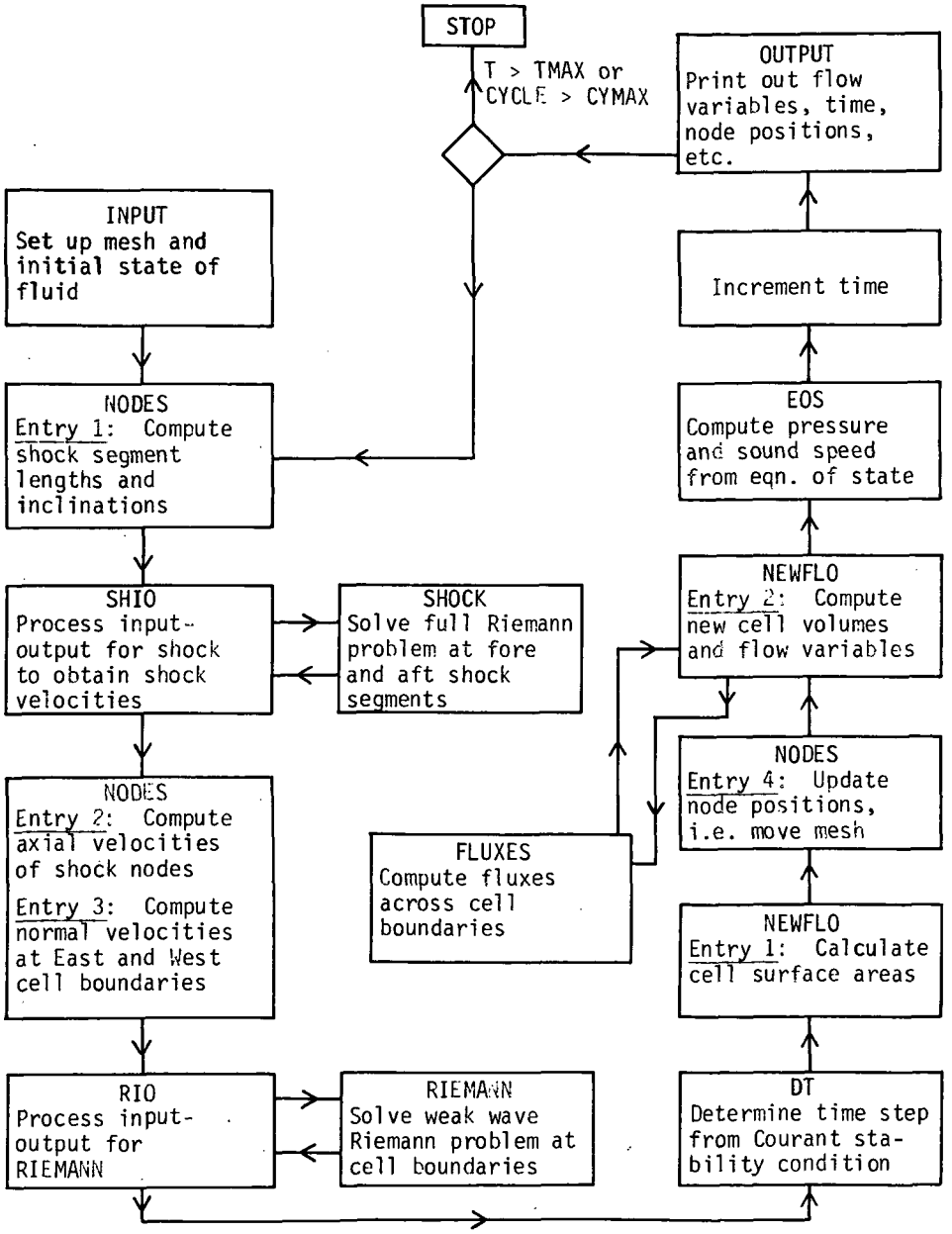

FIGURE A-1. GODUNOV FLOW CHART

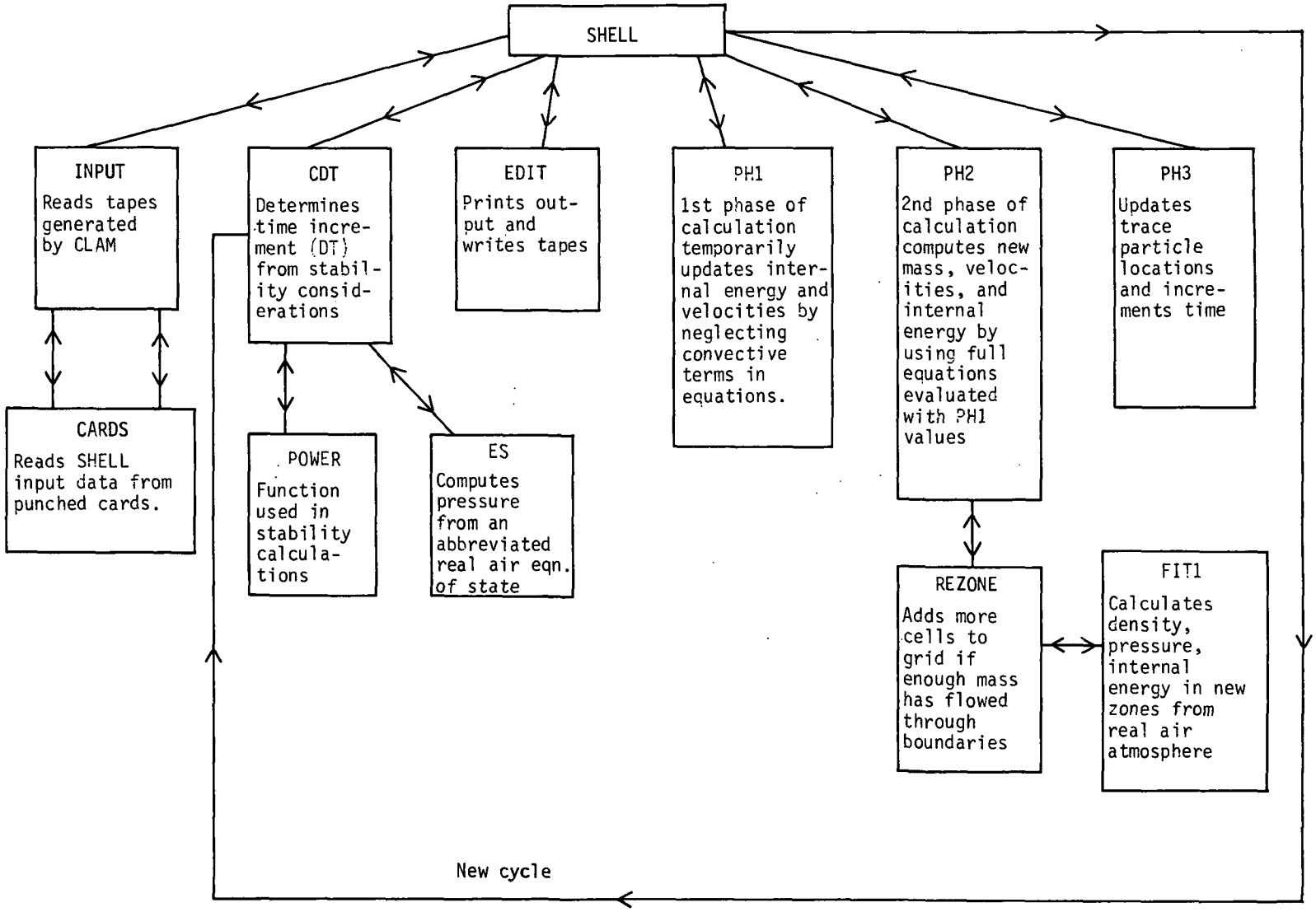

FIGURE A-2. SHELL FLOW CHART

TABLE 5-1

FOCUS FACTORS FOR POLYNOMIAL-FRONT
N-WAVE WITH DIFFERENT GRIDS

$$\frac{\Delta p_o}{p_o} = 10^{-3}$$

Number of Points radial x axial	$\frac{\Delta p_{max}}{\Delta p_o}$
20 x 7	6.4
100 x 7	12.4
200 x 7	13.1
400 x 7	12.9
100 x 12	16.2
200 x 12	18.8
100 x 20	18.7
* 50 x 7	13.1

* $a = \frac{\Delta r_j}{\Delta r_{i-1}} = 1.05$ (non-uniform spacing)

TABLE 5-2

FOCUS FACTORS FOR GAUSSIAN-FRONT
N-WAVE WITH DIFFERENT GRIDS

$$\frac{\Delta p_o}{p_o} = 10^{-3}$$

Number of points radial x axial	$\frac{\Delta p_{max}}{\Delta p_o}$
20 x 7	3.0
* 50 x 7	9.4
* 50 x 20	12.4
* 50 x 50	13.0

* $a = \frac{\Delta r_i}{\Delta r_{i-1}} = 1.05$ (non-uniform spacing)

REFERENCES

1. W. D. Hayes, R. C. Haefeli, and H. E. Kulsrud, "Sonic Boom Propagation in a Stratified Atmosphere with Computer Program," NASA CR-1299 (1969).

2. A. D. Pierce, "Maximum Overpressures of Sonic Booms Near the Cusps of Caustics," Noise and Vibration Control Engineering, M. J. Crocker, ed., Purdue Univ. Press (1971), pp. 478-87.

3. D. L. Lansing, "Application of Acoustic Theory to Prediction of Sonic Boom Ground Patterns from Maneuvering Aircraft," NASA TN D-1860 (1964).

4. J-C. L. Wanner, J. Vallée, C. Vivier, C. Thery, "Theoretical and Experimental Studies of the Focus of Sonic Booms," J. Acoust. Soc. Am., vol. 52, no. 1, pp. 13-32 (1972).

5. D. J. Maglieri, "Some Effects of Airplane Operations and the *Atmosphere on Sonic Boom Signatures*," *J. Acoust. Soc. Am.*, vol. 39, no. 5, pt. 2, pp. 536-542 (1966).

6. D. J. Maglieri, D. A. Hilton, V. Huckel, H. R. Henderson, and N. J. McLeod, "Measurements of Sonic Boom Signatures from Flights at Cutoff Mach Number," Third Conference on Sonic Boom Research, NASA SP-255, pp. 243-254 (1970).

7. W. D. Hayes, "Similarity Rules for Nonlinear Acoustic Propagation through a Caustic," NASA SP-165-171 (1968).

8. R. Seebass, E. M. Murman, and J. A. Krupp, "Finite Difference Calculation of the Behavior of a Discontinuous Signal Near a Caustic," NASA SP-155, pp. 361-371 (1971).

9. G. B. Whitham, "A New Approach to Problems of Shock Dynamics Part I Two-dimensional Problems," J. Fluid Mechanics, vol. 2, pp. 145-171 (1957).

10. S. K. Godunov, A. B. Zabrodin, and G. P. Prokopov, "A Difference Scheme for a Two-Dimensional Unsteady Problem in Gas Dynamics and the Calculation of a Flow with a Detached Shock Wave, USSR, Computational Mathematics and Mathematical Physics, vol. 1, no. 5, pp. 1187-1219 (1962).

11. T. D. Taylor and B. S. Masson, "Application of the Unsteady Numerical Method of Godunov to Computation of Supersonic Flows Past Bell Shaped Bodies," Journal of Computational Physics, vol. 5, pp. 443-454 (1970).

12. W. McNamara, "FLAME Computer Code for the Axisymmetric Interaction of a Blast Wave with a Shock Layer on a Blunt Body," J. Spacecraft, vol. 4, no. 6, pp. 790-795 (1967).

13. L. D. Landau and E. M. Lifshitz, Fluid Mechanics, p. 375 (Pergamon Press, 1959).

14. R. Collins and H-T. Chen, "Motion of a Shock Wave Through a Nonuniform Fluid," Lecture Notes in Physics, vol. 8, pp. 264-269 (Springer-Verlag, 1971).

15. G. T. Haglund and E. J. Kane, "Study Covering Calculations and Analysis of Sonic Boom During Operational Maneuvers," Boeing Report EQ 71-2 (February 1971).

16. A. D. Pierce, "Statistical Theory of Atmospheric Turbulence Effects on Sonic Boom Rise Times," J. Acoustical Soc. Am., vol. 49, no. 3, pt. 2, pp. 906-924 (1971).

"The aeronautical and space activities of the United States shall be conducted so as to contribute . . . to the expansion of human knowledge of phenomena in the atmosphere and space. The Administration shall provide for the widest practicable and appropriate dissemination of information concerning its activities and the results thereof."

—NATIONAL AERONAUTICS AND SPACE ACT OF 1958

NASA SCIENTIFIC AND TECHNICAL PUBLICATIONS

TECHNICAL REPORTS: Scientific and technical information considered important, complete, and a lasting contribution to existing knowledge.

TECHNICAL NOTES: Information less broad in scope but nevertheless of importance as a contribution to existing knowledge.

TECHNICAL MEMORANDUMS: Information receiving limited distribution because of preliminary data, security classification, or other reasons. Also includes conference proceedings with either limited or unlimited distribution.

CONTRACTOR REPORTS: Scientific and technical information generated under a NASA contract or grant and considered an important contribution to existing knowledge.

TECHNICAL TRANSLATIONS: Information published in a foreign language considered to merit NASA distribution in English.

SPECIAL PUBLICATIONS: Information derived from or of value to NASA activities. Publications include final reports of major projects, monographs, data compilations, handbooks, sourcebooks, and special bibliographies.

TECHNOLOGY UTILIZATION PUBLICATIONS: Information on technology used by NASA that may be of particular interest in commercial and other non-aerospace applications. Publications include Tech Briefs, Technology Utilization Reports and Technology Surveys.

Details on the availability of these publications may be obtained from:

SCIENTIFIC AND TECHNICAL INFORMATION OFFICE

NATIONAL AERONAUTICS AND SPACE ADMINISTRATION

Washington, D.C. 20546